AD

AD689490

RESEARCH AND DEVELOPMENT TECHNICAL REPORT
ECOM-0073-1

PROJECT THEMIS
PREDICTION OF ENVIRONMENTAL PARAMETERS

ANNUAL REPORT

By

K. C. Brundidge

William H. Clayton — Technical Director

E. L. Deacon

V. E. Moyer

November 1968

ECOM

UNITED STATES ARMY ELECTRONICS COMMAND · FORT MONMOUTH, N.J.

Contract DAAB07-68-C-0073

DEPARTMENTS OF METEOROLOGY AND OCEANOGRAPHY
TEXAS A&M UNIVERSITY
College Station, Texas 77843

DISTRIBUTION OF THIS DOCUMENT IS UNLIMITED

163

NOTICES

Disclaimers

The findings in this report are not to be construed as an official Department of the Army position, unless so designated by other authorized documents.

The citation of trade names and names of manufacturers in this report is not to be construed as official Government indorsement or approval of commercial products or services referenced herein.

Disposition

Destroy this report when it is no longer needed. Do not return to the originator.

TR ECOM-0073-1
NOVEMBER 1968

Reports Control Symbol
OSD-1366

PREDICTION OF ENVIRONMENTAL PARAMETERS
PROJECT THEMIS

First Annual Report

20 September 1967 to 20 September 1968

CONTRACT NO. DAAB07-68-C-0073

DA Project No. 1TO.14501.B81A.00.00

Project 542 (Themis)

Reference 68-23-A

Prepared by

K. C. Brundidge
William H. Clayton - Technical Director
E. L. Deacon
V. E. Moyer

TEXAS A & M RESEARCH FOUNDATION
College Station, Texas

For

U. S. Army Electronics Command, Fort Monmouth, New Jersey

ABSTRACT

The research efforts for the first year on Project Themis at Texas A&M University have been directed along five primary research paths: analysis and prediction of atmospheric structure through use of dual-frequency radars and associated ground facilities; cumulus cloud dynamics; modeling studies of the frictional boundary layer; installation of two automatic meteorological collection stations in an instrumented watershed which is in the pattern of the radars; and design of a facility for direct measurement of the fluxes of momentum, heat, and vapor. The activities under these various headings are reviewed separately herein.

ACKNOWLEDGEMENTS

The mobile meteorological stations employed in this study are provided by the Texas A&M Research Foundation and the U. S. Army Electronics Command (Contract DAAB07-68-C-0280).

The Research Council of Texas A&M University provides Themis employment of the General Purpose Analog Computer Facility, as well as some equipment and personnel support.

TABLE OF CONTENTS

LIST OF TABLES

LIST OF FIGURES

I. INTRODUCTION

The meteorological research program under Project Themis at Texas A&M has, since its inception, been divided into four main sub-areas as listed below.

Sub-task a.	Cumulus Cloud Development and Dissipation
Sub-task b.	Analysis and Prediction of Atmospheric Structure Through Dual Frequency Radar
Sub-task c.	Analog Modeling
Sub-task d.	Turbulent Flow Definition Through Reynolds Stresses Measurement

The single research goal under this program is the development of meteorological - mathematical models to improve objective forecast capability on all scales. Of course, it is an oversimplification to group research on all atmospheric scales under a single heading and therein really lies the reason for the subdivision. However, some need exists to show how these sub-areas make up the whole and it is to this point that this introductory section is directed.

The Themis research program derives in part from earlier research, conducted for the Atmospheric Sciences Laboratory of the United States Army, which led to the development of a model of the atmospheric boundary layer. The specific application of this model is from the surface to an elevation of 1000 meters and from the surface to a depth of two meters. This model and associated research revealed several deficiencies in

fundamental meteorological understanding that comprise a part of the investigations pursued in the sub-areas under Project Themis.

The analog modeling portion (Sub-task c) is not a continuation of this earlier modeling study but rather an investigation by analog means of the fundamental gaps in meteorological understanding, particularly, on the meso-scale. A significant example in this vein is the diabatic profile of wind, temperature, or vapor pressure. Of course, several "profile laws" exist and a couple of these have been cited so often in the literature that they enjoy the status of being widely known and, unfortunately, widely accepted. Unfortunately, since they are impractical in the sense of theoretical derivation and physical realism except for rather narrow and limited applications. Another example concerns the exchange coefficients, which, though widely used, are, as yet, without functional definition, and understanding is at best confused. Historically, as well as because of some practical necessities, this definition has been sought through mean-flow characteristics since the latter are the only parameters that can be routinely measured. To date, equivalence has not been determined and simultaneous direct measurement of Reynolds Stresses and pertinent mean parameters, under Sub-task d, is a logical path to follow.

A deficiency of the noted model, and other models, rests in the failure to include cloud formation and dissipation. For limited model areas, this is not too serious a problem but,

it becomes a most serious problem as the forecast area is extended vertically and horizontally, and the cumulus dynamics studies pursued under Sub-task a are addressed in part to this problem. Of course, turbulent flow definition under Sub-task d is also important to the cumulus dynamics study.

In general, existing models do not include precipitation, except in the total water balance sense, nor incorporate passage of frontal systems. The reason for this lack is twofold: 1) the functional definitions of involved phenomena are unknown; and 2) the measurement capability to provide necessary model input, assuming such understanding existed, is not routinely available. This introduces the dual frequency radar studies under Sub-task b which seeks to provide possible input through radar surveillance as well as permit incorporation of precipitation modeling. These studies also supplement the cumulus dynamics modeling.

As noted, these brief introductory remarks are intended only to show the relationship of the various sub-tasks under Project Themis to the overall project goals. Detailed information under these activities are reported separately on the following pages.

II. CUMULUS CLOUD DEVELOPMENT AND DISSIPATION

K. C. Brundidge

A. Introduction

The long-range objectives of this portion of the Themis program (Sub-task a) are:

1) to conduct numerical experiments on cumulus cloud initiation in which various conditions may be assigned with respect to heat and moisture sources, ambient wind, and exchange coefficients,

2) to extend, where possible, previous theoretical models of cumulus cloud development,

3) to compare the computed cumulus development with available observational data.

The accomplishment of these objectives will depend in part upon the observational program conducted in Sub-task b, and the determination of exchange coefficients as carried out in Sub-task d.

The specific goal of Sub-task a for this first year has been to formulate the mathematical procedures and models to be used in the study. The preparation and testing of the initial computer programs for the various models was then to be accomplished during the next 18-month period. In actuality, there has been some blending and realignment of these two phases during this first year. As a result, the moist convection model has not been completely formulated as yet; however, an initial program for a two-dimensional dry convection model has been written and has undergone some testing. This is in keeping with our decision to concentrate on the simplest of the various possible models as a first step. In particular, we have devoted most of our attention to a model of two-dimensional dry convection with zero ambient wind

field. The advantages of this procedure are that we can check the accuracy of our computer program with considerably less computer time than would be required for a more complicated model, and many of the developed sub-routines will have applicability in a more complicated model. Furthermore, we can determine the influences of various initial conditions and heating rates, multiple heat sources, and various assumptions for the eddy exchange coefficients on convection before bringing in the added influences of latent heat release.

In the following sections, we shall present the experimentation program which has been set up as a guideline, the details of the various models which are to be studied, the problems that have been encountered and their solution, and the numerical procedures which have been investigated.

<u>The basic equations</u>. The basic set of equations being used in this study is the anelastic system developed by Ogura and Phillips (1962). This system permits gravity wave solutions but filters out compression waves. The formulation of this system for moist convection will be stated at a later point. For dry convection and in dimensional form, it is

$$\frac{du}{dt} = -C_p \; \Theta \frac{\partial \pi'}{\partial x} + K_M \left[\nabla^2 u + a(z) u_z \right] \qquad 1)$$

$$\frac{dv}{dt} = -C_p \; \Theta \frac{\partial \pi'}{\partial y} + K_M \left[\nabla^2 v + a(z) v_z \right] \qquad 2)$$

$$\frac{dw}{dt} = -C_p \; \Theta \frac{\partial \pi'}{\partial z} + g \frac{\theta'}{\Theta} + K_M \left[\nabla^2 w + a(z) w_z \right] \qquad 3)$$

$$\nabla \cdot \rho_0 \mathbf{C} = 0 \tag{4)}$$

$$\frac{d\theta'}{dt} = K_H \left[\nabla^2 \theta' + a(z) \theta'_z \right] \tag{5)}$$

where $\rho_0 = \frac{P}{R\Theta}\left(1 - \beta z\right)^{\frac{1}{\kappa} - 1}$ and $a(z) = \rho_0^{-1} \frac{\partial \rho_0}{\partial z}$, $\beta = \frac{g}{C_p \Theta}$

P is a reference pressure (say, 1,000 mb), Θ is a constant reference potential temperature, K_M and K_H are the eddy coefficients for momentum and heat exchange, respectively, $\pi = \left(\frac{p}{P}\right)^{\kappa}$ where p is pressure, and

π' is the deviation of π from the distribution $\pi_0 = 1 - \beta z$, i.e.,

$\pi' = \pi - \pi_0$

θ' is the deviation of potential temperature from the value Θ, i.e.,

$\theta' = \theta - \Theta$

and other symbols in 1) - 5) have the usual meteorological meaning.

This system has been used by Ogura (1963) and Orville (1964, 1965), among others, in studies of convection in a vertical plane or in an axially-symmetric cylindrical coordinate system. These studies have been restricted to shallow convection, i.e., where the top of the model is at about 3 km. For the latter situation, Ogura and Phillips (op. cit.) have shown that 4) may be replaced with $\nabla \cdot \mathbf{C} = 0$. Then, the equations amount to the incompressible Boussinesq approximation. With this combination of circumstances, one may make use of the streamfunction and, furthermore, may replace 1) and 3), or their cylindrical coordinates equivalents, with the vorticity equation. Consequently, it is never necessary to compute π'.

However, it is our desire eventually to consider three-dimensional regions and deep convection (top of the region at about 10 km.). For this purpose, it is necessary to work with the primitive equations as given by 1) - 5) and this requires a means whereby π' can be determined. This is especially critical for moist, deep convection for then π' must be known in order to compute the saturation mixing ratio. A diagnostic equation for computing π' is obtained by forming the divergence equation from 1) - 3) and may be written as

$$C_p \Theta \nabla \circ \rho_0 \nabla \pi' = \frac{g}{\Theta}\frac{\partial \rho_0 \theta'}{\partial z} + \nabla \circ \rho_0 \mathbb{F} - \nabla \circ [\rho_0 ¢ \cdot \nabla ¢] \qquad 6)$$

where $\mathbb{F} = K_M \ (\hat{i} \nabla^2 u + \hat{j} \nabla^2 v + \hat{k} \nabla^2 w) + a(z) \ K_M \ (\hat{i} u_z + \hat{j} v_z + \hat{k} w_z)$.
Equations 1) - 6) form the basic system with which we are working, aside from modifications that must be brought in when an ambient wind field is considered or when moist convection is occuring.

The basic model. Natural convection in the atmosphere is a mechanism whereby heat and moisture are transported upward from their source region at the earth's surface. For air mass type convection, the lapse rate may be superadiabatic for several hundred feet above the ground. Accordingly, we have chosen to work with models which incorporate these features.

We consider a grid system in which Δx, Δy, and Δz are 100 m, except for a layer resting on the ground for which Δz is only 10 m. The surface temperature is a specified function of time which differs from one place to another so that "hot spots" may develop. Heat (and moisture) is transferred from the ground through the 10-m layer by turbulent diffusion.

The initial potential temperature distribution which has been chosen corresponds to conditions in the Dallas, Texas area for June 15, 1962 at 0900 CST. It is synthesized from the radiosonde observations at Amon Carter Field, observations on the Cedar Hill tower (Gerhardt et al, 1962), and observations on a micrometeorological tower (Clayton, 1963) located about 150 yds from the Cedar Hill tower. Since we have not as yet entered into the study of moist convection, the moisture distribution has not been abstracted; however, the data are at hand when the time comes. Incidentally, for the day in question Love Field, Dallas reported cumulus clouds with bases at 3000 ft starting at 1034 CST. This potential temperature distribution is given in Table II-1. It may be noted that the lapse rate is superadiabatic through the first 110 m.

Table II-1. Initial Temperature Distribution

Height [m]	θ [°K]
Ground	302.2
10	298.4
110	297.6
210	297.8
310	298.6
410	299.5
410-1510	$\frac{\partial\theta}{\partial z}$ = 0.3 deg/100m
1510-1710	$\frac{\partial\theta}{\partial z}$ = 2.25 deg/100m
1710-10km	$\frac{\partial\theta}{\partial z}$ = 0.35 deg/100m

__The experimental program__. The experimental program which has been set up is given below. This listing does not necessarily imply the order in which the various experiments are to be handled.

__Dry Convection__

i. Single heat source

  a. Numerical procedure experimentation

    1. Upstream differencing

    2. Others

  b. Other things constant, expand X dimension

  c. Other things constant, change power of heat source

  d. Other things constant, change initial lapse rate

  e. Other things constant, introduce non-linear diffusion

  f. Other things constant, introduce ambient wind field

    1. Vertical shear

    2. Vertical and horizontal shear (three-dimensional)

  g. Combinations as seen fit, particularly of e. and f.

ii. Two heat sources

  a. Other things constant, vary distance between sources

  b. Other things constant, vary relative power of sources

  c. Other things constant, vary relative size of sources

  d. Other things constant, introduce non-linear diffusion

  e. Other things constant, introduce ambient wind field

    1. Vertical shear

    2. Vertical and horizontal shear (three-dimensional)

  f. Combinations of the above as seen appropriate

iii. Cumulus initiation

a. Single heat source, surface inactive as moisture source

1.. All items in i

2. Other things constant, vary moisture distribution in x and z

b. Single heat source, moisture-active surface

1. All items in iii a

2. Other things constant, vary moisture sources at ground

c. Two heat sources

1. Surface inactive as moisture source

(a) All items in iii b

iv. Cumulus dissipation

B. The Two-Dimensional Dry Convection Model

General Features. As stated previously, this model has received most of our attention to date. It is the most simple model with which to begin, although it is somewhat unrealistic in that it assumes that motion occurs only in the x-z plane.

We visualize the region shown in Fig. II-1. It is assumed that

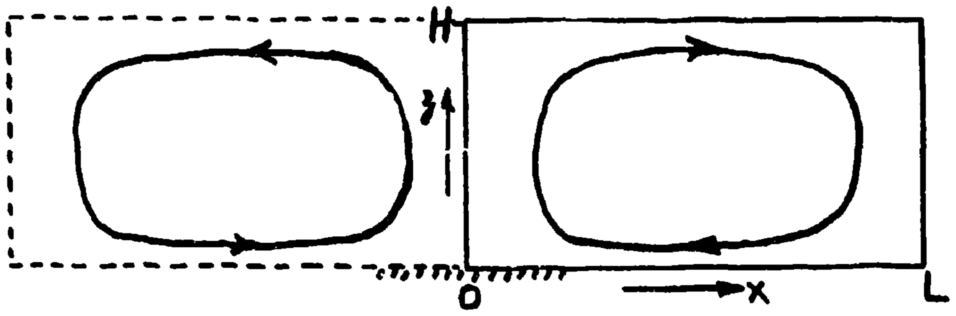

Fig. II-1 Two-Dimensional Dry Convection Model Area

initially in this region the pressure and potential temperature surfaces are horizontal and no motion exists. At the ground, differential rates of heating take place so that in a short time the stippled area in Fig. II-1 becomes a hot spot relative to the remainder of the lower boundary. Heat diffuses into the region from the lower boundary. The differential heating then acts as the energy source to initiate and maintain the motion field. The flow will be symmetric with respect to the vertical line $x = 0$, hence we need only consider the region with solid boundaries in Fig. II-1. We also assume symmetry exists across the vertical $x = L$.

For testing purposes, we are letting $L = 3$ km, $H = 4$ km, and the width of the hot spot be 1 km. The temperature-change rates imposed at the bottom boundary are as shown in Table II-2.

Table II-2. Surface Temperature Rates

Time [CST]

	09-10	10-12	12-14	14-15
Hot Spot	2 deg hr^{-1}	1 deg hr^{-1}	0.5 deg hr^{-1}	0.2 deg hr^{-1}
Exterior to Hot Spot	0.8 deg hr^{-1}	0.4 deg hr^{-1}	0.2 deg hr^{-1}	0.2 deg hr^{-1}

System of equations. The system of equations for this model are obtained directly from 1) - 6). They are as follows:

$$u_T = -u\,u_x - w\,u_z - C_p\,\Theta\pi_x' + K_M\left[u_{xx} + u_{zz} + a(z)u_z\right] \qquad 7)$$

$$w_T = -u\,w_x - w\,w_z - C_p\,\Theta\pi_z' + \frac{g\theta'}{\Theta} + K_M\left[w_{xx} + w_{zz} + a(z)w_z\right] \qquad 8)$$

$$\rho_0 \left(u_x + w_z\right) + w(\rho_0)_z = 0 \qquad 9)$$

$$\theta_t' = -u\,\theta_x' - w\,\theta_z' + K_H\left[\theta_{xx}' + \theta_{zz}' + a(z)\theta_z'\right] \qquad 10)$$

where the subscripts indicate differentation. When the continuity equation 9) is used to replace terms on the right-hand side of the divergence equation, the latter takes the form:

$$\left(\pi_{xx}' + \pi_{zz}'\right) + a\,\pi_z' = C1\left(\theta_z' + a\,\theta'\right) + \frac{1}{\pi_0^2}\left(\frac{-C7}{4}\frac{w}{\pi_0} + \frac{C8}{2}w_z - C9w^2\right)$$

$$+ C11\left(u_x w_z - u_z w_x\right) \qquad 11)$$

where $a = \frac{1}{\rho_0}(\rho_0)_z$

$C11 = \frac{2}{C_p\,\Theta}$

$C1 = \frac{R}{C_p\,\Theta^2}$

$C3 = \frac{R}{C_p\,\Theta}$

$C7 = \frac{5K_M C3^3}{C_p\,\Theta}$

$C8 = \frac{5K_M C3^2}{C_p\,\Theta}$

$C9 = \frac{8.75\,C3^3}{C_p\,\Theta}$.

We have chosen as values for the eddy coefficients in 7), 8) and 10) the following: $K_H = K_M = 7.5\times10^2\ cm^2\ sec^{-1}$ at the 10-m level but $K_H = K_M = 4\times10^4\ cm^2\ sec^{-1}$ at all higher levels. It may be noted that while K_H and K_M are not independent of height, this fact has been ignored in the formulation of the eddy diffusion term in 7), 8) and 10).

Boundary conditions. The boundary conditions were chosen to provide the symmetry conditions mentioned previously at the lateral boundaries, zero motion at the upper and lower boundaries, slip flow at the top and side boundaries, and a thermally-active lower boundary. These conditions are as follows:

Upper boundary: $w = 0, \; u_z = 0$

$\theta' =$ cons't w/r to x and t

$$\pi_z' = C1\theta' + \frac{K_M}{C_p \Theta}\left[w_{zz} + a(H)w_z\right]$$

Lower boundary: $w = 0, \; u = 0$

$\theta'(x,t) =$ specified function

$$\pi_z' = C1\theta' + \frac{K_M}{C_p \Theta}\left[w_{zz} + a(0)w_z\right]$$

Lateral boundaries: $u = 0, \; w_x = 0$

$\theta_x' = 0$

$\pi_x' = 0$

The conditions on π_z' at the upper and lower boundaries follow directly from 8) in conjunction with the other conditions assumed at these levels. In the same way, certain other conditions follow as results from 7) - 10). These are the following.

Upper boundary: $w_z = -u_x$

$w_{zz} = -a(H)w_z, \; \theta_{zz}' = -a(H)\theta_z'$

Lower boundary: $w_z = 0$

Lateral boundaries: $u_{xx} = 0$

These conditions permit the formulation of all terms in the various equations of the system in finite difference form. The special treatments needed to obtain certain of the terms in the balance equation will be presented later.

The pressure computation. When the balance equation is formulated in finite difference form and making use of the derivative boundary conditions, it is found that the determinent of the matrix of this elliptic equation is zero. As a consequence, the values of π' which result from solution, regardless of the procedure used, will be only relative values.

This would constitute no particular problem if we were concerned only with dry convection. The pressure (actually π')values are needed only to evaluate the pressure force terms in the equations of motion, and since these terms depend upon differences of pressure, relative values would be acceptable. However, as pointed out before, for the deep, moist convection model it will be necessary to know unique values of π' at every grid point in order to determine the saturation mixing ratio.

The unique values are obtained simply by specifying the value of π' at some point on the boundary for all time. The difference between this value and that computed for the same point then constitutes a correction factor to be applied at all grid points.

Another problem related to the pressure computation became apparent when we were trying to establish the initial pressure distribution. The basic form of the balance equation may be written

$$\nabla^2\pi' + a(z)\pi_z = Cl[\theta_z' + a(z)\theta'] + F(x,z) \qquad 12)$$

where $F(x,z)$ represents the motion terms on the right-hand side of 11). We assume that initially, the θ' and π'surfaces are horizontal and there is no motion. Thus, at the initial time, 12) becomes simplified to

$$\pi'_{zz} + a(z)\pi'_z = C1[\theta'_z + a(z)\theta'] \qquad 13)$$

from which one should be able to compute the initial π' distribution, given the initial θ' distribution. However, at the initial time the pressure field is hydrostatic and thus one also should be able to compute the π' field from

$$\pi'_z = C1\theta' \qquad 14)$$

or

$$\pi'_{zz} = C1\theta'_z \qquad 15)$$

Equation 14) can be solved by straightforward integration, assuming a value of π' at either the top or the bottom of the system. Equation 15) can be put in finite difference form and solved either by relaxation or as a system of simultaneous equations. Equations 14) and 15) give the same results. However, 13) which simply represents a combination of 14) and 15) did not give the same results when solved as a centered-difference system. This implied that once the motion was established, at which time 12) is the only available diagnostic relation for the computation of π', we could not expect to get correct values of π'.

The answer to this problem was found by working with various test cases. It was found that in order for 13) to give correct results, it was necessary to express π'_{zz} as a centered difference at the level in

question while expressing π_z' as a difference over the layer above or below the level of interest. At the upper and lower boundaries, the boundary condition for π_z' is applied in the usual manner.

This procedure, however, has a disadvantage in that it introduces different orders of truncation error in the finite difference formulation of π_z' and π_{zz}'. Thus, it was necessary to find a way to still express π_z' as a centered difference yet not introduce incorrect valu of π' at the initial time. Also, special consideration had to be given to the formulations at the second level in the model due to the unequal space increments above and below this level. The manner in which these problems were handled will be described in the next section.

C. Numerical Procedures

An extremely important aspect of the modeling problem is the choice of the numerical procedure which is to be used for the solution. The procedure must be stable, it should have as small a truncation error as possible and should not be such that it requires an excessive amount of computer time or exceeds the storage capabilities of the machine. Generally, some compromise of features will be required.

Numerical schemes which have been used successfully in the past in convection problems of the sort considered here have been the upstream differencing procedure used by Ogura (1962, 1963) and Orville (1964, 1965, 1968), and the two-step Lax-Wendroff (1960) method used by Árnason et.al. (1968). Molenkamp (1968) has investigated the features of these schemes and others by the application of each to the same

field in a situation for which the correct results were already known. His results confirm a feature that we had noted which is that the upstream scheme has a built-in fictitious diffusion which greatly smooths the field. On the other hand, the isolines of the field were advected at about the proper rate. The two-step Lax-Wendroff scheme, on the other hand, conserves maxima and minima of the field quite well but advects the isolines much too slowly. Other schemes discussed by Molinkamp have other draw-backs for grids of many points because of storage requirements or running time.

The programs which we have written up to this time have been based on a two-step upstream difference scheme which will be described below.

General features. We consider an equation of the form

$$\frac{\partial F}{\partial t} = -A\frac{\partial F}{\partial x} + K\frac{\partial^2 F}{\partial x^2} \qquad 16)$$

where the first term on the right-hand side represents advection and the second term represents diffusion. In finite upstream difference form 16) may be written as

$$F_n^{j+1} = F_n^j - r\left(F_n^j - F_{n-1}^j\right) + \gamma\left(F_{n+1}^j + F_{n-1}^j - 2F_n^j\right) \qquad 17)$$

where $x = n\Delta x$, $t = j\Delta t$, $r = \frac{A\Delta t}{\Delta x}$, $\gamma = \frac{K\Delta t}{\Delta x^2}$, $A > 0$, and Δx, Δt are the grid and time increments, respectively. With simple manipulation, 17) can be written

$$F_n^{j+1} = F_n^j - \frac{r}{2}\left(F_{n+1}^j - F_{n-1}^j\right) + \left(\frac{r}{2} + \gamma\right)\left(F_{n+1}^j + F_{n-1}^j - 2F_n^j\right) \qquad 18)$$

If, in turn, 18) is converted back into differential-equation form by using the Taylor Series through the second-order terms, one obtains

$$\frac{\partial F}{\partial t} = -A\frac{\partial F}{\partial x} + \left[\tfrac{1}{2}A\Delta x\left(1 - \frac{A\Delta t}{\Delta x}\right) + K\right]\frac{\partial^2 F}{\partial x^2} \qquad 19)$$

Thus, it is seen that representing the advection term in 16) as an up-stream difference actually amounts to the use of 19), thereby introducing an additional diffusion term with the coefficient,

$$\tfrac{1}{2}\ |A|\Delta x\left(1 - \frac{|A|\Delta t}{\Delta x}\right)$$

For values of $|A|$, Δx, and Δt which are typical of the convection problem, this coefficient is of the same order of magnitude as the real eddy coefficient, K. This, of course, presents a serious problem when one is interested in determining the influence of real diffusion on convective development. It can be shown that the same influence arises with the Lax-Wendroff Scheme; however, from Molenkamp's results the effect apparently is much smaller. Presumably, this is because the equation which involves the fictitious diffusion is used only for every other time step. Possibly this problem could be overcome by use of a real eddy coefficient whose magnitude increased as a function of the motion, i.e., along the lines of the non-linear diffusion discussed by Kuo (1962). However, the most satisfactory answer would be a numerical scheme which did not introduce a spurious diffusion. We have under study an implicit scheme which may prove to be superior to any of the schemes mentioned above.

__The two-step upstream difference scheme__. In this procedure 17) is computed in two steps for each time increment. First, intermediate values of F, called F', are determined on the basis only of diffusion. The intermediate values then are used to evaluate the advection term and to obtain the final predicted value of F. In two dimensions, the system becomes

$$\left(F'\right)^{j}_{n,\ell} = F^{j}_{n,\ell} + \gamma\left(F^{j}_{n+1,\ell} + F^{j}_{n-1,\ell} + F^{j}_{n,\ell+1} + F^{j}_{n,\ell-1} - 4F^{j}_{n,\ell}\right)$$

$$F^{j+1}_{n,\ell} = \left(F'\right)^{j}_{n,\ell} - r_1\left[\left(F'\right)^{j}_{n,\ell} - \left(F'\right)^{j}_{n-1,\ell}\right] \qquad 20)$$

$$- r_2\left[\left(F'\right)^{j}_{n,\ell} - \left(F'\right)^{j}_{n,\ell-1}\right]$$

where $x = n\Delta x$, $z = \ell\Delta z$, $t = j\Delta t$, $\Delta x = \Delta z$, $\gamma = \frac{K\Delta t}{\Delta x^2}$, $r_1 = U\frac{\Delta t}{\Delta x}$, $r_2 = W\frac{\Delta t}{\Delta x}$, and U and W are constant advection velocities.

Let,

$$F^{j}_{n,\ell} = A\phi^{j}\, e^{ikn\Delta x}\, e^{im\ell\Delta x}$$

$$\left(F'\right)^{j}_{n,\ell} = B\phi^{j}\, e^{ikn\Delta x}\, e^{im\ell\Delta x} \qquad 21)$$

where k and m are wave numbers in the x and z directions, respectively and $i = \sqrt{-1}$. When the relations in 21) are substituted into 20), one finds

$$\frac{B}{A} = 1 - 4\gamma\left(\sin^2\frac{k\Delta x}{2} + \sin^2\frac{m\Delta x}{2}\right) \equiv \Gamma$$

and the stability criterion becomes

$$|\phi| = \Gamma^2\Big\{[1-(r_1+r_2) + r_1 \cos k\Delta x + r_2 \cos m\Delta x]^2 \qquad 22)$$

$$+ [r_1 \sin k\Delta x + r_2 \sin m\Delta x]^2\Big\} \leq 1$$

It is seen that the criterion is a function of wavelength; however, the result for the shortest wavelength which can be resolved by the numerical scheme is found to hold for all longer wavelengths. Thus, if we assume wavelengths of $2\Delta x$ in both the x and z directions, the condition becomes

$$|\phi| = \Gamma^2[1-2(r_1+r_2)]^2 \leq 1 \qquad 23)$$

where

$$\Gamma = 1 - 8\gamma$$

In the event that the motion is zero, which is the initial condition in our cases unless an ambient wind field exists, r_1 and r_2 are zero and we must have $|\Gamma| \leq 1$. This condition is met if $\gamma \leq \frac{1}{4}$. We require that this condition shall always be met. Under these circumstances, the remainder of the criterion may be stated as

$$|1 - 2(r_1+r_2)| \leq 1$$

or 24)

$$|r_1|+|r_2| \leq 1$$

The absolute value signs have been applied in 24) to account for the modifications that arise in the formulations of the advective terms when the velocities are negative.

If we let

$$|r_1| = |r_2| = \frac{V_M}{\sqrt{2}} \frac{\Delta t}{\Delta x} \equiv r$$

where V_M is the magnitude of the maximum velocity vector in the field, the final results are that

$$\Delta t \le \frac{\Delta x^2}{4K} \quad \text{and} \quad \Delta t \le \frac{.707 \ \Delta x}{V_M} \qquad 25)$$

A schematic graph of the conditions in 25) is as follows

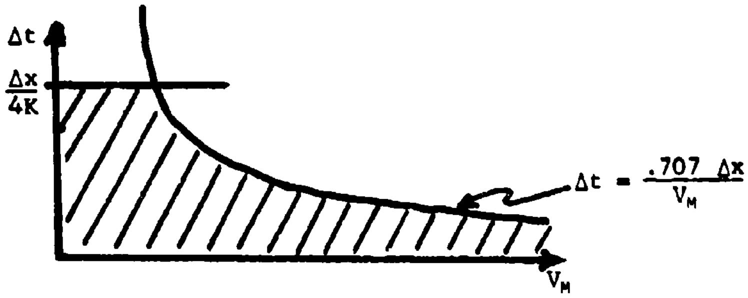

The allowable values of Δt fall in the hatched area. It follows that in the initial stages of a computation, Δt may be relatively large but it must be monitored and reduced as the motion develops and increases in magnitude.

The truncation error for the system given by 20) was determined in the same manner as that given by Williamson (1966), i.e., it is defined as the difference between the finite difference approximation equation and the original differential equation. The truncation error was found to be

$$T = 0(\Delta t) + 0(\Delta x)$$

<u>The finite difference relations for the two-dimensional case.</u> We consider here the finite difference formulations of 7), 8), 10) and 11). Rather than setting up the general relations for some point, it will be more suitable to examine the various terms, since in some instances rather special formulations are involved.

It will be convenient to drop the primes on π' and θ' in what follows and to let j,k stand for x,z, where $j = 1,2,\ldots,je$ and $k = 1,2,\ldots,ke$. The values $j = 1$, je and $k = 1$, ke denote points on the boundary. The size of the model is easily varied by changing the values of je and ke in the computer program. It will be recalled that $\Delta x = \Delta z = 100$ m except that $\Delta z = 10$ m between k=1 and k=2. In the following, we shall use Δx for a 100-m increment and Δz for the 10-m increment.

The time derivatives in 7), 8) and 10) are all evaluated as forward differences in time in accordance with the discussion given above on numerical stability. On the other hand, the exact form of the advection terms depends upon the signs of u and w. If we let α stand for u, w, or θ, the advection terms may be written as in the following table.

Term	$u > 0,\ w > 0$	$u < 0,\ w < 0$
$u\,\dfrac{\partial\alpha}{\partial x}$	$u_{j,k}\,\dfrac{\alpha_{j,k} - \alpha_{j-1,k}}{\Delta x}$	$u_{j,k}\,\dfrac{\alpha_{j+1,k} - \alpha_{j,k}}{\Delta x}$
$w\,\dfrac{\partial\alpha}{\partial z}$	$\begin{cases} w_{j,k}\,\dfrac{\alpha_{j,k} - \alpha_{j,k-1}}{\Delta x};\ k > 2 \\ w_{j,2}\,\dfrac{\alpha_{j,2} - \alpha_{j,1}}{\Delta z} \end{cases}$	$w_{j,k}\,\dfrac{\alpha_{j,k+1} - \alpha_{j,k}}{\Delta x}$

Because of the boundary conditions, all of the advection terms vanish at the corners of the region and along the bottom boundary. At the top only $u u_x$ is computed and at the lateral boundaries $w w_z$ and $w \theta_z$ are computed.

The Laplacian terms in 7), 8) and 10) are evaluated in the usual manner at the interior points as

$$\nabla^2 \alpha \simeq \frac{\alpha_{j+1,k} + \alpha_{j-1,k} + \alpha_{j,k+1} + \alpha_{j,k-1} - 4\alpha_{j,k}}{\Delta x^2} \qquad 26)$$

except at the second level. At this level one obtains by use of the Taylor Series expansion through the second order terms,

$$\left(\nabla^2 \alpha\right)_2 \simeq \frac{\alpha_{j+1,k} + \alpha_{j-1,k} - 2\alpha_{j,k}}{\Delta x^2} + DN4\alpha_{j,k+1}$$

$$+ DN5\alpha_{j,k-1} - DN6\alpha_{j,k} \qquad 27)$$

where $DN4 = \frac{2}{\Delta x(\Delta x+\Delta z)}$, $DN5 = \frac{2}{\Delta z(\Delta x+\Delta z)}$, and $DN6 = \frac{2}{\Delta x \Delta z}$

Expressions then are needed for u_{zz} at the upper boundary and w_{xx} and θ_{xx} at the lateral boundaries. The boundary conditions described in Section B permit these derivatives to be expressed as

$$\frac{\partial^2 \alpha}{\partial n^2} \simeq \frac{2(\alpha_1 - \alpha_0)}{\Delta x^2} \qquad 28)$$

where n is in the normal direction to the boundary, α_1 is the value of α at the point just interior to the boundary, and α_0 is the boundary value.

The first derivative terms in the diffusion quantities of 7), 8) and 10) are treated as centered differences and take the form

$$\frac{\partial \alpha}{\partial z} \simeq \frac{\alpha_{j,k+1} - \alpha_{j,k-1}}{2\Delta x} \qquad 29)$$

except at level two where again a special formulation is required. Using the Taylor Series expansion through the second order terms, one obtains for this level the expression

$$\left(\frac{\partial \alpha}{\partial z}\right)_2 \simeq DN1\alpha_{j,k+1} - DN2\alpha_{j,k-1} + DN3\alpha_{j,k} \qquad 30)$$

where $DN1 = \frac{\Delta z}{\Delta x(\Delta x+\Delta z)}$, $DN2 = \frac{\Delta x}{\Delta z(\Delta x+\Delta z)}$, and $DN3 = \frac{\Delta x - \Delta z}{\Delta x \Delta z}$

The pressure force term in 7) is approximated by

$$\frac{\partial \pi}{\partial x} \simeq \frac{\pi_{j+1,k} - \pi_{j-1,k}}{2\Delta x} \qquad 31)$$

at all interior points and along the upper boundary. The pressure term in 8) also is represented by a centered difference; however, this choice must be considered in conjunction with the way the buoyancy term is formulated and also must be consistent with the way the terms are handled in 11). Thus, we shall take this up in the following discussion of 11).

The pressure computation must be carried out at the boundary points as well as at the interior points of the grid. Therefore, a means must be found to express all of the terms in 11) which involve a first or second derivative that is taken normal to a boundary and which are not already accounted for in the boundary conditions stated in Section 5.

Specifically, at the lateral boundaries we need π_{xx} and u_x. Using the conditions at these boundaries that $\pi = 0$ and $u = 0$, we can express π_{xx} in the same form as that shown in 28) while u_x becomes

$$\frac{\partial u}{\partial x} \simeq \pm \frac{u_1 - u_0}{\Delta x} \qquad 32)$$

where the + sign applies at the left-hand boundary and the - sign applies at the right-hand boundary.

At both the upper and lower boundaries we must have π_{zz}. These expressions are readily obtained in centered difference form by using the upper boundary condition $\pi_z = Cl\theta$, and the lower boundary condition $\pi_z = Cl\theta + \frac{K_M}{C_p\theta}\frac{2w_z}{\Delta z^2}$. Accordingly, we obtain at the upper boundary,

$$\left(\frac{\partial^2\pi}{\partial z^2}\right)_{ke} \simeq \frac{2\left(\pi_{j,ke-1} - \pi_{j,ke}\right) + 2\Delta x Cl\theta_{ke}}{\Delta x^2} \qquad 33)$$

and at the lower boundary,

$$\left(\frac{\partial^2\pi}{\partial z^2}\right)_1 \simeq \frac{2\left(\pi_{j,2} - \pi_{j,1}\right)}{\Delta z^2} - \frac{2}{\Delta z}\left(Cl\theta_{j,1} + \frac{K_M}{C_p\theta}\frac{2w_{j,2}}{\Delta z^2}\right) \qquad 34)$$

Statements for θ_z also are required at the upper and lower boundaries. An attempt to use the thermal equation 10) as a diagnostic relation to obtain θ_z at these boundaries failed because the resulting balance equation could not provide a hydrostatic distribution of pressure at the initial time. Consequently, these derivatives are approximated by inward differences. Then at the upper boundary we have

$$\left(\frac{\partial\theta}{\partial z}\right)_{ke} \simeq \frac{\theta_{ke} - \theta_{ke-1}}{\Delta x} \qquad 35)$$

and at the lower boundary

$$\left(\frac{\partial\theta}{\partial z}\right)_1 \simeq \frac{\theta_2 - \theta_1}{\Delta z} \tag{36)}$$

The expression for θ_z at level k = 2 had to be derived by special means. We consider the region at the initial time when there is no motion, the θ surfaces are horizontal, and the heating at the bottom is set equal to zero. At this time, the pressure is hydrostatic and 15) could be used to compute the distribution. An integration of 15) with respect to z yields

$$\left(\frac{\partial\pi}{\partial z}\right)_{ke} - \left(\frac{\partial\pi}{\partial z}\right)_1 = C1\int_0^H \frac{\partial\theta}{\partial z}\,dz$$

$$= C1\left(\theta_{ke} - \theta_1\right)$$

which, of course, agrees with the boundary conditions. If the integral of θ_z is expanded using the trapezoidal rule, we must have

$$\begin{aligned}\theta_{ke} - \theta_1 = &\left[(\theta_z)_1 + (\theta_z)_2\right]\frac{\Delta z}{2} \\ &+ \left[\tfrac{1}{2}(\theta_z)_2 + (\theta_z)_3 + \cdots + \tfrac{1}{2}(\theta_z)_{ke}\right]\Delta x\end{aligned} \tag{37)}$$

On the right-hand side we use 35) and 36), and

$$\left(\frac{\partial\theta}{\partial z}\right)_k \simeq \frac{\theta_{k+1} - \theta_{k-1}}{2\Delta x}; \quad k \neq 1,2 \text{ or ke}$$

Thus, 37) is an equation for $(\theta_z)_3$. After cancellation of many terms and rearrangement, the result is

$$\left(\frac{\partial\theta}{\partial z}\right)_3 \simeq \frac{\theta_3 - \theta_1}{\Delta x + \Delta z} \qquad 38)$$

The final quantities to be considered in 11) [and also in 8)] are the terms $a(z)\pi_z$ and $C1a(z)\theta$. These terms are related to one another at the upper and lower boundaries, as already noted. Elsewhere, as pointed out in Section B, it was found that at the initial time the only way the balance equation 11) could give the same results as the hydrostatic equation 14) was if π_z and θ' were evaluated for the layer above or below the level of interest. Let the level of interest be denoted by k. Then the hydrostatic equation gives

$$\frac{\pi_{k+1} - \pi_k}{\Delta x} = C1\left(\frac{\theta_{k+1} + \theta_k}{2}\right)$$

and 39)

$$\frac{\pi_k - \pi_{k-1}}{\Delta x} = C1\left(\frac{\theta_k + \theta_{k-1}}{2}\right)$$

Thus, one can satisfy the hydrostatic relation at level k by combining these two equations into the single relationship

$$\frac{\pi_{k+1} - \pi_{k-1}}{2\Delta x} = C1\left(\frac{\theta_{k+1} + 2\theta_k + \theta_{k-1}}{4}\right) \qquad 40)$$

At level two, this becomes

$$\frac{\pi_3 - \pi_1}{\Delta x + \Delta z} = \frac{C1\ \Delta x \Delta z}{2(\Delta x+\Delta z)} \left(\frac{\theta_2 + \theta_1}{\Delta x} + \frac{\theta_3 + \theta_2}{\Delta z}\right) \qquad 41)$$

In this manner, π_z is expressed as a centered difference while θ is represented by a weighted average in 8) and 11). After the initial moment, the heating at the ground disturbs the hydrostatic distribution of pressure which in turn gives rise to accelerations in 7) and 8).

Equation 11) is solved for π by an iterative relaxation technique (Liebman process). The finite-difference form of 11) at interior points ($3 \le k \le ke-1$) is

$$\frac{1}{\Delta x^2}\left(\pi_{j+1,k} + \pi_{j-1,k} + \pi_{j,k+1} + \pi_{j,k-1} - 4\pi_{j,k}\right)$$
$$+ \frac{a(k)}{2\Delta x}\left(\pi_{j,k+1} - \pi_{j,k-1}\right) = F_{j,k} \qquad 42)$$

All of the terms on the right-hand side of 11) are included in $F_{j,k}$ (x,z). At the boundaries, the special formulations of derivatives given above must be used.

At the level k=2, 11) takes the form:

$$\frac{1}{\Delta x^2}\left(\pi_{j+1,2} + \pi_{j-1,2} - 2\pi_{j,2}\right)$$
$$+ \pi_{j,3}\frac{2}{\Delta x(\Delta x+\Delta z)} + \pi_{j,1}\frac{2}{\Delta z(\Delta x+\Delta z)} - \pi_{j,2}\frac{2}{\Delta x \Delta z}$$
$$+ a_{j,2}\frac{\pi_3 - \pi_1}{\Delta x + \Delta z} \qquad 43)$$
$$= F_{j,2}$$

Either 42) or 43) can be solved for $\pi_{j,k}$, so that

$$\pi_{j,k} = H_{j,k}$$

where H contains all other terms in 42) or 43).

The next approximation for π is found as π^*:

$$\pi^*_{j,k} = \pi_{j,k} - m\left(\pi_{j,k} - H\right)$$

Here, m is the underrelaxation factor which gives convergence in the case $0 < m < 1$. The convergence of the described relaxation process was established by several numerical experiments with various values of m. The fastest convergence was found to occur for $m = 0.5$.

Integral Constraints. It is standard procedure in modeling work to form the mechanical energy equation for the system. For a closed system, such as is usually dealt with, this amounts to a statement of the conservation of the sum of the kinetic and available potential energies. The relation may then be used as a check on the accuracy of the numerical integration.

In the present study, the system is open to energy input which is reflected in a somewhat more complicated relation for the energy equation. The derivation follows in the usual manner from the equations of motion. For dry, deep convection, we obtain from 1) - 3) the relation,

$$\begin{aligned} \frac{d}{dt}\left(\frac{u^2+v^2+w^2}{2}\right) = {} & -C_p\,\Theta\mathbf{C}\cdot\nabla\pi' + wg\frac{\theta'}{\Theta} + K_M\left[u\nabla^2 u + v\nabla^2 v + w\nabla^2 w\right] \\ & + K_M\,a(z)\left[u\frac{\partial u}{\partial z} + v\frac{\partial v}{\partial z} + w\frac{\partial w}{\partial z}\right] \end{aligned} \qquad 44)$$

When 44) is multiplied through by ρ_0 and the continuity equation is used, we obtain

$$\frac{\partial}{\partial t}\left(\rho_0 K - \frac{g\rho_0\theta' z}{\Theta}\right) = -\nabla\circ\rho_0 K\mathbb{C} - C_p\,\Theta\nabla\circ\rho_0\pi'\mathbb{C} + \frac{g}{\Theta}\,\nabla\circ\rho_0\theta' z\mathbb{C}$$

$$- \frac{g\rho_0 z}{\Theta}\frac{d\theta'}{dt} + \rho_0 K_M\ a(z)\left[u\nabla^2 u + v\nabla^2 v + w\nabla^2 w\right] \qquad 45)$$

$$+ \rho_0 K_M\ a(z)\,\frac{\partial K}{\partial z}$$

where $K = \frac{u^2+v^2+w^2}{2}$. The fourth term on the right may be reexpressed by using 5). When 45) is integrated over the volume of the model under conditions of a zero ambient wind field and use is made of the boundary conditions, the resulting equation is,

$$\frac{\partial}{\partial t}\int \rho_0\left(K - \frac{g\theta' z}{\Theta}\right)d\upsilon = \frac{gK_H}{\Theta}\int \rho_0\,\frac{\partial\theta'}{\partial z}\,d\upsilon - \frac{gK_H}{\Theta}\int\left(\rho_0 z\,\frac{\partial\theta'}{\partial z}\right)_H dxdy$$

$$-K_M\int\rho_0\left[\left(\frac{\partial u}{\partial x}\right)^2 + \left(\frac{\partial u}{\partial y}\right)^2 + \left(\frac{\partial u}{\partial z}\right)^2 + \left(\frac{\partial v}{\partial x}\right)^2 + \left(\frac{\partial v}{\partial y}\right)^2\right. \qquad 46)$$

$$\left. + \left(\frac{\partial v}{\partial z}\right)^2 + \left(\frac{\partial w}{\partial x}\right)^2 + \left(\frac{\partial w}{\partial y}\right)^2 + \left(\frac{\partial w}{\partial z}\right)^2\right]d\upsilon$$

where H stands for the upper boundary of the system and $d\upsilon = dxdydz$. The left-hand side of 46) expresses the change of kinetic and available potential energy. The dissipation terms on the right-hand side appear because the thermal energy equation 5) does not contain a term accounting for the frictional transformation of kinetic into heat energy.

A somewhat simpler relationship may be derived from the thermal energy equation. In this case, we multiply 5) by ρ_0 and integrate over the volume of the model. From this we obtain after application of the boundary conditions

$$\frac{\partial}{\partial t}\int \rho_0\theta' dv = \int\left(\rho_0 K_H \frac{\partial\theta}{\partial z}\right)_H dxdy - \int\left(\rho_0 K_H \frac{\partial\theta}{\partial z}\right)_0 dxdy \qquad 47)$$

Thus, in this case, the change in sensible heat of the region is seen to depend upon the heat fluxes at top and bottom of the system.

The two-dimensional versions of 46) and 47) follow directly by setting v and $\frac{\partial}{\partial y}$ equal to zero.

D. The Ambient Flow Model

General features This model follows in a straightforward manner from the anelastic system given previously by 1) - 6) if the coriolis force is incorporated for purposes of modeling the large-scale flow.

It is assumed here that the atmosphere consists of a stationary, hydrostatic state as represented by the zero-order equations given by Ogura and Phillips (op.cit.). Superimposed upon this is a large-scale basic or ambient flow which for simplicity may be taken as zonal and steady-state. This flow may be modeled to include a friction layer in which vertical eddy momentum transfer occurs. Geostrophic flow may be assumed above the friction layer, and both horizontal and vertical shear may be permitted. A convective perturbation may then be added which is ageostrophic and of the same order of magnitude as the ambient flow.

An x-z plane representation of the model is given in Fig. II-2. It is assumed that initially $\pi_x' = 0$, $\theta_x' = 0$ and only the ambient flow exists.

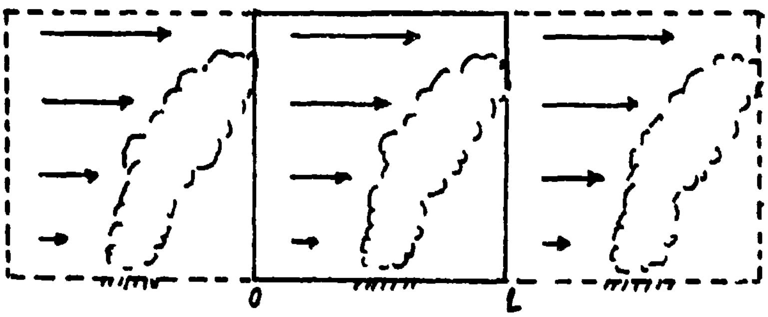

Fig. II-2 Ambient Flow Model (x-y plane)

As in the previous model, differential heating takes place along the ground leading to the development of hot spots. As shown in Fig. II-2, it is assumed that conditions in the model section (solid boundaries) are repeated in the sections upstream and downstream relative to the basic flow.

System of equations. In the following discussion we let the subscript 1 refer to ambient flow and the subscript 2 refer to the convective fields. The dependent variables of the system may then be represented by:

$$
\begin{aligned}
u &= u_1\ (y,z) + u_2\ (x,y,z,t) \\
v &= v_2\ (x,y,z,t) \\
w &= w_2\ (x,y,z,t) \qquad\qquad 48) \\
\pi' &= \pi_1\ (y,z) + \pi_2\ (x,y,z,t) \\
\theta' &= \theta_1\ (y) + \theta_2\ (x,y,z,t)
\end{aligned}
$$

It may be noted that the lapse rate for the ambient flow is adiabatic but there is a north-south temperature gradient. For a two-dimensional version of this model, θ_1, may be set equal to zero which means that the

ambient flow isentrope is given by Θ, and $\pi_1 = \pi_0$. From 1) - 5), the ambient flow equations are given by:

$$0 = -\frac{\partial \pi_1}{\partial x}$$

$$0 = -C_p \Theta \frac{\partial \pi_1}{\partial y} - f u_1 + K_M \left[\frac{\partial^2 u_1}{\partial z^2} + a(z) \frac{\partial u_1}{\partial z}\right]$$

$$0 = -C_p \Theta \frac{\partial \pi_1}{\partial z} + g \frac{\theta_1}{\Theta} \qquad 49)$$

$$\frac{\partial \theta_1}{\partial t} = 0$$

$$\frac{\partial u_1}{\partial x} = 0$$

When the statements in 48) are substituted into 1) - 6) and cancellations are made in accordance with 49), we obtain for the three-dimensional model:

$$\frac{du_2}{dt} + u_1 \frac{\partial u_2}{\partial x} + v_2 \frac{\partial u_1}{\partial y} + w_2 \frac{\partial u_1}{\partial z} = -C_p \Theta \frac{\partial \pi_2}{\partial x} + K_M\left[\nabla^2 u_2 + a(z) \frac{\partial u_2}{\partial z}\right]$$

$$\frac{dv_2}{dt} + u_1 \frac{\partial v_2}{\partial x} = -C_p \Theta \frac{\partial \pi_2}{\partial y} + K_M\left[\nabla^2 v_2 + a(z) \frac{\partial v_2}{\partial z}\right]$$

$$\frac{dw_2}{dt} + u_1 \frac{\partial w_2}{\partial x} = -C_p \Theta \frac{\partial \pi_2}{\partial z} + g \frac{\theta_2}{\Theta} + K_M\left[\nabla^2 w_2 + a(z) \frac{\partial w_2}{\partial z}\right] \qquad 50)$$

$$\frac{d\theta_2}{dt} + u_1 \frac{\partial \theta_2}{\partial x} + v_2 \frac{\partial \theta_1}{\partial y} = K_H\left[\nabla^2 \theta_2 + a(z) \frac{\partial \theta_2}{\partial z}\right]$$

$$\nabla \cdot \rho_0 w_2 + \frac{\partial \rho_0 w_2}{\partial z} = 0$$

$$\nabla^2 \pi_2 + a(\pi_2)_z = C1[(\theta_2)_z + a\theta_2] + \frac{1}{\pi_0^2}\left[\frac{-C7}{4}\frac{w_2}{\pi_0} + \frac{C8}{2}(w_2)_z - C9w_2^2\right]$$

$$+ C11[(w_2)_x\ (u_2-u_1)_z - (u_2)_x\ (w_2)_z + (v_2)_x\ (u_2-u_1)_y$$

$$- (u_2)_x\ (v_2)_y + (v_2)_z\ (w_2)_y - (v_2)_y\ (w_2)_z] \qquad 50)$$

These equations with appropriate assumptions may form the basis for several different dry models.

1) A zonal basic flow with vertical shear (two-dimensional)
2) A zonal basic flow with vertical shear (three-dimensional)
3) A zonal basic flow with horizontal and vertical shear (three-dimensional)

It is possible, also, with some alterations to include the influence of horizontal convergence in the ambient flow. The possibility of moist convection will be considered at a later point.

Boundary conditions. The boundary conditions for this model are in most respects the same as those for the model with zero ambient flow. The primary difference occurs in the conditions in the x direction. As indicated in Fig. II-2, all dependent variables are repeated periodically in the x direction. Thus, $Q(x) = Q(x+L)$, where Q is any one of the variables. In addition, the following conditions are assumed.

Upper boundary: $w_2 = 0,\ (u_2)_z = 0,\ (u_1)_z = 0,\ (v_2)_z = 0$

θ_2 = cons't. w/r to x, y, and t.

$$(\pi_2)_z = C1\theta_2 + \frac{K_u}{C_p \Theta}\left[(w_2)_{zz} + (H)(w_2)_z\right]$$

Lower boundary: $w_2 = 0,\ u_2 = 0,\ u_1 = 0,\ v_2 = 0$

$\theta_2\ (x,y,t) =$ specified function

$$(\pi_2)_z = C1\theta_2 + \frac{K_M}{C_p\,\Theta_-}\left[(w_2)_{zz} + a(0)(w_2)_z\right]$$

North-South boundaries: $(w_2)_y = 0,\ (u_2)_y = 0,\ v_2 = 0,$

$(u_1)_z =$ specified function

$(\theta_2)_y = 0$

$(\pi_2)_y = 0$

When these boundary conditions are applied to 50), the following additional relations are found:

Upper boundary: $(u_2)_x + (v_2)_y + (w_2)_z = 0$

$w_{zz} = -a(H)w_z$

Lower boundary: $(w_2)_z = 0$

North South boundaries: $(v_2)_{yy} = 0$

E. Moist Convection

General Considerations. This model, especially with the inclusion of an ambient wind field, is the ultimate goal in our work although it has received the least attention in this early phase of the project.

Dr. P. Das has concentrated most of his effort on the development of relations which will incorporate the microphysics of the phase changes in a convective cloud. A summary of this work will be given at a later point in this section. However, for the time being we again turn to the anelastic system devised by Ogura and Phillips (op.cit.), which is suitable for modeling the macroscale aspects of cumulus development, assuming a reversible, saturation adiabatic process.

The applications of this system (Ogura, 1963; Orville, 1965 and 1968) have always been to shallow convection, apparently to avoid the complication which arises in the computation of the saturation mixing ratio due to its dependence upon pressure. As shown by Ogura (1963), an approximation to the saturation vapor pressure is given by

$$e_s(T) = e_s(T_0)\left[1 + \frac{L}{R_v T_0} T' + \frac{1}{2}\left(\frac{L}{R_v T_0^2}\right)^2 T'^2\right]$$

where L is the latent heat, R_v is the specific gas constant for vapor, and T_0 is the reference atmosphere temperature. For shallow convection, T' is the deviation of temperature from the reference value; however, for deep convection T' is related to the potential temperature and pressure deviations through the relationship,

$$\frac{T'}{T_0} = \frac{\theta'}{\Theta} + \frac{\pi'}{\pi_0}$$

More will be said about this shortly.

<u>System of equations</u>. In this system the predictive equation for potential temperature deviation is replaced by one for the specific entropy of the moist air. Also, a term is added to the third equation of motion which accounts for the negative buoyancy of the liquid portion of the water substance. The complete system is:

$$\frac{du}{dt} = -C_p \Theta \pi_x' + K_M\left[\nabla^2 u + a(z) u_z\right] \qquad 51)$$

$$\frac{dv}{dt} = -C_p \Theta \pi_Y' + K_M[\nabla^2 v + a(z)v_z] \quad 52)$$

$$\frac{dw}{dt} = -C_p \Theta \pi_z' + \frac{g\theta'}{\Theta} - g\, q_L + K_M[\nabla^2 w + a(z)w_z] \quad 53)$$

$$\nabla \circ p_0 \text{¢} = 0 \quad 54)$$

$$\frac{dq}{dt} = K_Q[\nabla^2 q + a(z)q_z] \text{ where } q = q_v + q_L \quad 55)$$

$$\frac{d\varphi}{dt} = K\varphi[\nabla^2\varphi + a(z)\varphi_z] \quad 56)$$

$$\varphi = \frac{\theta'_{UNS}}{\Theta} + \frac{L}{C_p T_0} q_v \quad \text{or} \quad \varphi = \frac{\theta'_s}{\Theta} + \frac{L}{C_p T_0} q_{vs} \quad 57)$$

$$q_{vs} = \frac{.622\ e_s(T_0)}{p}\left[1 + \frac{L}{R_v T_0}\left(\frac{\theta'_s}{\Theta} + \frac{\pi'}{\pi_0}\right) + \frac{1}{2}\left(\frac{L}{R_v T_0}\right)^2 \left(\frac{\theta'_s}{\Theta} + \frac{\pi'}{\pi_0}\right)^2\right] \quad 58)$$

where q_v and q_L are the mixing ratios for vapor and liquid, φ is the specific entropy of the moist air (the entropy of the liquid is neglibly small), and θ'_{UNS} and θ'_s are the potential temperature deviations for unsaturated and saturated air, respectively. Equation 58) expresses the saturation mixing ratio where $p = P\pi^{1/k} \approx P(\pi_0 + \pi')^{1/k}$. The divergence or balance equation for the system is given by,

$$\nabla^2\pi' + a(z)\pi_z' = C1[\theta_z' + a(z)\theta'] - C3[(q_L)_z + a(z)q_L]$$
$$+ \frac{1}{\pi_0^2}\left[\frac{-C7}{4}\frac{w}{\pi_0} + \frac{C8}{2}w_z - C9w^2\right] \quad 59)$$
$$+ C11[w_x u_z - u_x w_z + v_x u_y - u_x v_y + v_z w_y - w_z v_y]$$

In order to determine whether or not condensations has occured at any given grid point, one solves 55) and 56) for a q and φ at the point. These values are then used in the first expression of 57) to compute θ'_{UNS}. The value of φ again is used in the second expression of 57) which is solved simultaneously with 58) to get θ'_s and q_{vs}. If $\theta'_s < \theta'_{UNS}$, then $q_L = 0$ and $\theta' = \theta'_{UNS}$. However, if $\theta'_s > \theta'_{UNS}$, then $\theta' = \theta'_s$ and $q_L = q - q_{vs}$. The special problem that arises in this procedure is because of the dependency of 58) on π', which must be known. However, π' is computed from 59) which depends upon θ' and q_L. Thus, a dilemma is created as to how to start the computation.

Tentatively, at least, we propose to use an iterative scheme for the solution, as outlined below. The first step is to assume for the moment that the air is saturated. Then from the second expression in 57)

$$\theta' = \theta'_s = \Theta\varphi - \frac{L\Theta}{C_p T_0} q_{vs}$$

Also, 60)

$$q_L = q - q_{vs}$$

If the expressions in 60) are substituted into 59), the latter becomes,

$$\begin{aligned} \nabla^2 \pi' + a(z)\pi' = C3\Big\{&\left(\varphi_z + a\varphi\right) - \left(q_z + aq\right) - \left(\frac{L}{C_p T_0} - 1\right) \\ &\left[\left(q_{vs}\right) + aq_{vs}\right] + \frac{L}{C_p T_0^2} (T_0)_z \; q_{vs}\Big\} \\ &+ \frac{1}{\pi_0^2}\left[\frac{-C7}{4}\frac{w}{\pi_0} + \frac{C8}{2} w_z - C9w^2\right] \end{aligned} \qquad 61)$$

$$+ C11[(w_x u_z - u_x w_z) + (v_x u_y - u_x v_y) + (v_z w_y - w_z v_y)] \quad 61)$$

Equation 61) then expresses the pressure field for saturated air; however, it holds equally well for unsaturated air if q_{vs} is replaced by q.

Now, at the end of a given time step we have the fields of q and φ but we do not yet have θ', π' and q_L. Assume the old value of π' as a first estimate in 58) and solve 58) simultaneously with the second expression in 57) to obtain a first estimate of the θ_s' and q_{vs} fields. Substitute the values of φ, q and q_{vs} into 61) to get a new estimate of the π' field. Use the new estimates of π' in 58) and solve as before for second estimates of θ_s' and q_{vs}. This procedure may be repeated until the desired degree of accuracy is obtained for π', θ_s' and q_{vs}, assuming that convergence occurs.

Now compute θ_{UNS}' from the first expression in 57) using φ and q, and compare θ_{UNS}' with θ_s'. If $\theta_s' > \theta_{UNS}'$, then saturation has occurred and the last values of π, θ_s' and q_{vs} are the desired values. q_L can be obtained explicitly from $q_L = q - q_{vs}$. If $\theta_s' < \theta_{UNS}'$, then saturation has not occurred and θ_s' is the desired value of θ'. π' is then computed from 61) by setting $q_{vs} = q$.

It is evident that this model will require considerable storage capacity in the computer and the procedure will involve large amounts of computer time per forecast period. This would be true, particularly, if the model were modified to include a shearing ambient wind field with

precipitation and in three dimensions. Therefore, it well may be that we shall have to restrict our experiments to relatively simple cases when we get to this model.

The microphysics of moist convection. At this point, we give a brief review of Das's work which is concerned with certain aspects of phase change and liquid water storage in a convective cloud.

A theoretical and numerical study of moist convection is complicated by the various physical factors related to the nature of phase transition of water substances. In the classical approach to the moist-adiabatic process one assumes that all the water vapor above the saturation value condenses and that in the presence of liquid-water particulates the cloud air is always just saturated. Even this simple assumption entails serious difficulties in numerical modeling although unfortunately, it can afford only a very simple picture of moist convection.

In order to examine what is involved in a more r[illegible]c modeling of moist convection, a reexamination of the thermodynamic equation was taken up for an alternative form which would take care of the microphysical implications of the process of condensation and evaporation in convective drafts. The alternative picture arrived at replaces the moist-adiabatic equation by a set of three equations, viz., 1) a moisture equation,

$$\frac{d\xi_v}{dt} = - \int_0^\infty N_r \left(\frac{D}{Dt}\right)_r m_r \, dr$$

2) the thermodynamic equation,

$$\frac{d\phi_d}{dt} + \frac{L}{T}\frac{d\xi_v}{dt} = 0$$

and 3) an equation of continuity for N_r,

$$\frac{dN_r}{dt} = -\frac{1}{\rho_d}\nabla\cdot(n_r\vec{V}_r) - \frac{\partial}{\partial_r}\left(N_r\frac{dr}{dt}\right)$$

which includes the effect of condensation-evaporatior but not coagulation.

The symbols have the following meanings:

$\frac{d}{dt} = \frac{\partial}{\partial t} + \vec{V}\cdot\nabla$ where $\vec{V}$ is the velocity of air motions,

$\left(\frac{D}{Dt}\right)_r = \frac{d}{dt} + \vec{V}_r\cdot\nabla$,

$\vec{V}_r$ = velocity of the particulate products of condensation relative to air motions,

ξ_v = humidity mixing ratio,

N_r = number of particles taking part in the processes of condensation and evaporation per unit mass of dry air,

m_r = effective water mass of the particles of condensation of radius r,

φ_d = entropy per unit mass of dry air,

L = latent heat of condensation,

T = temperature of cloud air,

ρ_d = density of dry air

$n_r = \rho_d N_r$ = number of particles of condensation per unit volume of cloud.

The equation for N_r, which does not include the effect of coagulation, can be made to do so by including an additional set of terms. Fortunately, over the last few years this aspect of cloud processes has received able consideration from Golovin (1963), Twomey (1964,1966), Berry (1965), Bartlett (1966) and Warshaw (1967) and the cloud dynamicist will find the treatment ready for inclusion in a model when he has one tractable enough within the existing computation abilities.

The immediate achievement of the new thermodynamic equation is incorporating in one equation the effects discussed by McDonald (1962), Kamburova and Ludlam (1966), and Das and Subba Rao (1968)*. McDonald considers the anomalous thermodynamic consequences of supersaturation in an updraft containing a population of condensation nuclei. There are circumstances available when the adiabatic ascent of a parcel can also be isothermal. On the other hand Kamburova and Ludlam, and Das and Subba Rao have shown that a thunderstorm downdraft containing all its water in the form of drops will be unsaturated and its temperature lapse rate closer to the dry adiabatic when the water-content is divided into larger drops. In other words, the thermodynamic system envisaged by the new thermodynamic adiabatic process dispenses with the saturation assumption of the classical moist adiabatic process.

A paper incorporating the results of the above studies was communicated to the Journal of the Atmospheric Sciences. It has been revised in view of the referees' comments and resubmitted for publication.

*Unpublished work

Introducing the microphysics of cloud formation into the problem will involve obvious complications but in its simplest aspects might provide an important consequence. Since sub- or super-saturation will be a matter of rule, the calculations will be less sensitive to the exact point where saturation occurs.

A simple way to start introducing the effects of the microphysics is by assuming nuclei of a single size with an assumed but realistic concentration. This will not be much more difficult than working with the pseudo-adiabatic form of the thermodynamic equation. However, the introduction of a population of nuclei, and then, of coagulation effects will involve considerably more sophistication and computer time.

The details of the application of these concepts to the moist convection problem are not as yet worked out.

F. Summary

The foregoing summarizes the various models which are to be studied and the lines along which our work will proceed in the next two years. The programs for the dry convection model which have been run on the computer to date have been for testing purposes; therefore, there are no computational results to present at this time.

Two graduate students presently are doing their thesis research in connection with this project. Captain R. L. Croft (USAF) is working with the ambient wind field model with vertical shear. Captain J. L. Conley (USAF) has initiated a theoretical study along the lines of the

work done by Kuo (op.cit.), Saltzman (1962), and others. The latter, if successfully concluded for the boundary conditions with which we are working, should compliment the numerical computations and greatly enhance our understanding of the results.

GLOSSARY

A	a constant east-west component of wind	(cm/sec)
$a(z)$	percentage rate of change of reference-atmosphere density with height	(1/cm)
$\mathbb{C}$	three-dimensional velocity vector	(cm/sec)
C_p	specific heat of air at constant pressure	(ergs/gm deg)
e_s	saturation vapor pressure	(dynes/cm^2)
$\mathbb{F}$	three-dimensional friction vector	(dynes/gm)
g	acceleration of gravity	(cm/sec^2)
H	height of top boundary of system	(cm)
$\hat{i}, \hat{j}, \hat{k}$	unit vectors in the x,y,z directions, respectively	(dimensionless)
i	$\sqrt{-1}$	(dimensionless)
j	grid point number along time coordinate or x coordinate, as indicated in text	(dimensionless)
k	grid point number along z coordinate or a wave number in x direction, as indicated in text	(dimensionless) or (1/cm)
K_M, K_H, K_Q, K_Φ	exchange coefficient for momentum, heat, water substance, and entropy, respectively	(cm^2/sec)
K	a general exchange coefficient	(cm^2/sec)
ℓ	grid point number along z coordinate	(dimensionless)
L	latent heat of vapor[illegible]tion for water	(ergs/gm)
m	wave number in the z direction	(1/cm)
m_r	effective water mass of particles of condensation of radius, r	(gm)

n	grid point number along x coordinate	(dimensionless)
n_r	number of condensation particles per unit volume of cloud	$(1/cm^3)$
N_r	number of particles involved in evaporation and condensation per unit mass of dry air	(1/gm)
p	pressure of air	$(dynes/cm^2)$
P	a reference pressure for air	$(dynes/cm^2)$
q_v	mixing ratio for water vapor	(dimensionless)
q_L	mixing ratio for liquid water	(dimensionless)
q	mixing ratio for water substance	(dimensionless)
q_{vs}	mixing ratio for water vapor at saturation	(dimensionless)
R	specific gas constant for dry air	(ergs/gm deg)
R_v	specific gas constant for water vapor	(ergs/gm deg)
r_1	the ratio $U\Delta t/\Delta x$	(dimensionless)
r_2	the ratio $W\Delta t/\Delta x$	(dimensionless)
t	time	(sec)
T	absolute temperature	(deg)
T_0	reference-atmosphere absolute temperature	(deg)
T'	deviation of temperature from the reference value	(deg)
u	component of velocity in the x direction	(cm/sec)
U	a constant component of velocity in the x direction	(cm/sec)
v	component of velocity in the y direction	(cm/sec)
V_M	the maximum velocity in the x,z plane	(cm/sec)

w	component of velocity in the z direction	(cm/sec)
W	a constant component of velocity in the z direction	(cm/sec)
x	west-east coordinate, positive eastward	(cm)
y	north-south coordinate, positive northward	(cm)
z	vertical coordinate, positive upward	(cm)
α	a dummy variable for u, w, or θ	(cm/sec) or (deg)
Δx	grid increment of 100 m	(m)
Δz	grid increment of 10 m	(m)
Δt	time increment	(sec)
θ	potential temperature	(deg)
Θ	reference -atmosphere potential temperature	(deg)
θ'	potential temperature deviation	(deg)
θ_s'	potential temperature deviation at saturation	(deg)
θ_{UNS}'	potential temperature deviation for unsaturated conditions	(deg)
κ	ratio of R/C_p	(dimensionless)
υ	volume	(cm^3)
ξ_v	mixing ratio for water vapor	(dimensionless)
π	a pressure variable, $(p/P)^\kappa$	(dimensionless)
π_0	reference-atmosphere pressure variable	(dimensionless)
π'	pressure deviation	(dimensionless)
ρ_0	reference-atmosphere density	(gm/cm^3)

ρ_d	density of dry air	(gm/cm^3)
φ	specific entropy of moist air	(dimensionless)
ϕ_d	specific entropy of dry air	(cals/gm deg)

REFERENCES

Arnason, G., Greenfield, R.S., and E.A. Newburg, 1968: A numerical experiment in dry and moist convection including the rain stage. J. Atmos. Sci., 25, 404-415.

Bartlett, J.T., 1966: The growth of cloud droplets by coalescence. Quart. J. Roy. Meteor. Soc., 92, 93-104.

Berry, E.X., 1965: Cloud droplet growth by collection: a theoretical formulation and numerical calculation. Ph.D. dissertation, University of Chicago, Chicago.

Clayton, W.H., 1963: An automatic micrometeorological data--collection station. Final Rpt. Contract AF19 (604)-6200. Texas A&M University, 127pp.

Gerhardt, J.R., W.S. Mitcham and A.W. Straiton, 1962: A 1400-ft meteorological tower with automatic data readout. Proc. IRE, 50, 2263-2271.

Glovin, A.M., 1963: The solution of the coagulation equation for cloud droplets in a rising air current. Izv. Ak. Nk. SSSR. (Geophys. Ser.), 5, 783-791.

Kamburova, P.L., and F.H. Ludlam, 1966: Rainfall evaporation in thunderstorm downdrafts. Quart. J. Roy. Meteor. Soc., 92, 510-518.

Kuo, H.L., 1962: On the controlling influences of eddy diffusion on thermal convection. J. Atmos. Sci., 19, 236-243.

Lax, P.D., and B. Wendroff, 1960: Systems of conservation laws. Comm. Pure Appl. Math., 13, 217-237.

McDonald, J.E., 1962: A note on anomalous adiabatic cooling rates in clouds. J. Atmos. Sci., 19, 309-312.

Molenkamp, C.R., 1968: Accuracy of finite-difference methods applied to the advection equation. J. Appl. Met., 7, 160-167.

Ogura, Y. and N.A. Phillips, 1962: Scale analysis of deep and shallow convection in the atmosphere. J. Atmos. Sci., 19, 173-179.

Ogura, Y., 1962: Convection of isolated masses of buoyant fluid: A numerical calculation. J. Atmos. Sci., 19, 492-502.

________, 1963: The evolution of a moist convective element in a shallow, conditionally unstable atmosphere: a numerical calculation. J. Atmos. Sci., 20, 407-424.

Orville, H.D., 1964: On mountain upslope winds. J. Atmos. Sci., 21, 622-633.

________, 1965: A numerical study of the initiation of cumulus clouds over mountainous terrain. J. Atmos. Sci., 22, 684-699.

________, 1968: Ambient wind effects on the initiation and development of cumulus clouds over mountains. J. Atmos. Sci., 25, 385-403.

Saltzman, B., 1962: Finite amplitude free convection as an initial value problem---I. J. Atmos. Sci., 19, 329-341.

Twomey, S., 1964: Statistical effects in the evolution of a distribution of cloud droplets by coalescence. J. Atmos. Sci., 21, 553-557.

________, 1966: Computations of rain formation by coalescence. J. Atmos. Sci., 23, 405-411.

Warshaw, M., 1967: Cloud-droplets coalescence: statistical foundations and a one-dimensional sedimentation model. J. Atmos. Sci., 24, 278-286.

Williamson, D., 1966: Stability of difference approximations to certain partial differential equations of fluid dynamics. J. Comp. Phy., 1, 51-67.

III. ANALYSIS AND PREDICTION OF ATMOSPHERIC STRUCTURE THROUGH USE OF DUAL FREQUENCY RADAR

V. E. Moyer

A. Introduction

The objectives of this phase of the Themis program (Sub-task b) are:

1) Observe, record, and analyze precipitation echo strength and patterns using two carefully calibrated radars which, while operating at different wave lengths, are matched with respect to pulse-repetition rate, pulse length, receiver band-pass characteristics, antenna-beam pattern, and antenna height;

2) Observe precipitation intensity and amounts using calibrated raingages over a watershed;

3) Observe accompanying meteorological and electromagnetic propagation conditions at and near the radar antennas and the watershed area;

4) Investigate cell motion versus line motion;

5) Develop prediction techniques for cell and line motion; and

6) Construct conceptual and quantitative models of precipitation phenomena and develop and test realistic and effective prediction techniques for precipitation parameters including rainfall intensity, liquid-water content, drop-size distribution, surface visibility, and precipitation amount.

B. Procedures

Through the first year, the work has proceeded with the above goals in view. From the initiation of the project, a 24-hour radar watch was set up to record all precipitation echoes that appeared inside the 125-mile and outside the 25-mile range markers. The observing technique that was used was that of sequential

gain-reduction of the receivers. At the same time, efforts to optimize the equipment went forward.

By the end of August 1968, the following characteristics of the equipment had been achi..ed.

Table III-1. Characteristics of Texas A&M Dual-frequency Radar System

	AN/CPS-9	WSR/TAM-1
Peak power, P_T	$2X10^5$ w	$2X10^5$ w
Pulse repetition frequency, PRF	186 sec^{-1}	186 sec^{-1}
Wavelength, λ	3.2 cm	10.3 cm
Pulse length, τ	5.0 μsec	5.0 μsec
Pulse length, h	$1.5X10^5$ cm	$1.5X10^5$ cm
Antenna shape	Paraboloidal	Paraboloidal
Antenna diameter	$1.52X10^2$ cm	$4.57X10^2$ cm
Conical beam width, $\theta(=\phi)$	1.60 deg	1.60 deg
Antenna gain, G	$1.4X10^4$	$8.0X10^3$
Minimum detectable signal	$1.6X10^{-14}$ w	$1.3X10^{-14}$ w

The receiver band-pass characteristics of the two main components have been matched by tuning the WSR/TAM-1 receiver (originally from an AN/CPS-6 radar) from 1.2 Mhz to 1.0 Mhz and the AN/CPS-9 receiver from 0.5 Mhz to 1.0 Mhz, both on long pulse. The receivers are calibrated using two signal generators: TS-147D/UP for the 3.2-cm set, and TS-155C/UP for the 10.3-cm set. Calibration is accomplished no less frequently than once a week, more frequently as operating conditions permit.

An unsuccessful effort was made to acquire from the National Science Foundation funds to procure a mono-pedestal capable of supporting a single array of three antennas with the centers of the dishes at the same height above the ground. It now appears that such acquisition must await completion of the new 11-story Oceanography and Meteorology Building that has been approved by the Board of Directors of the Texas A&M System. The pedestal has been included as special equipment for this building, which it is hoped will be ready for occupancy no later than September 1971.

Meteorological conditions near the antenna site are being recorded by means of standard instruments mounted on the AN/CPS-9 tower (wind speed and direction) and on the observing platform near the base of the WSR/TAM-1 tower (short-wave radiation, IR radiation, temperature, dew point, rainfall). Hourly airways observations are filed from the Federal Aviation Agency station at Easterwood Field, 2 miles southwest of the radar site. Conditions representative of the East Yegua Creek Watershed will be determined during the coming year by means of two automatic micrometeorological stations recently installed (see Fig. III-1). A description of these stations is given in Section IV of this report.

The first year of the work has been devoted largely to the collection of data. By chance, the eastern portion of Texas has been subjected to unusually heavy amounts of precipitation during

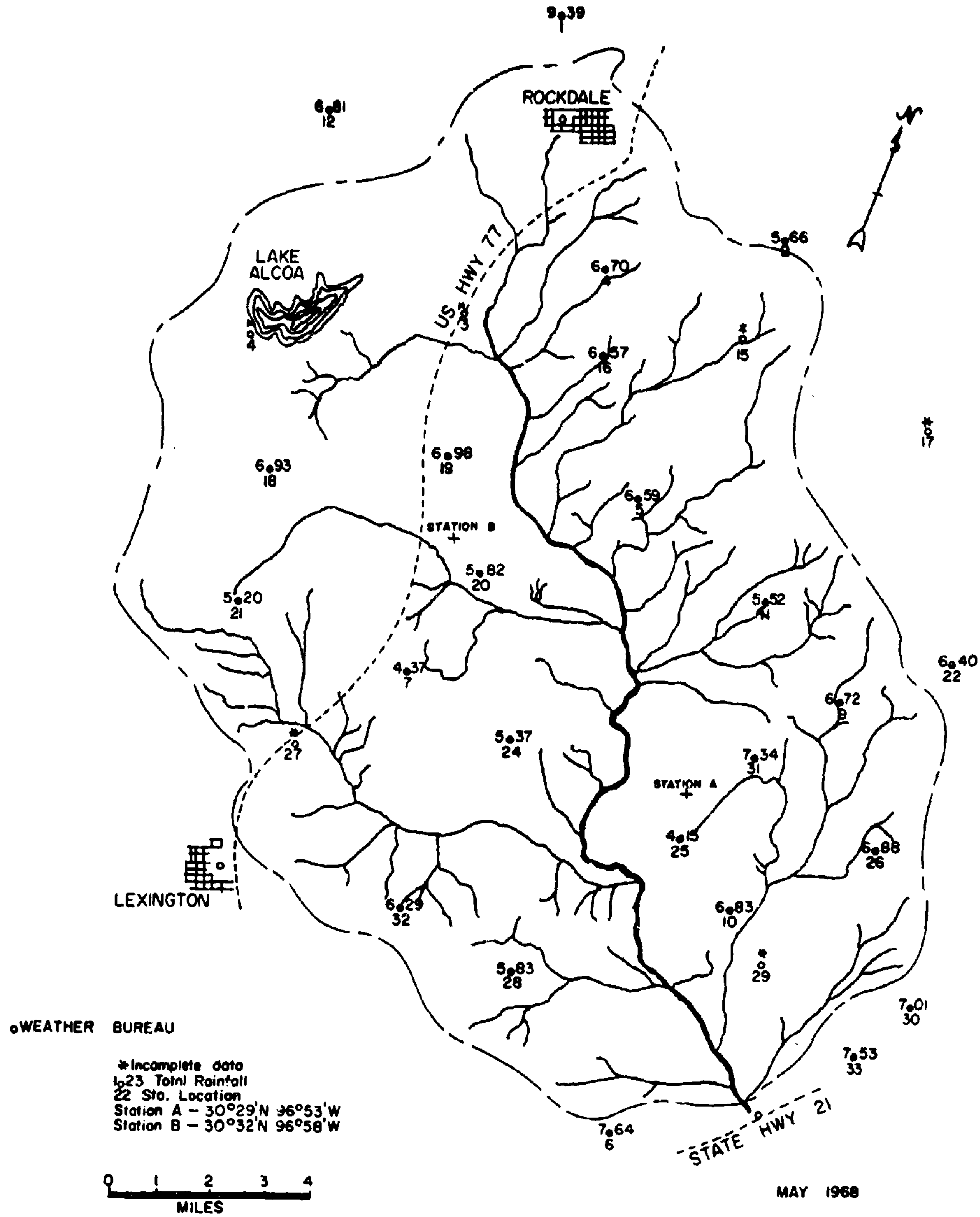

FIG. III-1 EAST YEGUA BASIN NEAR DIME BOX, TEX.

this period[*], and consequently project personnel have been kept busy just operating the radars. Some data extraction has been accomplished, although analysis of the data will have to await compilation of meaningful statistical samples.

The Principal Investigator of Sub-task b has devoted a primary portion of his research time to an investigation of an observation of unusual "angel" echoes that was recorded on both radars on May 23, 1968. (Examples of the PPI and RHI photographs were presented in Quarterly Progress Report #3.) These observations were made during a period when an instrumented aircraft from the National Center for Atmospheric Research was flying cloud penetrations for the Department of Meteorology. The aircraft was sent aloft into the area of radar returns; a straight climb-out from the ground was conducted to 10,000 feet, with a deck of stratocumulus being encountered between 2,800 and 5,500 feet. No clouds were visible above this layer. A spiral ascent then was made from 10,000 to 20,000 feet in the area of radar echo. Numerous fragments of inversion layers (as indicated by stratified concentrations of haze) were visible above and around the aircraft on all sides. When the aircraft reported an altimeter-indicated altitude of 18,000 feet, the radar-indicated elevation was 12,000 feet and a strongly enhanced return was received from the 10-cm transponder on the aircraft.

---

[*]For example, the climatological rainfall average for College Station is 38.7 inches per annum; by July 9, 1968, more than 42 inches had been recorded in 1968 -- with almost 6 months of the year to go! This is the first time that the annual average had been exceeded before the end of July.

This enhancement of signal (as indicated on the A-scope) persisted throughout the flight.

The aircraft was outfitted to record observations of static pressure, temperature, dew point, liquid-water content, true air speed, and heading, among other parameters. Because of the unique appearance of the echoes (no such returns previously had been observed from this site), the Principal Investigator will continue to devote his attention to the analysis of the attendant propagation conditions. It is anticipated that the assistance of a graduate student will be enlisted.

Drs. Runnels, Moyer, and Clark collaborated in a paper* that was presented at the 13th Radar Meteorology Conference, Montreal, Quebec, August 20-23, 1968. Appropriate acknowledgment of Project Themis support was given.

C. Summary

The following table shows some operational statistics of Subtask b during the first year.

Table III-2. Operational Statistics 1967-68

Number of Storm Days Observed	136
Number of Aircraft Research Flights Tracked	21
Hours Spent in Collecting Radar Data	1,252

*Runnels, R. C., Moyer, V. E., and Clark, R. A., "Uncertainties in the Measurement of Liquid-Water Content Using the Gain-Step Technique," pp. 388-391, Proceedings, 13th Weather Radar Conference, Montreal, August 20-23, 1968.

Table III-2—Continued

Hours Spent in Tracking Research Aircraft	28
Man-Hours Spent in Support of Aircraft Flights	364
Man-Hours Spent in Calibrating Radars	165
Man Hours Spent in Maintaining Radars	1,078
Man-Hours Spent in Maintaining Rain-Gage Network	218
Man-Hours Spent in Extracting Radar Data	241
Man-Hours Spent in Analyzing Radar Data	554
Feet of Radar Film Exposed	28,850
Feet of Radar Film Developed	25,250
Feet of Radar Film Edited	25,900
Feet of Radar Film from Which Data have been Extracted	615
Feet of Radar Film Catalogued	49,800

The activities for the second year will necessarily follow a similar pattern with increasing analyses as the data bank approaches significant levels.

IV. MODIFICATION AND INSTALLATION OF AUTOMATIC METEOROLOGICAL STATIONS

William H. Clayton

A. Station Modifications

These stations, designated Station A and Station B, were previously employed in Project Green Glow and the Dallas Tower Network program to provide measurement of: wind speed, wet bulb temperature, and dry bulb temperature at 1/4, 1/2, 1, 2, 4, 8, 16, and 32 m; wind direction at 6 m; soil temperature at 3, 6, 12, 25, 40, 65, and 100 cm; insolation; albedo; net radiation; and soil heat flux. Recording of these data is according to the format shown in Table IV-1. The term "automatic", as applied to these stations, designates a capability for remote operation, plus the fact that all sensor outputs, through suitable function generation and amplification, are recorded in conventional meteorological parameter form. More correctly, the sensor outputs are converted to DC voltages with scale factors of 1, 10, or 100. The output, in addition to the hard copy format indicated in Table IV-1, is also stored on punched paper tape.

Inasmuch as the design, construction, and operation of these stations has been fully reviewed in another report (Clayton and Eckelkamp, 1963), discussion here will be limited to the modifications incorporated in the stations for Project Themis use plus station location details.

The purpose of these stations in the current research program is twofold. The first of these, associated with Sub-task b, is to

```
09131121   2934 2409 2858 2350 2784 2289 2820 2217 2726 2173 2478 2158 2732 2130 2731 2126 4000 4000 2287 0389 1944-0049
09131122   2993 2510 2868 2412 2831 2289 2762 2249 2738 2206 2726 2160 2717 2137 2717 2136 4000 4000 2288 0389 1947-0400
09131123   2869 2372 2836 2275 2866 2201 2834 2194 2864 2249 2830 2211 2862 2174 2860 2174 4000 4000 2288 0379 1935 1399
09131124   2983 2499 2852 2409 2773 2266 2789 2207 2854 2269 2807 2276 2812 2200 2807 2190 4000 4000 2296 0389 1936 3173
09131125   4373 4430 4428 4482 4447 4481 4453 0029
09131125   0142      0190      0202      0236      0251      0287      0330      0345
```

First Minute - Line 1
Date/time, 1/4-m dry bulb, 1/4-m wet bulb, 1/2-m dry bulb, 1/2-m wet bulb, 1-m dry bulb, 1-m wet bulb, 2-m dry bulb, 2-m wet bulb, 4-m dry bulb, 4-m wet bulb, 8-m dry bulb, 8-m wet bulb, 16-m dry bulb, 16-m wet bulb, 32-m dry bulb, 32-m wet bulb, dry-bulb reference, wet-bulb reference, insolation, reflected insolation, net radiation, wind direction.

Second Minute - Line 2 - Same as Line 1 format

Third Minute - Line 3 - Same as Line 1 format

Fourth Minute - Line 4 - Same as Line 1 format

Fifth Minute - Line 5
Date/time, 3-cm soil temperature, 6-cm soil temperature, 12-cm soil temperature, 25-cm soil temperature, 40-cm soil temperature, 65-cm soil temperature, 100-cm soil temperature, soil heat flux.

Fifth Minute - Line 6
Date/time, 1/4-m wind speed, 1/2-m wind speed, 1-m wind speed, 2-m wind speed, 4-m wind speed, 8-m wind speed, 16-m wind speed, 32-m wind speed.

The sixth minute would begin a new five-minute cycle.

DATE/TIME	TEMPERATURE	INSOLATION, ALBEDO, NET RADIATION, SOIL HEAT FLUX	WIND DIRECTION	WIND SPEED
xx xx xx xx Month Day Hour Minute	xx.xx°C	.0xxxx cal/cm^2/sec	xxx.x degrees from North	xxxx cm/sec

Table V-1. Printing Format for Any Five-Minute Period

seek methods to correlate radar coverage with the micrometeorological environment. The second, associated with Sub-task d, is to provide measurements on a mean scale, with simultaneous direct measurements of the Reynold's stresses, from other facilities, in order to investigate postulated concepts concerning equivalence of the latter in terms of the former.

The modifications effected to these automatic meteorological stations prior to installation in the Yegua Watershed are listed below.

1. Elimination of the soil heat flux measurements in favor of surface temperature measurements.
2. Replacement of Beckman Whitley Radiometers (Model N188-01) by Thornthwaite Radiometers (Model 605).
3. Replacement of wind speed measurements at 8 levels through hard tube circuitry and stepping switch logic with solid state components.

Elimination of the soil heat flux measurements is primarily a consequence of analyses of data collected at Dallas, Texas and Richland, Washington that shows the soil heat flux is rarely, if ever, accurately measured by soil heat plates (King, 1963). The soil heat flux can be determined from measurements of soil temperature profiles, which are already incorporated in the measurement complex; however, measurement of surface temperature, unless made directly, must be extrapolated from the soil and air profiles which necessarily degrades the flux computations.

Another requirement also entered in the decision to replace soil heat flux measurements in favor of measurements of surface temperature. This requirement is based on the following equation employed in a soil model under study in Sub-task c.

$$q_{s,o} = (T_o - T_o')/G \qquad 1)$$

This equation, first introduced by Halstead, et al. (1957), relates the soil heat flux at the surface to the surface temperatures from the air side and the soil side, and these values will differ according to the thermal insulation provided by vegetation and other surface debris. Virtually, nothing is known quantitatively of this factor of thermal resistance (G) other than its value for typical surfaces which appear to range between 100 to 5000 cm^2/sec deg/cal. Analyses of collected data, from these stations at Dallas and Richland, to evaluate G from Equation 1) have been something less than useful. However, assuming that overly large errors were not made in these analyses in determining T_o and T_o' by extrapolation, and $q_{s,o}$ by application of the Fourier conduction equation; it would appear that G is not a constant for a particular surface but varies rather widely with soil moistness and air temperature. On the other hand, if a mean value of G for a particular surface is assumed constant, the scatter of T_o and, particularly, T_o' values are within reasonable limits of extrapolation error. Hopefully, direct measurement of T_o will resolve this question.

Several means for measuring surface temperature were investigated and the method of infrared thermometry (Barnes, Model IT-3) was chosen. The sensor is mounted on the tower at approximately a 6 ft elevation and "sees" the surface near the base of the tower. Inasmuch as the output of the device for the normal temperature ranges is essentially linear, no function generation is employed in converting the sensor output before recording. Also, in view of the relatively high cost of this sensor and its, as yet, unproved capability to actually measure the surface temperature, only one unit is employed (Station A). Subsequently, assuming operation is satisfactory, an additional unit will be installed at Station B and function generation will be incorporated in the measurement circuitry to compensate for the nonlinearity involved between -50 and +50° C. Inasmuch as the surface temperature measurement replaces the soil heat flux measurement, it will be recorded as indicated in Table IV-1; that is, at the end of the fourth minute of each five minute interval.

Replacement of the Beckman Whitley net exchange radiometer by the Thornthwaite radiometer is based on testing of both instruments during the Dallas Tower Program. In the tests of the Beckman Whitley device, which were comparison rather than calibration tests inasmuch as the latter was not possible to project facilities, five radiometers including one standard (normally maintained in sealed storage) were mounted side by side and near simultaneous

measurements were made in up-wind, down-wind, and cross-wind configurations. Also measurements in an inverted position in the same wind orientation were made. These tests show that the variability of one instrument to another with regards to tracking capabilities was no better than 20%, and that the instrument response was strongly affected by wind velocity. Oddly enough, the cross-wind configuration yielded better results than the down-wind configuration which is recommended by the manufacturer. The instrument response was not significantly varied by plate reversal.

Similar comparison with two Thornthwaite radiometers (supplied by Dr. L. Fritschen for test purposes) showed that the tracking capabilities under all conditions were no worse than 5% and, of course, the sensors were unaffected by wind flow.

Modification of the wind measurements system applies to the conversion of the sensor output rather than the sensors themselves. In actuality the basic correction sought in this system was replacement of the wind counters (Neuron Type 7005D90AS) by more reliable counters. However, investigation of several other counters did not demonstrate significant potential for improvement in this regard. Since counter failure often occurred in the units digit (highest operating frequency), replacement of the five digit counter by single digit counters appeared to afford operational capability which was equivalent to an improvement in counter reliability, in that a single counter failure would not require replacement of a

complete five digit counter as had been the case previously. This modification, because of the radically different operating characteristics of the single counters, introduced the necessity for several other modifications which in total exceeded the efforts and cost associated with the design of a completely new wind measurement system.

In the following description of the modified wind system, the discussion is patterned after that given in the previously cited report covering the operation of these automatic meteorological stations and, specifically, replaces pages 37-40 and 88-90; Figures 20, 21, and 33; and Tables 4a, 4b, and 18 in that report.

The hardware modifications to the wind system consists of nine types of printed circuit subassemblies and a mainframe that holds these assemblies as well as the Veeder-Root (Model AG-196901)* decade counters. The latter directly replaces the Neuron counters of the old wind system. Of these printed circuit assemblies, seven are removable while the other two are permanently mounted on the front panel. Each of the assemblies is identifiable by a title corresponding to the circuit schematic as listed in the following figures.

Fig. IV-1. 7/11 and Input (8)

Fig. IV-2. Reset and Set 20 Detector (1)

Fig. IV-3. Power Driver (2)

Fig. IV-4. Lamp Driver (3)

*The counters have been altered internally such that they reset to 9 rather than 9 or 0.

Fig. IV-5.   Control (1)

Fig. IV-6.   Control Relay (1)

Fig. IV-7.   Type Relay (1)

Fig. IV-8.   Type Control I (1)

Fig. IV-9.   Type Control II (1)

The numbers in parentheses by each figure title indicates the number of assemblies employed in the complete system.

The signal coding employed in the above listed figures is described in Table IV-2. Use of this coding in the circuit schematic descriptions, which follow, would likely be a factor of complication and is avoided. However, the correlation to the signal coding is obvious

a. Fig. IV-1 7/11 and Input

As implied by the title, this circuit receives the anemometer input and converts the anemometer pulses so that for every 11 input pulses there are seven output pulses. This is accomplished by a scale-of-sixteen binary counting circuit that resets at the count of eleven. The reset is accomplished by detecting when the '1', '2', and '8' outputs are all logic '1' (5 volts). The three-input NAND gate which detects this logic state then sends a logic '0' signal (0 volts or absence of logic '1') to another three-input NAND which has its inputs strapped together. The second NAND then supplies a logic '1' to a third and final three-input NAND whose output drives the 'direct clear' input on the scale-of-sixteen circuit. The

Table IV-2. Signal Coding

SIGNAL CODE	LOCATION	FUNCTION
D1R	TB1, TB2	DIGIT 1 READ COMMAND
D2R	TB1, TB2	DIGIT 2 READ COMMAND
D3R	TB1, TB2	DIGIT 3 READ COMMAND
D4R	TB1, TB2	DIGIT 4 READ COMMAND
ED	TB1, TB2	TYPING ERROR DETECT
EDC	TB1, TB2	ERROR DETECTOR RESET
H	TB1, L7-19	TYPE HYPHEN COMMAND
HP	TB2, L7-4	HIGH PUNCH COMMAND
HPR	TB1, TB2	HIGH PUNCH READ COMMAND
OSC	TB2, U10-2	ERROR DETECTOR DRIVE
RE	TB1, TB2	RESET ENABLE COMMAND (AFTER BUFFERS)
REB	TB1, TB2	RESET ENABLE COMMAND (BEFORE BUFFERS)
RS	TB1, U10-14	RESET COMMAND
RSF-1	TB1, U1-18, L5,-5	RESET FAIL - REGISTER 1
RSF-2	TB1, U2-18, L5-7	RESET FAIL - REGISTER 2
RSF-3	TB1, U3-18, L5-9	RESET FAIL - REGISTER 3
RSF-4	TB1, U4-18, L5-11	RESET FAIL - REGISTER 4
RSF-5	TB2, U5-18, L5-13	RESET FAIL - REGISTER 5
RSF-6	TB2, U6-18, L5-15	RESET FAIL - REGISTER 6
RSF-7	TB2, U7-18, L5-17	RESET FAIL - REGISTER 7

Table IV-2—Continued

SIGNAL CODE	LOCATION	FUNCTION
RSF-8	TB2, U8-18, L5-19	RESET FAIL - REGISTER 8
R1	TB1, TB2	TYPE '1' ENABLE
R2	TB1, TB2	TYPE '2' ENABLE
R3	TB1, TB2	TYPE '3' ENABLE
R4	TB1, TB2	TYPE '4' ENABLE
R5	TB1, TB2	TYPE '5' ENABLE
R6	TB1, TB2	TYPE '6' ENABLE
R7	TB1, TB2	TYPE '7' ENABLE
R8	TB1, TB2	TYPE '8' ENABLE
R9	TB1, TB2	TYPE '9' ENABLE
R0	TB1, TB2	TYPE '0' ENABLE
R1R	TB1	READ REGISTER 1
R2R	TB1	READ REGISTER 2
R3R	TB1	READ REGISTER 3
R4R	TB1	READ REGISTER 4
R5R	TB1, TB2	READ REGISTER 5
R6R	TB1, TB2	READ REGISTER 6
R7R	TB1, TB2	READ REGISTER 7
R8R	TB1, TB2	READ REGISTER 8
R1-D1	TB1	READ REGISTER 1 - DIGIT 1
R1-D2	TB1	READ REGISTER 1 - DIGIT 2
R1-D3	TB1	READ REGISTER 1 - DIGIT 3

Table IV-2—Continued

SIGNAL CODE	LOCATION	FUNCTION
R1-D4	TB1	READ REGISTER 1 - DIGIT 4
R2-D1	TB1	READ REGISTER 2 - DIGIT 1
R2-D2	TB1	READ REGISTER 2 - DIGIT 2
R2-D3	TB1	READ REGISTER 2 - DIGIT 3
R2-D4	TB1	READ REGISTER 2 - DIGIT 4
R3-D1	TB1	READ REGISTER 3 - DIGIT 1
R3-D2	TB1	READ REGISTER 3 - DIGIT 2
R3-D3	TB1	READ REGISTER 3 - DIGIT 3
R3-D4	TB1	READ REGISTER 3 - DIGIT 4
R4-D1	TB1	READ REGISTER 4 - DIGIT 1
R4-D2	TB1	READ REGISTER 4 - DIGIT 2
R4-D3	TB1	READ REGISTER 4 - DIGIT 3
R4-D4	TB1	READ REGISTER 4 - DIGIT 4
R5-D1	TB2	READ REGISTER 5 - DIGIT 1
R5-D2	TB2	READ REGISTER 5 - DIGIT 2
R5-D3	TB2	READ REGISTER 5 - DIGIT 3
R5-D4	TB2	READ REGISTER 5 - DIGIT 4
R6-D1	TB2	READ REGISTER 6 - DIGIT 1
R6-D2	TB2	READ REGISTER 6 - DIGIT 2
R6-D3	TB2	READ REGISTER 6 - DIGIT 3
R6-D4	TB2	READ REGISTER 6 - DIGIT 4

Table IV-2—Continued

SIGNAL CODE	LOCATION	FUNCTION
R7-D1	TB2	READ REGISTER 7 - DIGIT 1
R7-D2	TB2	READ REGISTER 7 - DIGIT 2
R7-D3	TB2	READ REGISTER 7 - DIGIT 3
R7-D4	TB2	READ REGISTER 7 - DIGIT 4
R8-D1	TB2	READ REGISTER 8 - DIGIT 1
R8-D2	TB2	READ REGISTER 8 - DIGIT 2
R8-D3	TB2	READ REGISTER 8 - DIGIT 3
R8-D4	TB2	READ REGISTER 8 - DIGIT 4
S2F-1	TB1, U1-17, L5-5	SET 20 FAIL - REGISTER 1
S2F-2	TB1, U2-17, L5-7	SET 20 FAIL - REGISTER 2
S2F-3	TB1, U3-17, L5-9	SET 20 FAIL - REGISTER 3
S2F-4	TB1, U4-17, L5-11	SET 20 FAIL - REGISTER 4
S2F-5	TB2, U5-17, L5-13	SET 20 FAIL - REGISTER 5
S2F-6	TB2, U6-17, L5-15	SET 20 FAIL - REGISTER 6
S2F-7	TB2, U7-17, L5-17	SET 20 FAIL - REGISTER 7
S2F-8	TB2, U8-17, L5-19	SET 20 FAIL - REGISTER 8
T	TB2, L7-20	TYPE TABULATE COMMAND
TC	TB1, L7-18	TYPE COMPLETE COMMAND
TE	TB1, TB2	TYPE ENABLE
TGR	TB1, TB2	TYPE TABULATE ENABLE
1	TB2, L6-20	TYPE '1' COMMAND

Table IV-2—Continued

SIGNAL CODE	LOCATION	FUNCTION
2	TB2, L6-19	TYPE '2' COMMAND
3	TB2, L6-18	TYPE '3' COMMAND
4	TB2, L6-17	TYPE '4' COMMAND
5	TB2, L6-6	TYPE '5' COMMAND
6	TB2, L6-5	TYPE '6' COMMAND
7	TB2, L6-4	TYPE '7' COMMAND
8	TB2, L6-3	TYPE '8' COMMAND
9	TB2, L6-2	TYPE '9' COMMAND
0	TB2, L6-21	TYPE '0' COMMAND

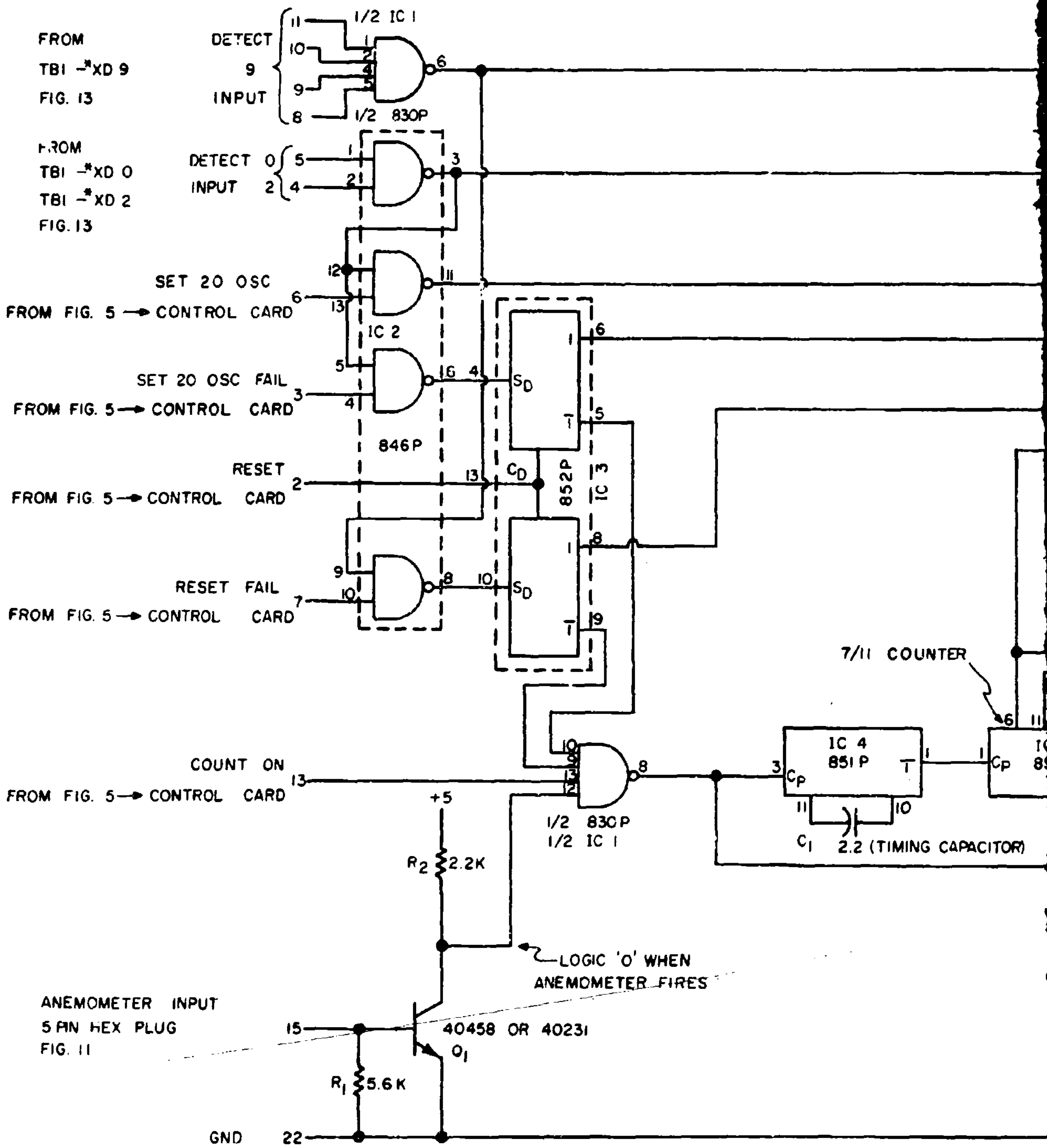

A

*X = 1,2,3,4,5,6,7,8

FIG. IV-1 INPUT

NOTE: (1) NUMBERS AT THE END OF A SIGNAL LINE DENOTE INPUT OR OUTPUT PINS ON CIRCUIT BOARD.
(2) NUMBERS AROUND COMPONENTS INDICATE CONNECTIONS ON IC'S.

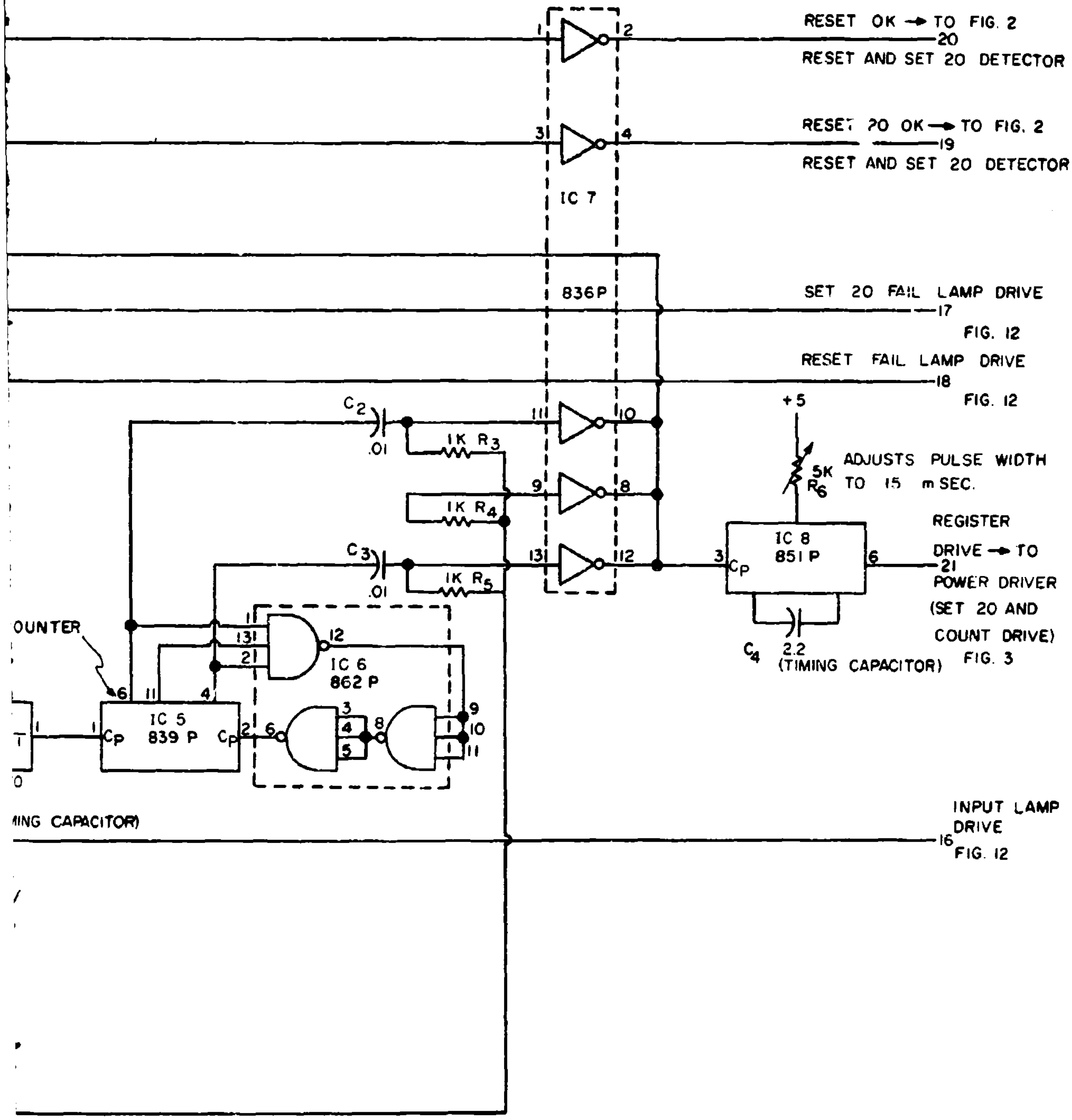

INPUT AND 7/11 CIRCUIT (CARDS U1 → U8 FIG. 11)

B

reason for this cascading is to allow sufficient delay between the fall of the input pulse, which caused the count of eleven to appear, and the clear signal. If this were not done the counter might clear and enter another count on the fall of the same pulse. The seven pulses are picked off through two R-C networks which drive two inverting stages whose outputs are strapped in parallel. This combined output then drives a monostable circuit (monostable) that supplies the final output from the printed circuit assembly (card). The width of the output is adjusted to 15 msec by a potentiometer located on the card. This pot is available from the front of the mainframe cabinet when the cabinet is open.

From the diagram it is apparent that the input pulse drives the scale-of-sixteen circuit through a four-input gate and a monostable. The purpose of the monostable is to shape the pulse for reliable counting. The gate is connected to three lines which come from the 'count on' line, and from the reset outputs of the dual flip-flop circuit (F/F) located on the card. The gate is enabled whenever all three lines have logic '1' appearing on them. Whenever this condition is met the output of the gate follows the input pulses from the anemometer. The 'count on' line is energized by the control card and the F/F's are in the reset condition whenever the counters reset properly after the preceding RESET signal. The purpose of these F/F's is to detect reset and 'set 20' errors and in the event of no errors the F/F's remain reset. In the event

that failure occurs in resetting, either one or both F/F's will set. If this happens, an error lamp will light on the front panel and the typewriter will type four hyphens to indicate failure. Each time a RESET is received from the external main system the wind system circuitry will attempt to reset all counters. Consequently, counters which are intermittently failing to reset will be returned to the system whenever they reset properly and will be blocked from the system whenever they fail to reset.

Failure to reset and failure to 'set 20' signals are generated by the control card and will be discussed later.

The two-input NAND gate, with inputs marked '0' input and '2' input, and the four-input NAND, with inputs marked '9's input', detect when the counter assembly associated with a particular input card has reset to a reading of 9999 and when it has set a reading of 0020. The outputs of these gates send a signal through an inverting stage to the system reset and 'set 20' detector card and, also, either block or enable the reset and 'set 20' F/F inputs.

b. Fig. IV-2. Reset and Set 20 Detector

As each of the register or counter assemblies resets to a reading of 9999 the input card associated with a particular set of registers generates a logic '1' signal. When all eight register assemblies have completed resetting,the reset detector circuit generates a logic '1' signal which is sent to the control card. The control card then changes modes of operation and begins to set 0020

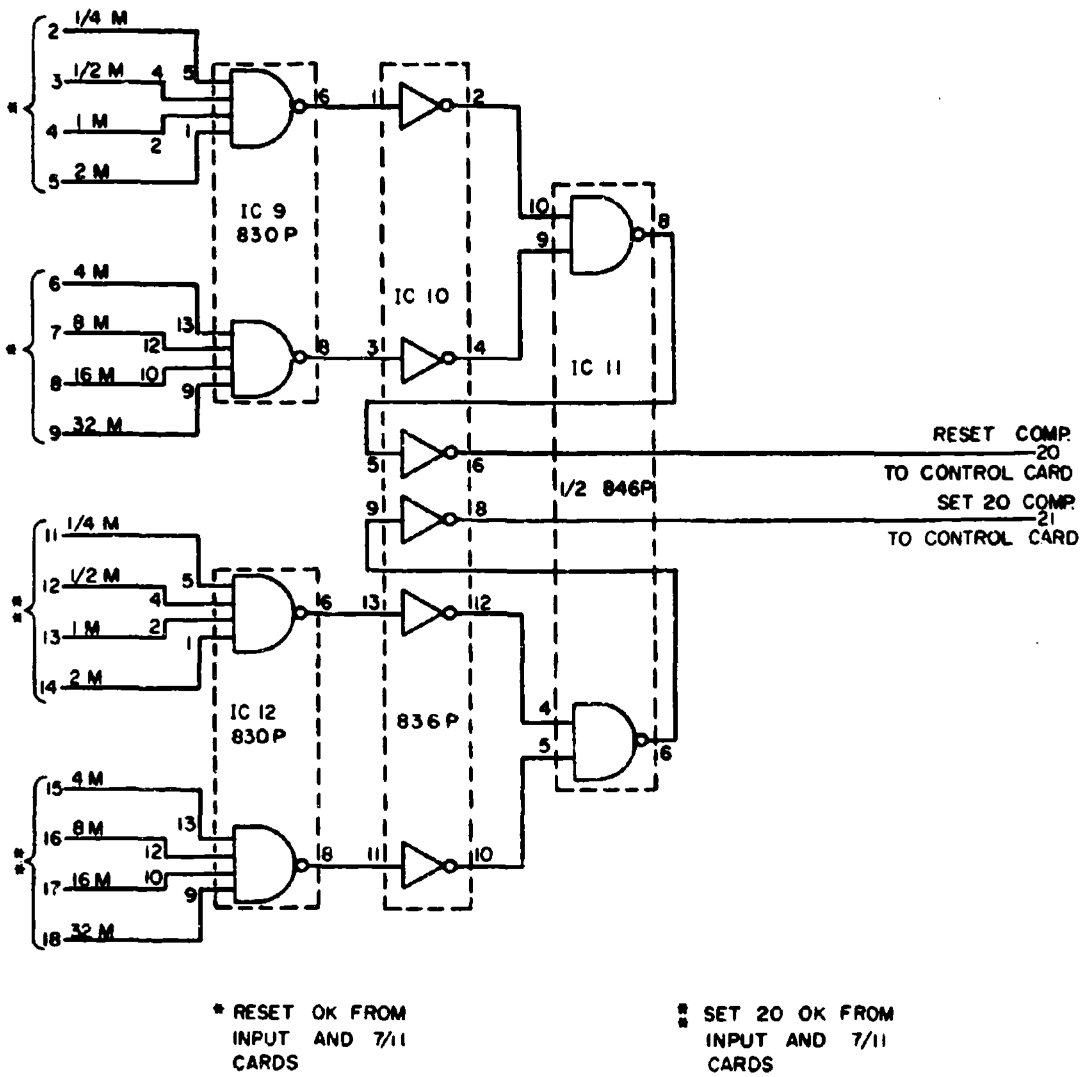

FIG. IV-2 RESET AND SET 20 DETECTOR
(CARD U9 FIG. 11)

on the registers. As each register arrives at 0020 the 'set 20 complete' lines from each input card go to logic '1' state. When all register assemblies read 0020 the 'set 20' detector sends a logic '1' signal to the control card. The control card then stops generating the 'reset 20' signal and generates a 'reset complete' signal to the main system.

c. Fig. IV-3. Power Drivers

The power drivers are used to drive the count and reset inputs of the counter assemblies. In the case of the count inputs, each of the eight power transistors on the card receives pulses from the 7/11 output of the input cards and actuates the count input of the register assembly associated with the input card from which the pulses were received. The reset inputs receive pulses from the second power driver board whose input comes from the 30 cycle (5 volts) reset oscillator output on the control card.

d. Fig. IV-4. Lamp Drivers

The lamp driver boards receive their inputs from three sources: anemometer input 'set 20 fail' and 'reset fail'. The lamp driver in the anemometer circuit supplies one of the lamps associated with a particular register assembly to indicate whenever an input pulse is received. The 'reset fail' lamp driver receives its inputs from the 'reset fail' outputs on each input board and lights a lamp on the front panel in case of RESET failure. The 'set 20 fail' lamp driver also receives its inputs from the input board and when

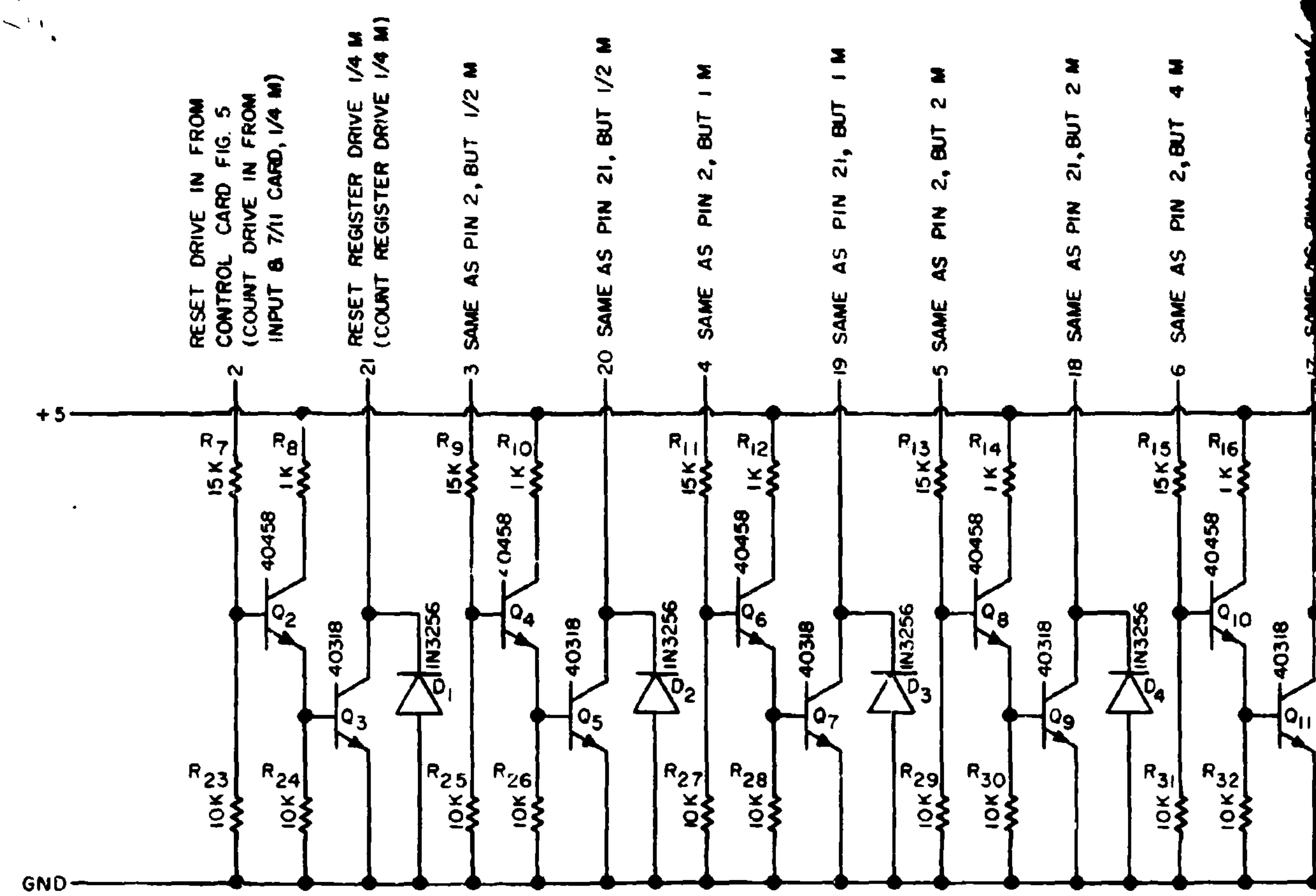

A

FIG. IV-3 POWER DRIVER (CAR

NOTE: DESCRIPTIONS IN ( ) INDICATE INPUTS OR OUTPUTS ON COUNT POWER DRIVER, OTHERWISE DESCRIPTIONS ARE FOR RESET POWER DRIVER.

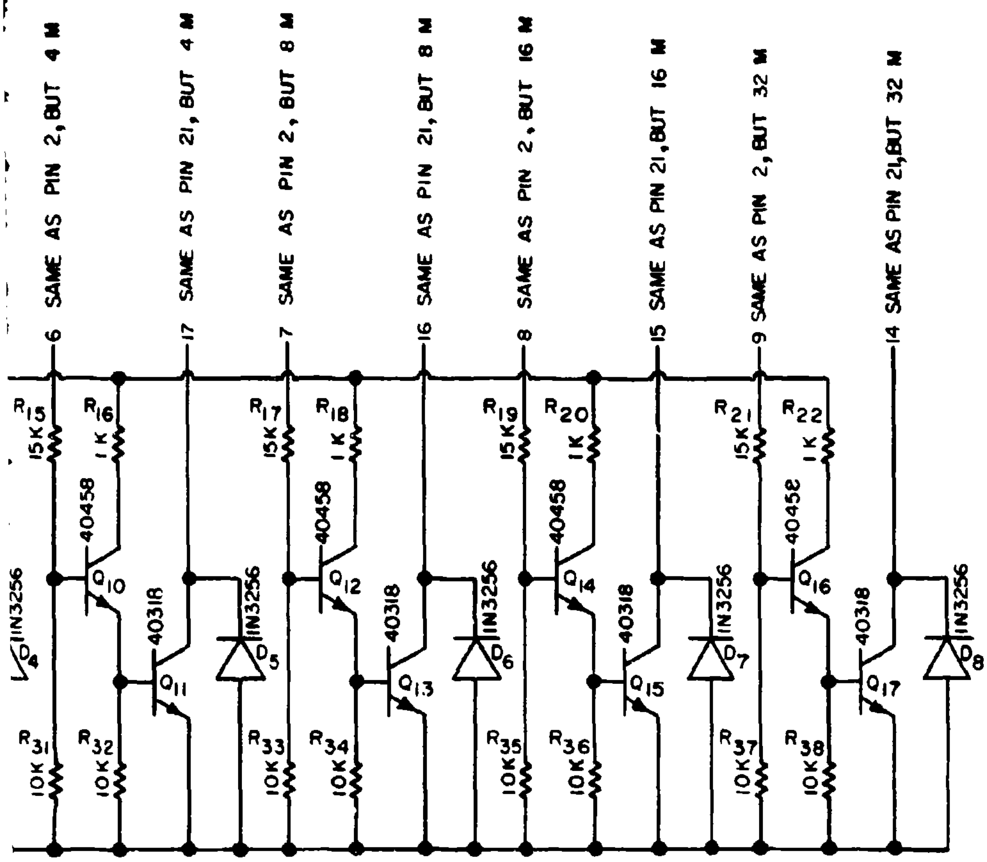

B

/ER (CARDS L1 & L2 FIG. 11)

NOTE: INPUTS TO THESE CARDS ALL COME FROM INPUT AND 7/11 CARDS.
OUTPUTS GO TO RESPECTIVE LAMPS.

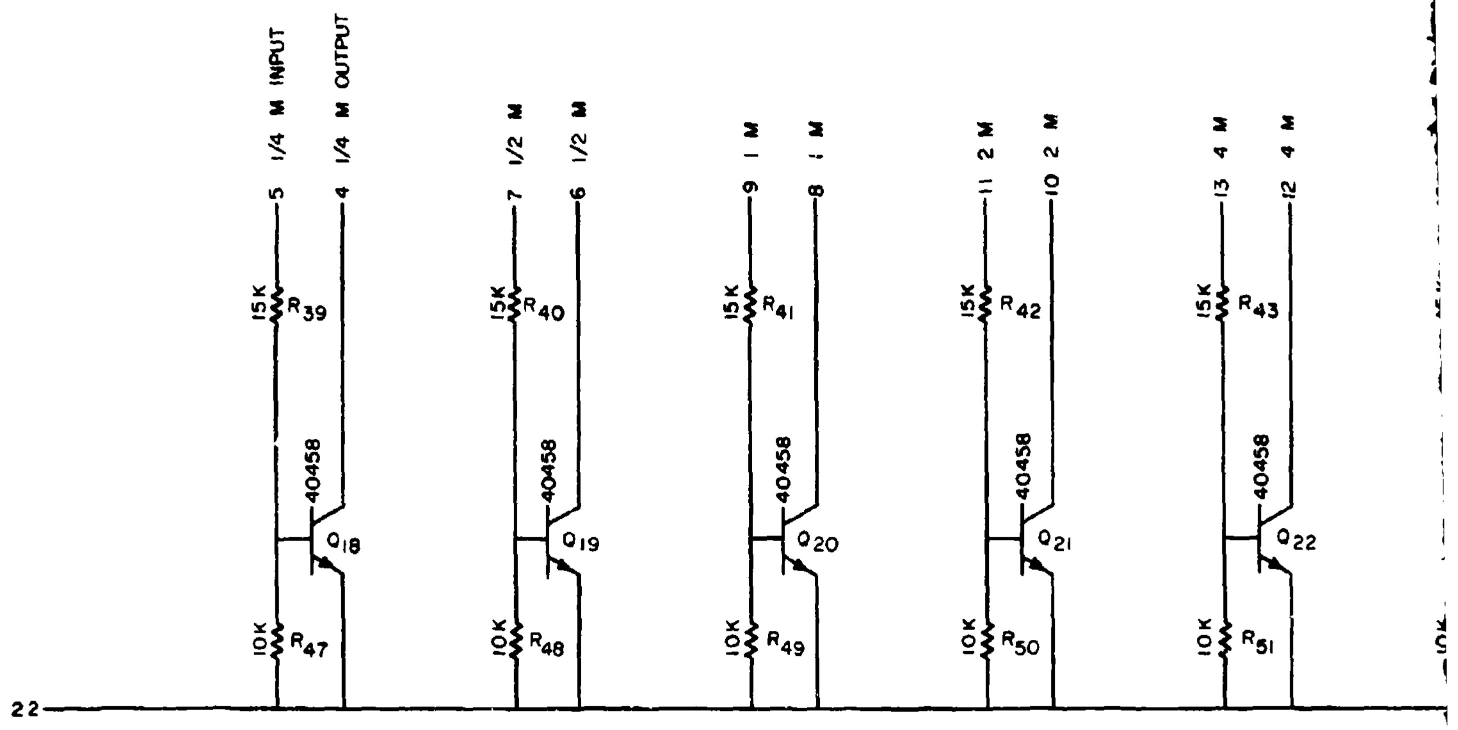

FIG. IV-4 LAMP DRIVER (CARDS

A

AND 7/11 CARDS.

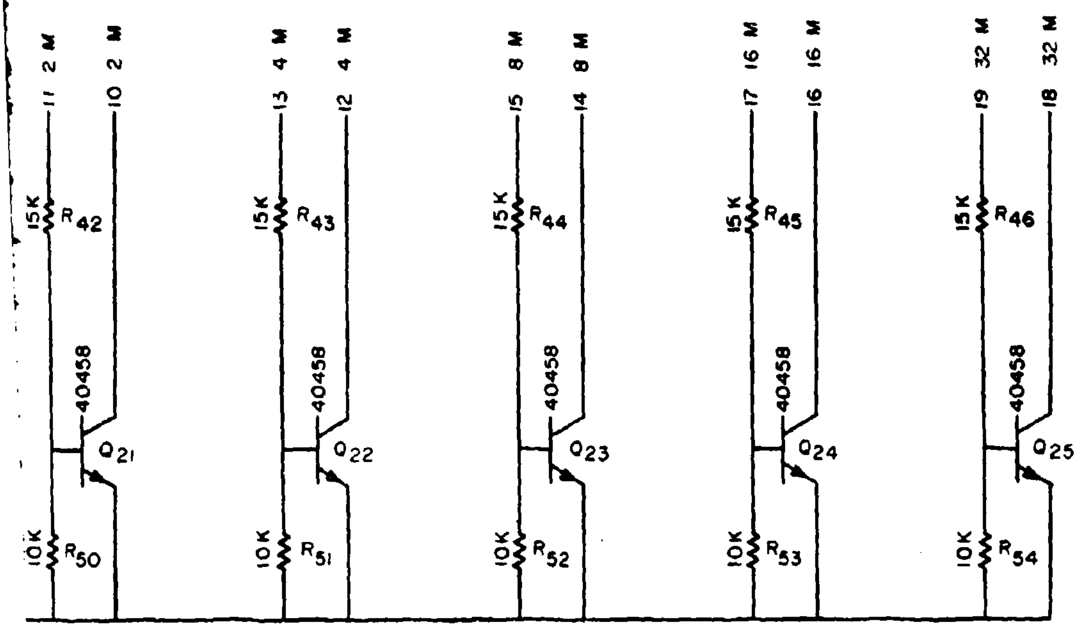

LAMP DRIVER (CARDS L3→L5 FIG. 11)

B

applicable, lights a lamp on the front panel to indicate that a particular register assembly has failed to set 0020.

e. Fig. IV-5. Control

With the exception of the typing format the control card provides internal instructions to the wind measurement system. The instructions are; 'count on', reset, 'reset oscillator', 'set 20 oscillator', 'reset fail', and 'set 20 fail'. A 30 cycle square wave is also provided by this card as well as a 50 volt signal back to the main system indicating when the wind counters have completed resetting. The control card receives signals from both the counters and the main system. From the main system it receives 50 volt pulses which instruct the counter assemblies to start and stop counting, and to reset. The control card receives logic signals from the register assemblies and 'set 20' detector card to indicate when reset and 'set 20' instructions have been completed. Also, a 60 cycle signal is fed to the control card for reduction to 30 cycles. In normal operation the sequency of signals would be start, stop, reset, 'reset complete' and 'set 20 complete'. On receipt of a start pulse from the main system the count F/F is set. The count F/F, when set, supplies a logic '1' signal to all input cards to enable the input gate. Counting in all registers then proceeds until a stop pulse is received from the external main system. Since the typing cards function independently they will be discussed later. After typing is complete the main system generates a 50 volt RESET

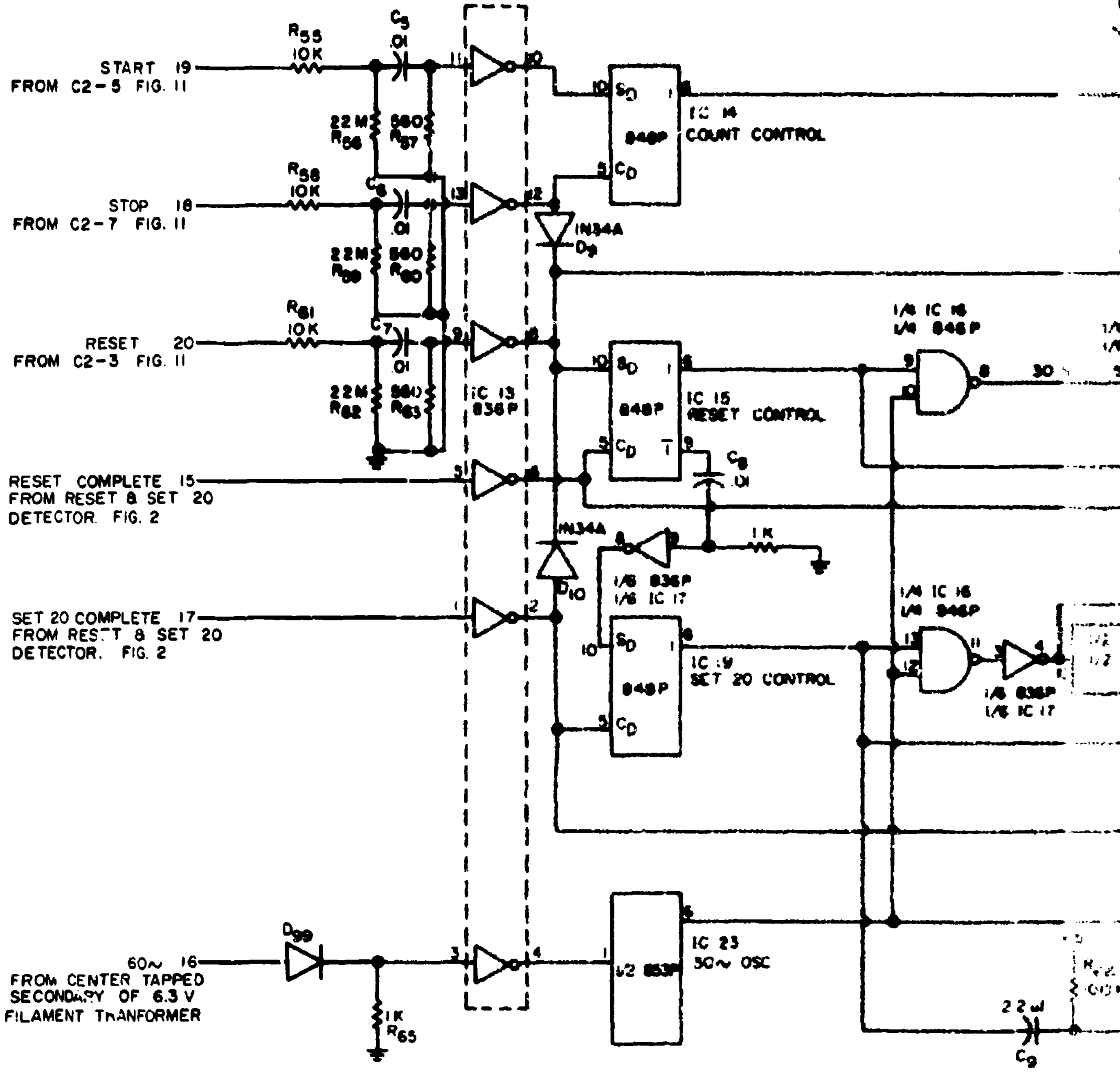

FIG. IV-5 CONTROL

A

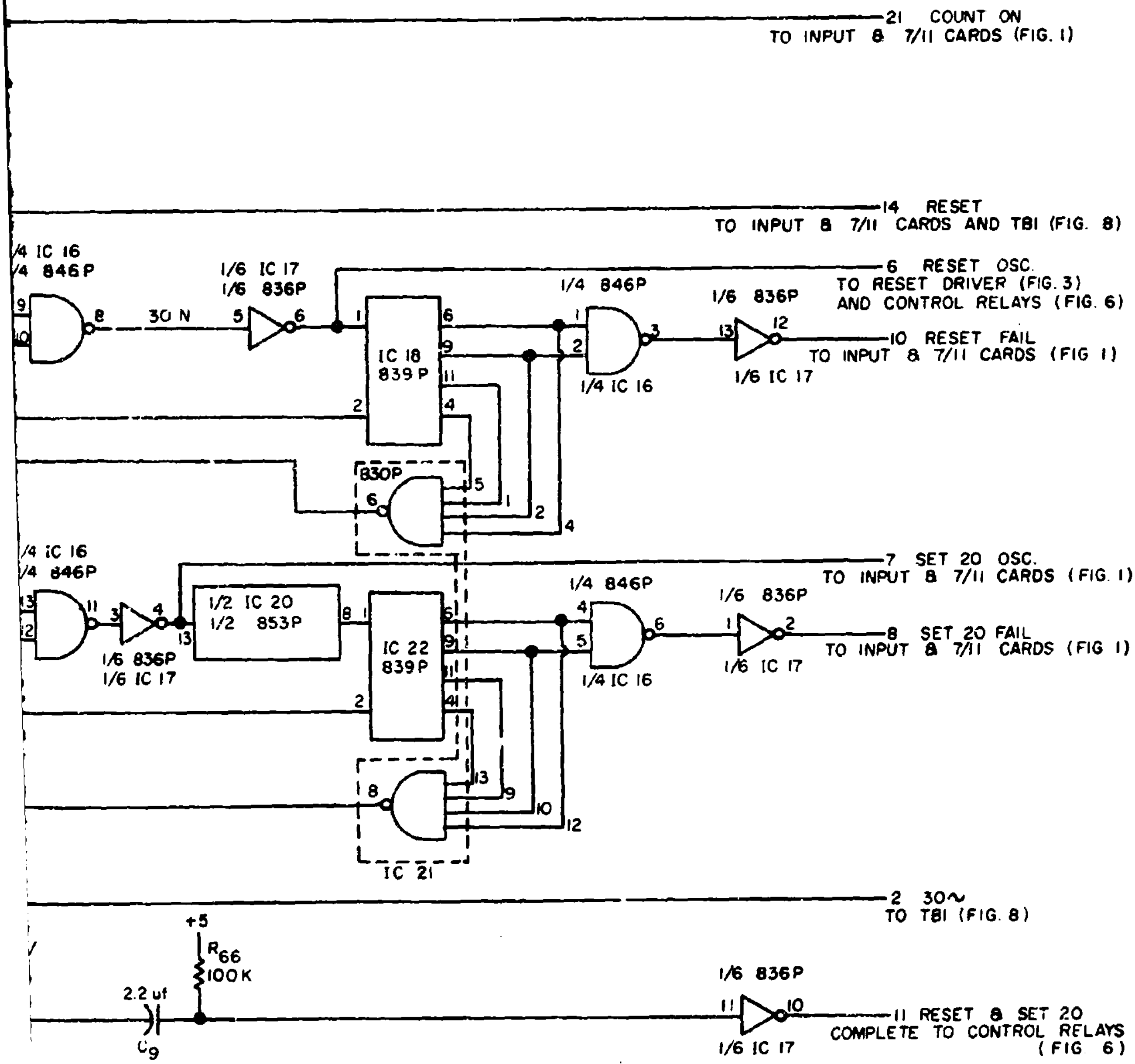
21 COUNT ON
TO INPUT & 7/11 CARDS (FIG. 1)
14 RESET
TO INPUT & 7/11 CARDS AND TBI (FIG. 8)
1/4 IC 16
1/4 846P
30 N
1/6 IC 17
1/6 836P
IC 18
839P
6 RESET OSC.
TO RESET DRIVER (FIG. 3)
AND CONTROL RELAYS (FIG. 6)
10 RESET FAIL
TO INPUT & 7/11 CARDS (FIG 1)
830P
7 SET 20 OSC.
TO INPUT & 7/11 CARDS (FIG. 1)
1/2 IC 20
1/2 853P
IC 22
839P
8 SET 20 FAIL
TO INPUT & 7/11 CARDS (FIG 1)
IC 21
2 30~
TO TBI (FIG. 8)
+5
R66
100K
2.2 uf
C9
11 RESET & SET 20
COMPLETE TO CONTROL RELAYS
(FIG 6)

CONTROL

B

command which resets the failure F/F's on the input boards and resets the typing boards. When the reset F/F is set, a two-input NAND gate is enabled which allows the 30 cycle signal to be applied to an inverter which drives a scale-of-sixteen counter and the inputs of the reset power drivers. When all registers are reset, the 'reset complete' signal resets the F/F to remove the 30 cycle output. The function of the scale-of-sixteen counter is to determine when 12 pulses (30 cycle) have been supplied to the reset drivers. If 12 pulses are supplied without a 'reset complete' signal, the counter interprets this as an indication of reset failure, since a maximum of only nine pulses are required to reset the system, and generates a 'reset fail' signal of logic '1' through the two-input NAND gate and inverter and holds this signal until a count (30 cycle) of 15 is received. At a count of 15 the counter sends a logic '0' signal back from the four-input NAND gate to reset the reset F/F and clear the counter. When this occurs the 'reset oscillator' and 'reset fail' signals are removed. Further, through the combination of a R-C network and inverter connected to the reset output of the reset F/F, a signal is generated to set the 'set 20' F/F. This in turn, enables a two-input NAND to permit transmission of the 30 cycle signal to the input cards and to a F/F. The input cards then proceed to count 21 pulses (48 volts) into the register assemblies (the number required to go from 9999 to 0020). As each register sets 0020, the input card prevents further pulses

from being sent to the register by disabling a two-input NAND gate on the input board. When all registers have set 0020, a logic '1' signal is sent from the reset and 'set 20' detector card which resets the 'set 20' F/F. The output of the F/F which was being driven by the 'set 20' oscillator signal drives the input of a second scale-of-sixteen counter. This counter is connected in in the same way as the one associated with the reset circuit except that it counts only every other pulse because of the F/F preceding it. This allows 24 'set 20' pulses to occur before a failure signal is generated. A 'set 20' failure is held for six counts rather than for three as in the case of the reset F/F. When the 'set 20' F/F is reset it generates a logic '1' output through the R-C and inverter combination which indicates to the main system that the total wind system has been reset.

f. Fig. IV-6. Control Relays

The control relays are required to transform the logic levels (5 volts) used in the wind measurement system to the 50 volt level used by the main system. There are six relays and driving circuits on this card and they supply signals for the following functions:

1. system reset complete
2. typewriter hyphen
3. typewriter tabulate
4. high punch on tape
5. type wind complete
6. tape leader advance

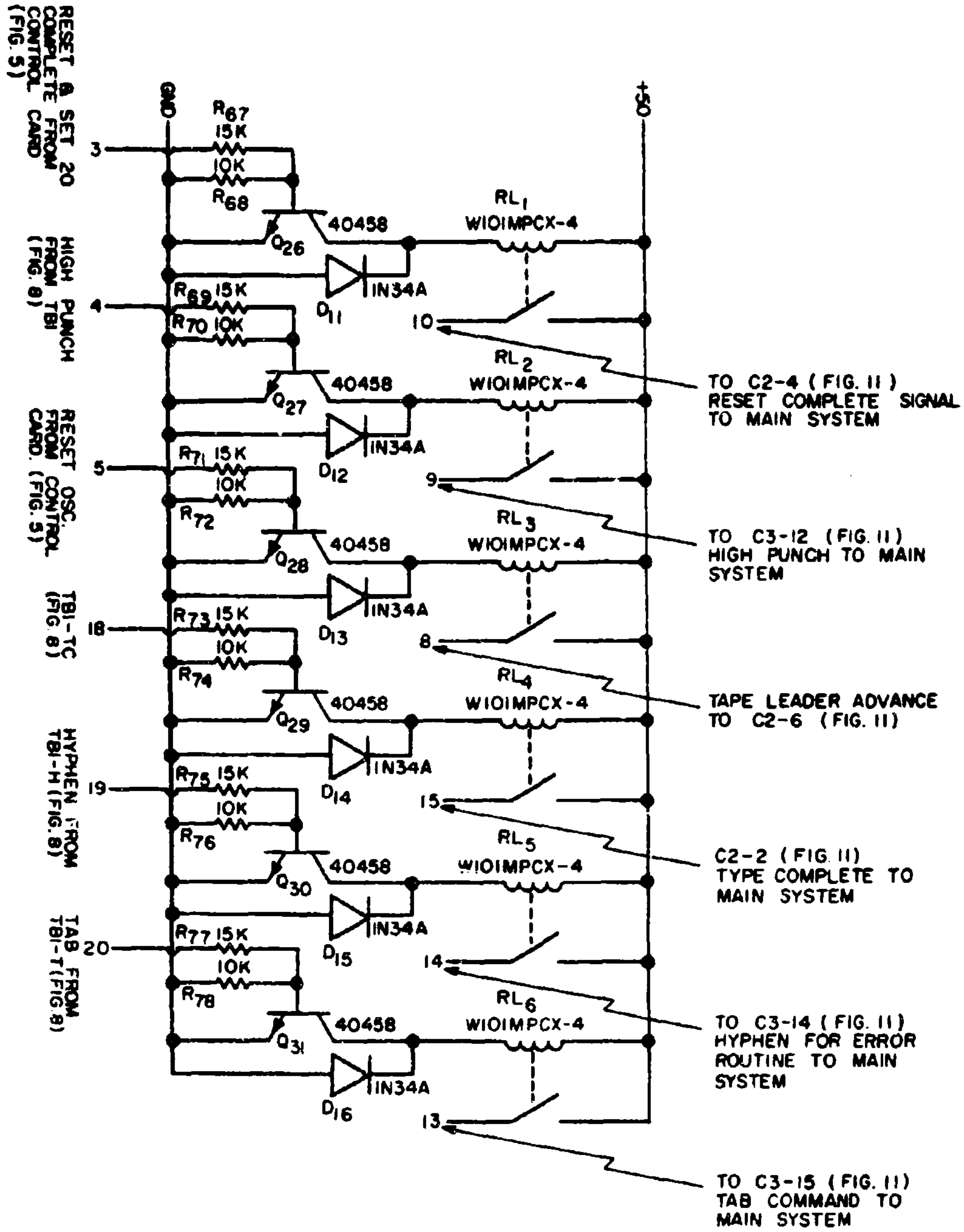

FIG. IV—6 CONTROL RELAYS

The inputs for each relay driving circuit are:

1. system reset complete from control card
2. typewriter hyphen from type control I
3. typewriter tabulate from type control II
4. high punch from type control II
5. type wind complete from type control I
6. tape leader advance from reset oscillator output

g. Fig. IV-7. Type Relays

The type relays are used to type and punch the digits 0 through 9 and receive their inputs from type control II.

h. Fig. IV-8. and IV-9. Type Control I and II

The type control system contains two shift registers which are used in conjunction to identify the particular digit to be typed. One of the shift registers is a five-bit unit which is closed on itself while the other register is an eight-bit unit which is open at the end. The five-bit register is used to identify the digit to be read while the eight-bit register is used to identify the counter assembly. These registers make up the basic logic of the system while the balance of the logic is used to decode the outputs of the shift registers and to supply the necessary control functions.

On receipt of a 'type wind' command, the type F/F is set and the two shift registers have a logic '1' set into the first bit location. When the type F/F is set, the type AND gate is enabled and a logic '1' is applied to the digit AND gates. With the logic '1' in the first bit locations of the shift registers, a logic '1'

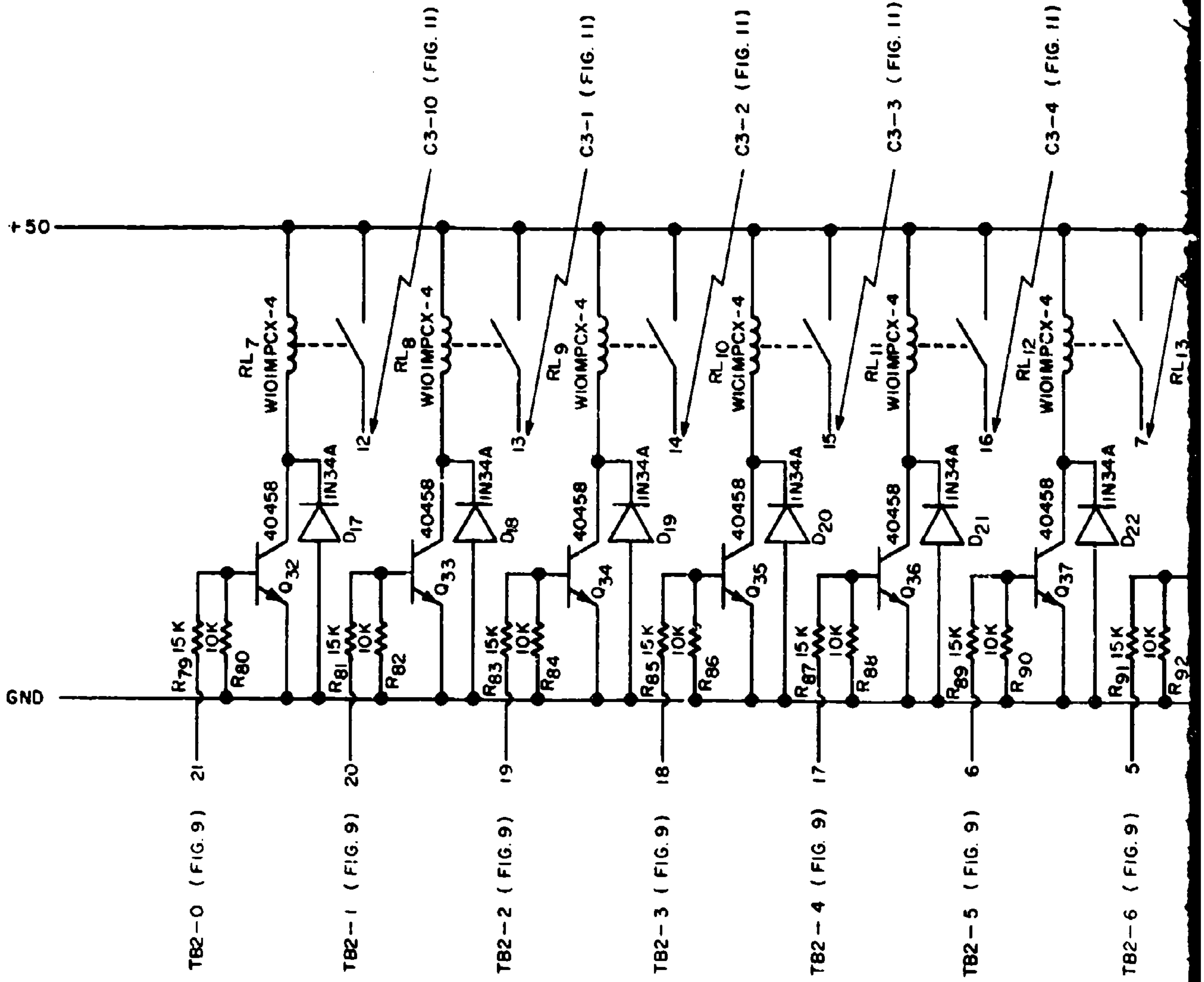

FIG. IV-7 TYPE RELAYS

A

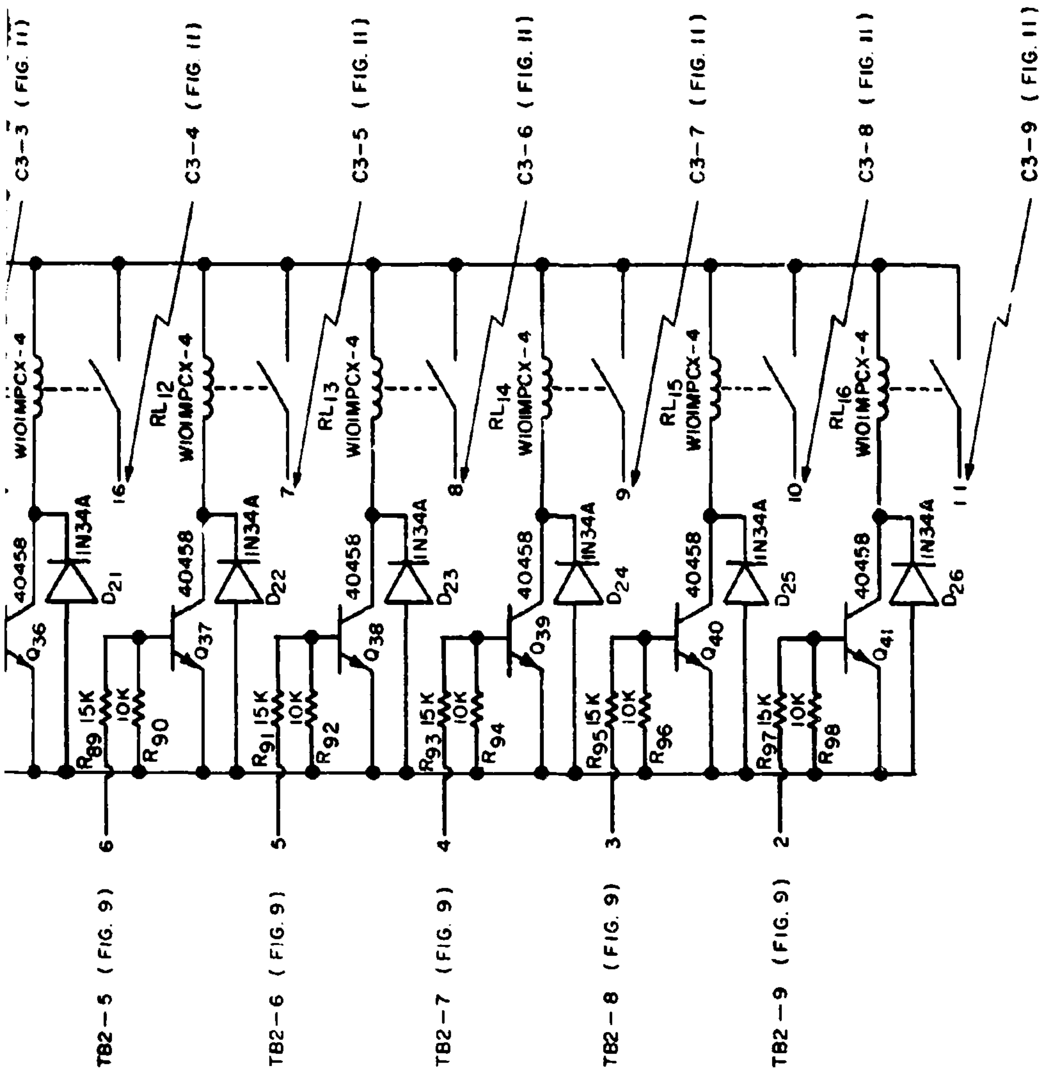
C3-3 (FIG. 11)
C3-4 (FIG. 11)
C3-5 (FIG. 11)
C3-6 (FIG. 11)
C3-7 (FIG. 11)
C3-8 (FIG. 11)
C3-9 (FIG. 11)
W101MPCX-4
RL12 W101MPCX-4
RL13 W101MPCX-4
RL14 W101MPCX-4
RL15 W101MPCX-4
RL16 W101MPCX-4
16
7
8
9
10
11
1N34A
40458
Q36
Q37
Q38
Q39
Q40
Q41
D21
D22
D23
D24
D25
D26
15K
10K
R89
R90
R91
R92
R93
R94
R95
R96
R97
R98
6
5
4
3
2
TB2-5 (FIG. 9)
TB2-6 (FIG. 9)
TB2-7 (FIG. 9)
TB2-8 (FIG. 9)
TB2-9 (FIG. 9)

E RELAYS

B

* EXAMPLE OF CODING: READ 1-DIGIT 1 R1-D1
READ 1-DIGIT 2 R1-D2
READ 2-DIGIT 3 R2-D3

RSF-1 RESET FAIL 1/4M REGISTERS
S2F-2 SET 20 FAIL 1/2M REGISTERS

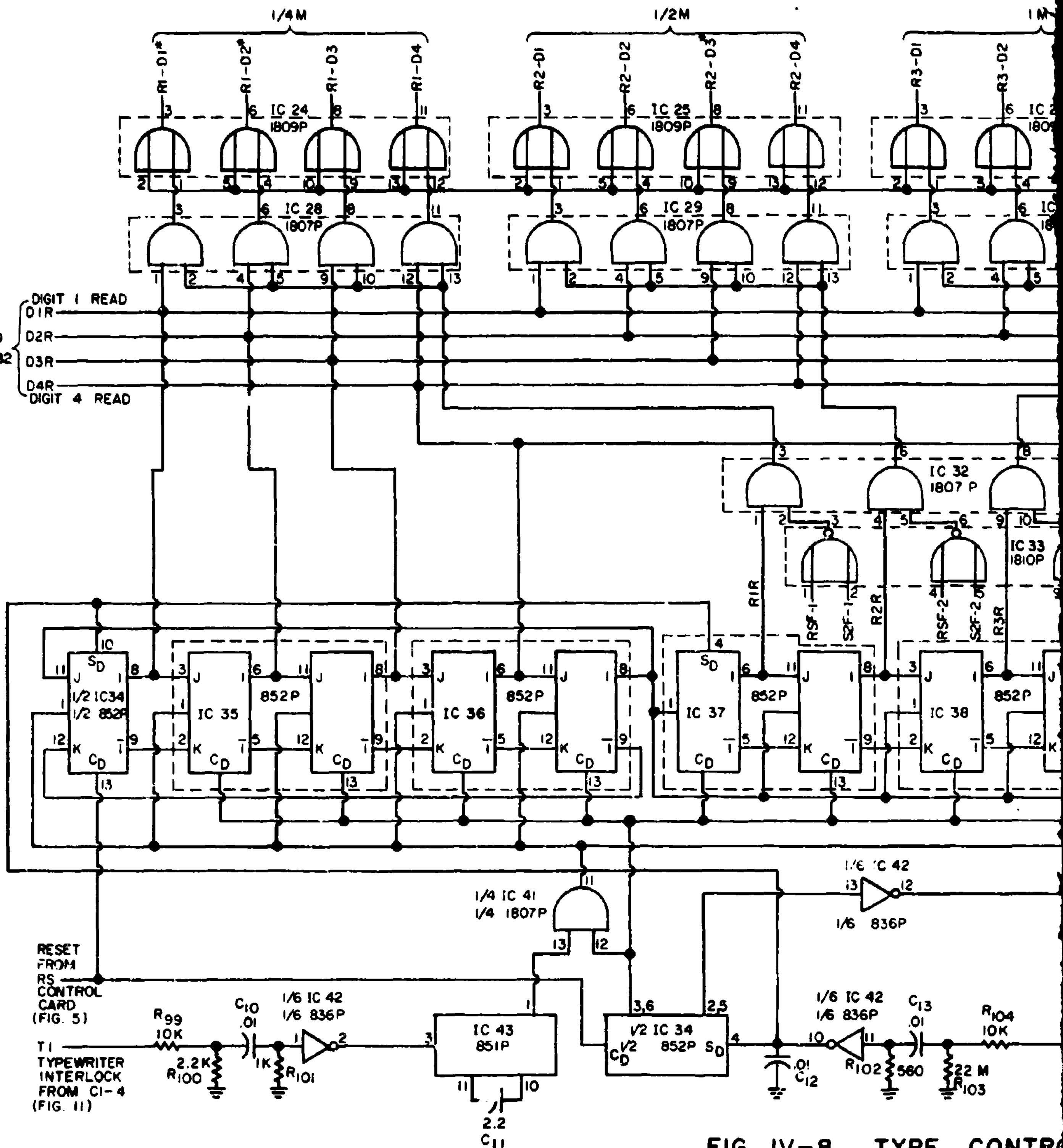

FIG. IV-8 TYPE CONTR

A

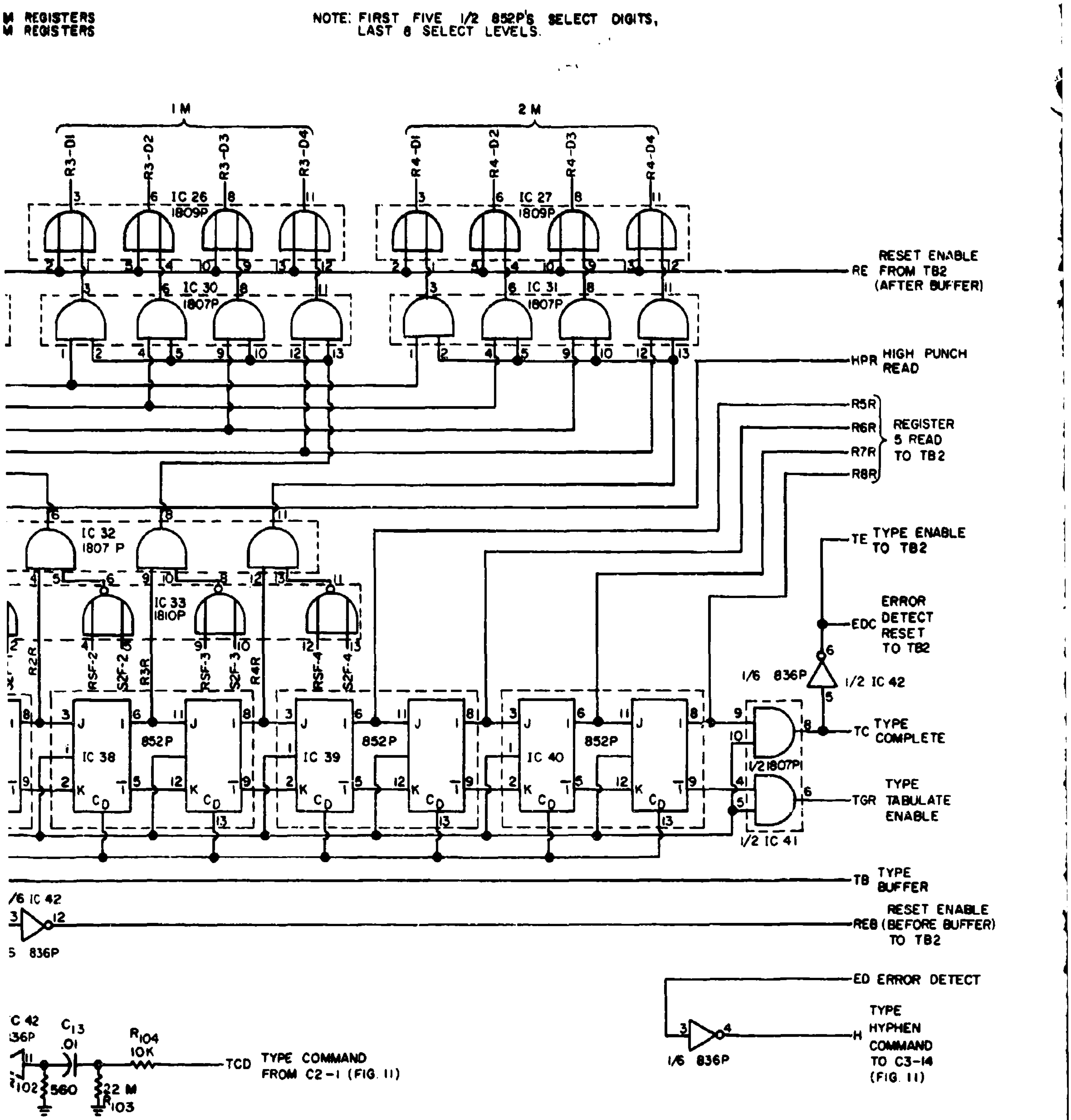

TYPE CONTROL I

B

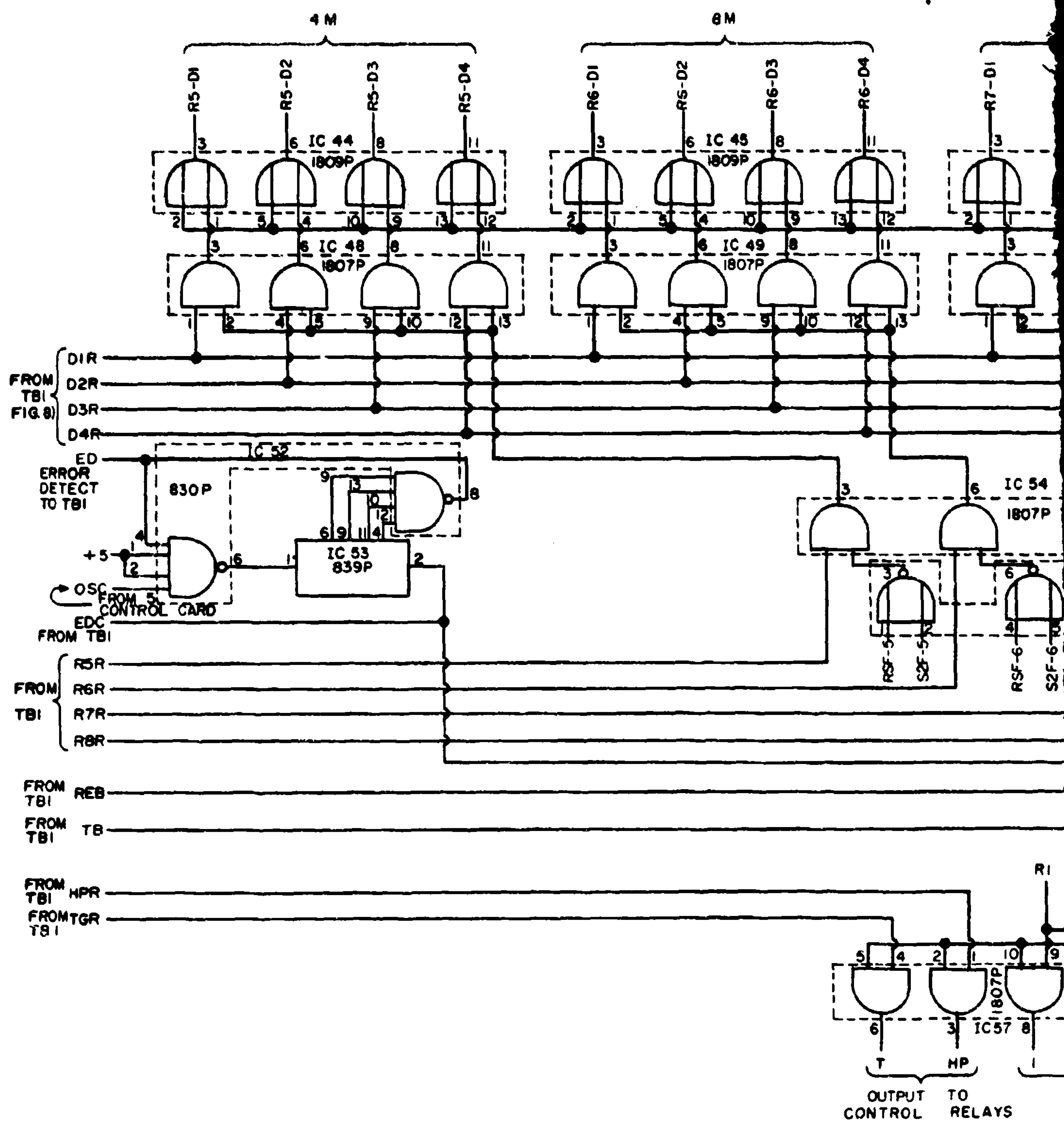

FIG. IV-9 TYPE

A

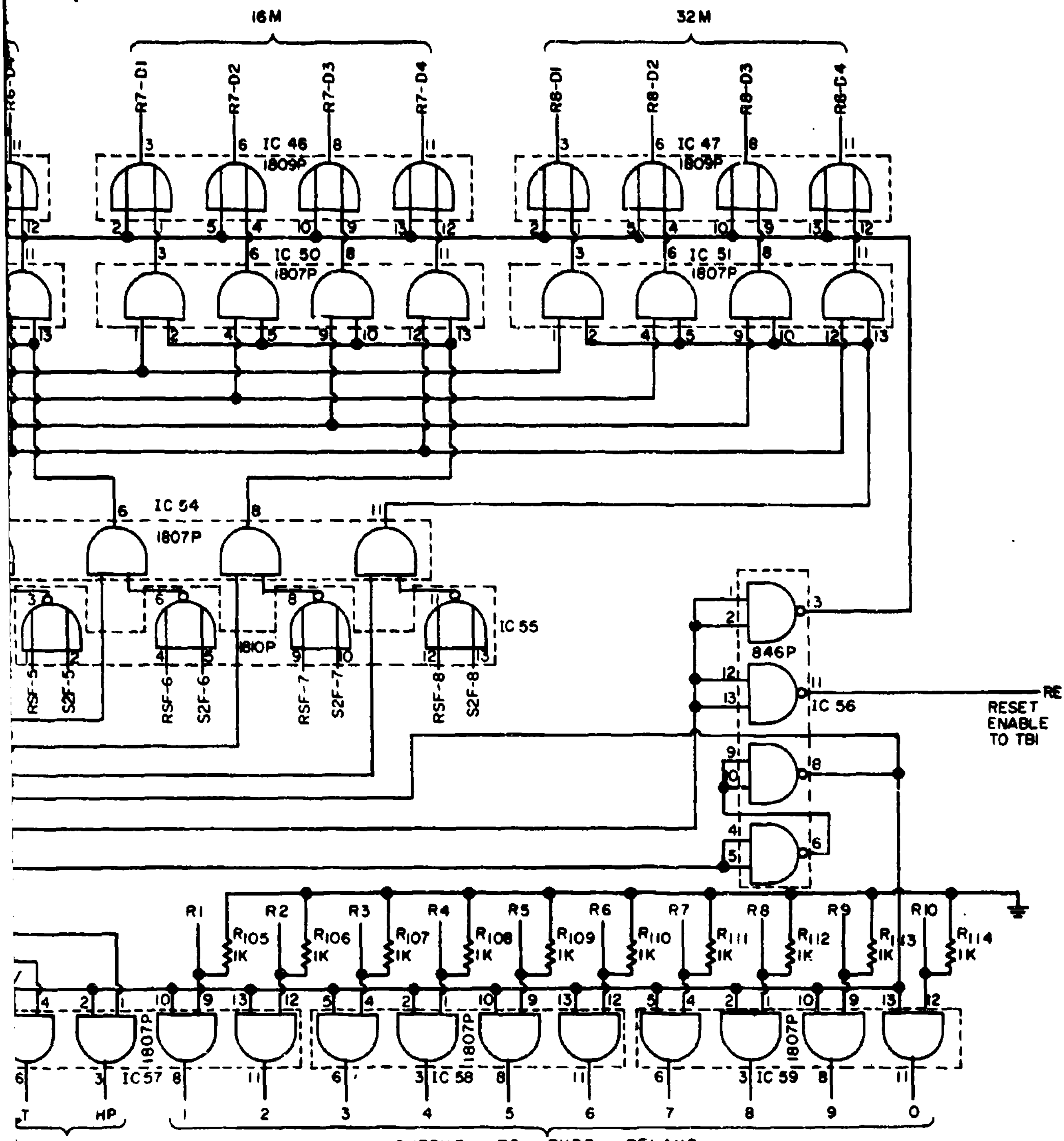

UTPUT TO
TROL RELAYS

. IV-9 TYPE CONTROL II

B

signal will be applied to the common line of the first digit in the first wind counter assembly. Depending on the reading contained in this assembly, this logic '1' signal will appear on one of the digit AND gates. This signal, together with the signal from the type AND gate, causes one of the 'type digit' relays to be energized. When a 'type digit relay is energized, a 50 volt signal is applied to an output line to drive the appropriate solenoid on the typewriter. On completion of typing a digit, the typewriter returns a 50 volt typewriter interlock signal to the type control board. This signal causes the monostable, which is connected to the type AND gate, to drive to a logic '0' state. This removes the logic '1' signal from the digit AND gates and shifts the logic '1' signal in the first bit location of the five-bit register to the second bit location. After the monostable has delayed for approximately 35 msec, it returns to logic '1'. The digit AND gates are again enabled, and the second digit in the first counter assembly is typed. After all four digits are typed, the fifth bit in the five-bit register energizes the tab AND gate and the typewriter tabulates to the next position. On receipt of the typewriter interlock signal after tabulation the five-bit register again has a logic '1' in the first bit location. When the fifth bit goes from logic '1' to logic '0' it advances the logic '1' in the first bit location of the eight-bit register to the second bit location. This sequencing of digits and registers continues until the fourth digit in the eight counter assembly has been typed. At this time, the tab signal

is disabled and a type complete signal is generated which sends a 50 volt pulse back to the main system.

In the event a digit should fail to type after the digit AND gates have been energized, the system generates a command to type a hyphen. This command is generated by a scale-of-sixteen circuit which begins counting a 30 cycle signal as soon as the digit AND gates are enabled. If the count reaches 15 without a typewriter interlock signal being received, the scale-of-sixteen circuit generates the type hyphen command. As each digit is typed the scale-of-sixteen circuit is reset so that each digit is allowed a half second in which to type before a hyphen is typed in its place. This failure circuit is also used whenever a counter has failed to reset properly. If reset or 'set 20' failure occurs, the output from the eight-bit register, associated with the particular counter assembly, is disabled so that when the data in that register is to be typed, the common lines to each of its digits are not energized and therefore cannot be typed. As a result this is interpreted as four successive failures and the system types four hyphens. Thus, a typed group of four hyphens indicates that a particular counter assembly has failed to reset properly or has failed (all digits) to read out properly.

All of the preceding references to typewriter control apply also to simultaneous punched paper tape commands.

Table IV-3. Wind Speed Cabling

Connector	Pin #	Function	Connects to
	A	Photocell supply voltage +5 VDC	Anemometer, Pin 2
A-1	B	Photocell input	Anemometer, Pin 3
through	D	3 VAC	Anemometer, Pin 4
A-8	E	Ground	Anemometer, Pin 1
	H	Ground	Anemometer, Pin 1
	1	Type Wind	Main programmer, Pin W
	2	Wind typed	Main programmer, Pin N
	3	Reset	Main programmer, Pin a; timer Pin J
C-1	4	Counter reset	Main programmer, Pin Z
	5	Start counters	Timer, Pin B
	6	NC	
	7	Stop counters	Timer, Pin C
	8	NC	
	1	115 VAC	
	2	+50 VDC	
	3	T. I.	
C-2	4	Tape advance	Typer/punch Junction box, 10 Pin, Pin I
	5	50 VDC return	
	6	115 VAC	

Table IV-3.—Continued

Connector	Pin #	Function	Connects to
	1	Typewriter punch junction box	15-Pin, Pin 1
	2	Typewriter punch junction box	Pin 2
	3	Typewriter punch junction box	Pin 3
	4	Typewriter punch junction box	Pin 4
	5	Typewriter punch junction box	Pin 5
	6	Typewriter punch junction box	Pin 6
	7	Typewriter punch junction box	Pin 7
C-3	8	Typewriter punch junction box	Pin 8
	9	Typewriter punch junction box	Pin 9
	10	Typewriter punch junction box	Pin 10
	11	Typewriter punch junction box	Pin 11
	12	Typewriter punch junction box	Pin 12
	13	Typewriter punch junction box	Pin 13
	14	Typewriter punch junction box	Pin 14
	15	Typewriter punch junction box	Pin 15

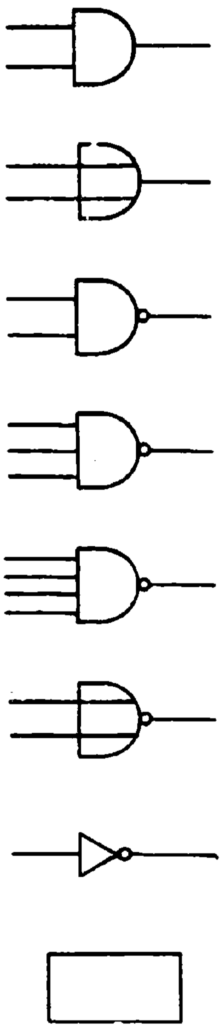

2 INPUT AND (1807P)

2 INPUT OR (1809P)

2 INPUT NAND (846P)

3 INPUT NAND (862P)

4 INPUT NAND (830P)

2 INPUT NOR (1810P)

INVERTER (836P)

FLIP-FLOP, MONOSTABLE, OR COUNTER

FLIP-FLOP: 852P, 853P, OR 848P
MONOSTABLE: 851P
COUNTER: 839P

FIG. IV-14 DIGITAL LOGIC SYMBOLS

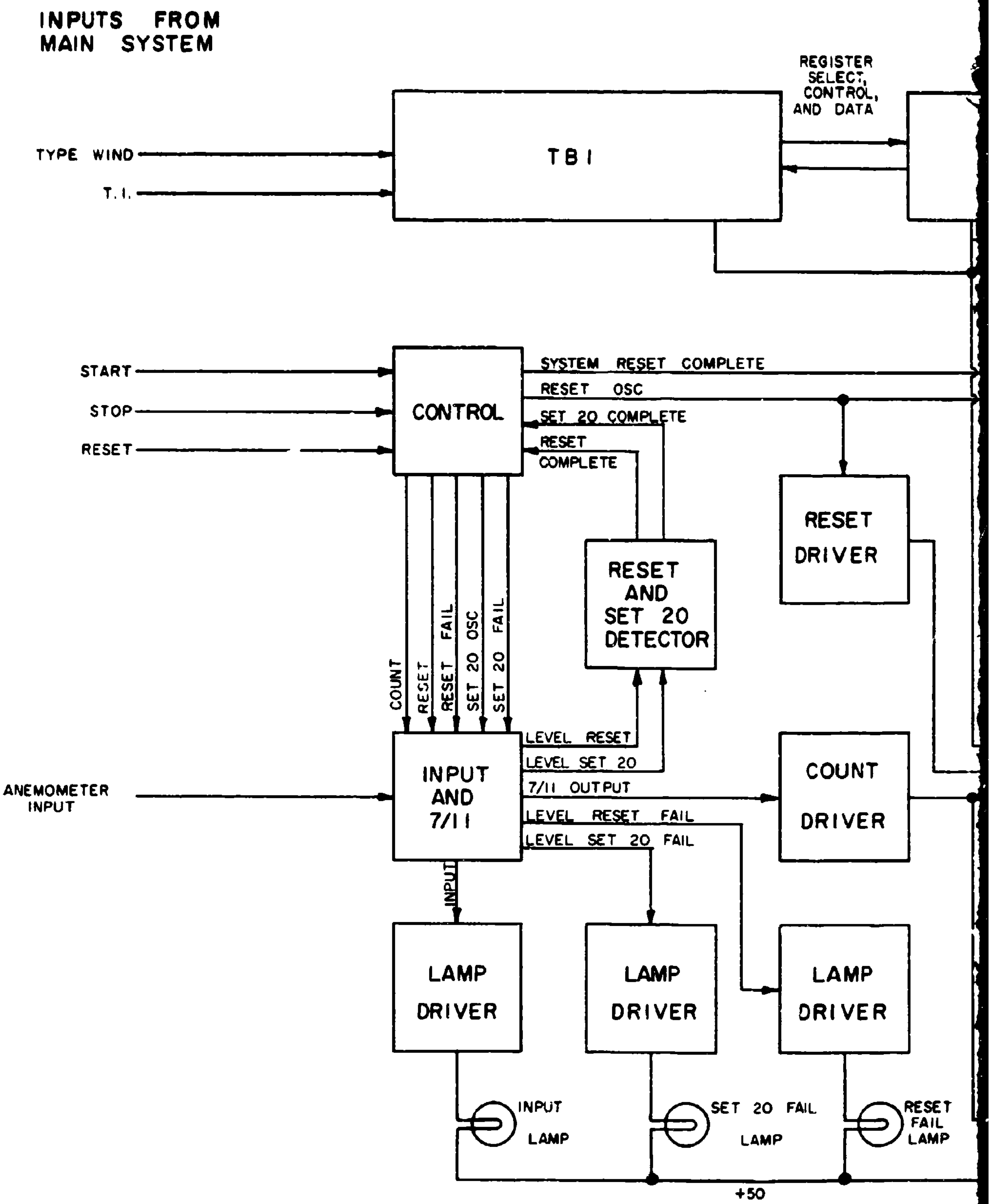

FIG. IV-10 SIGNAL FLOW

A

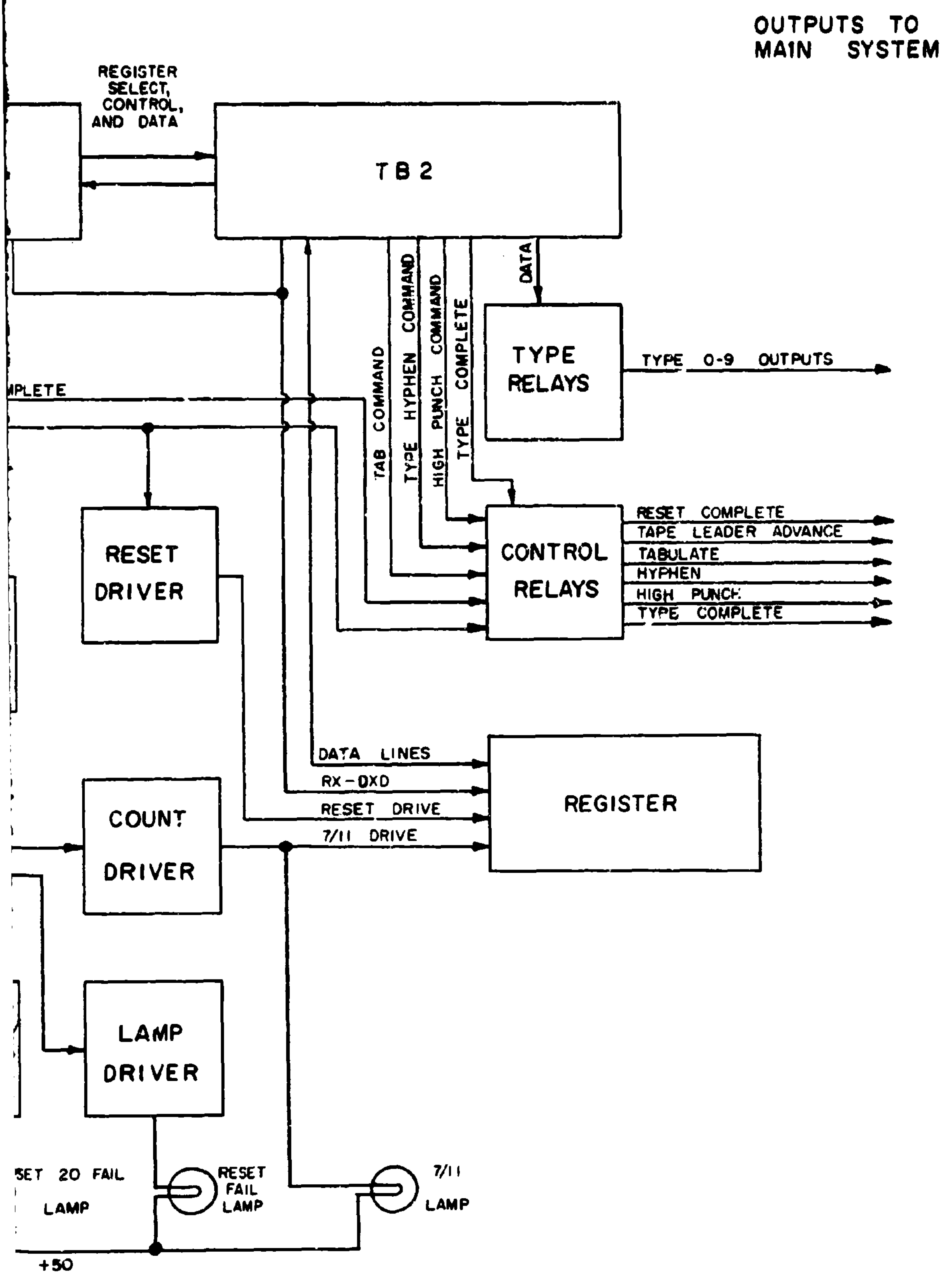

SIGNAL FLOW

B

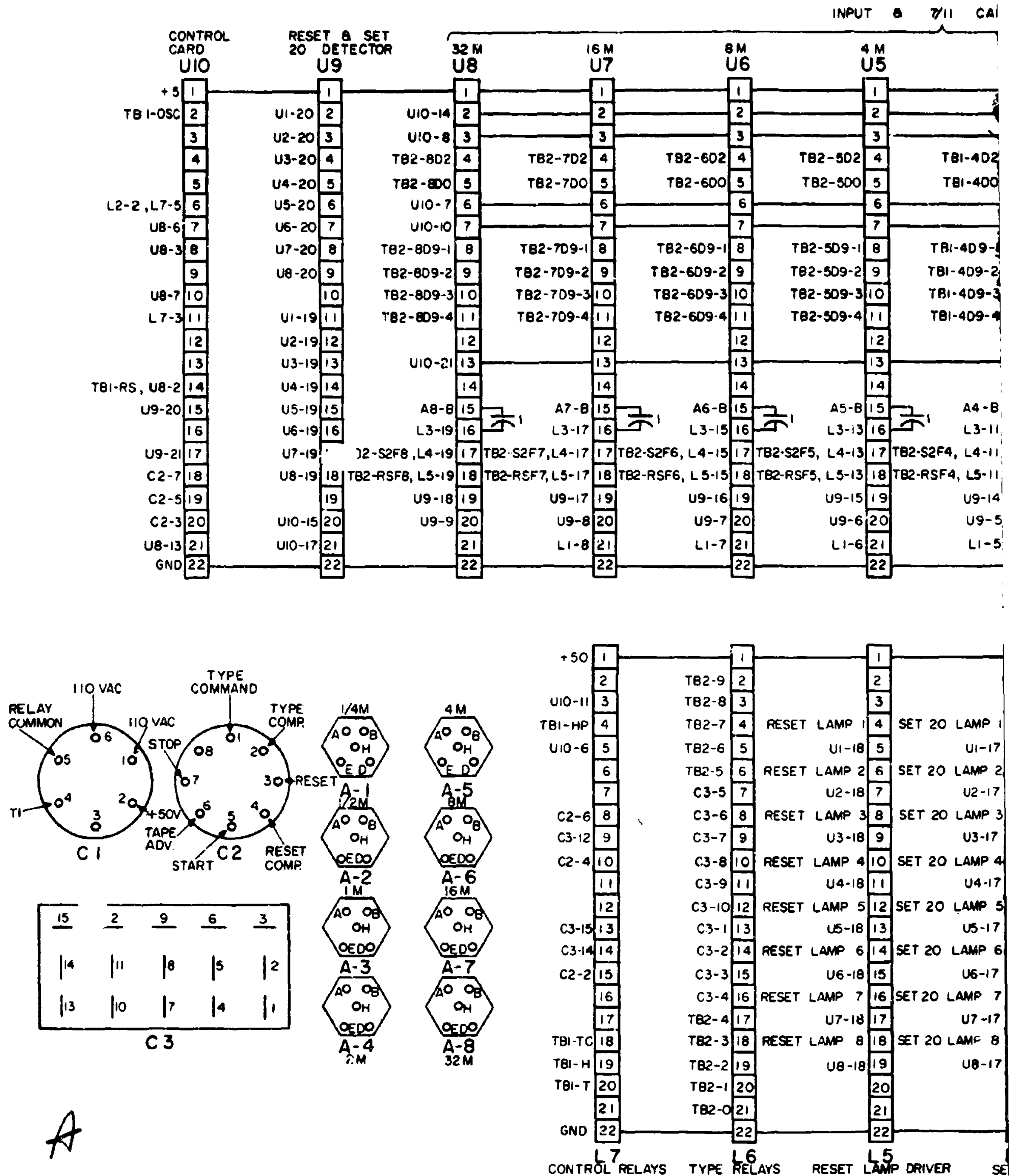

FIG. IV-11 MAIN FRAME

A

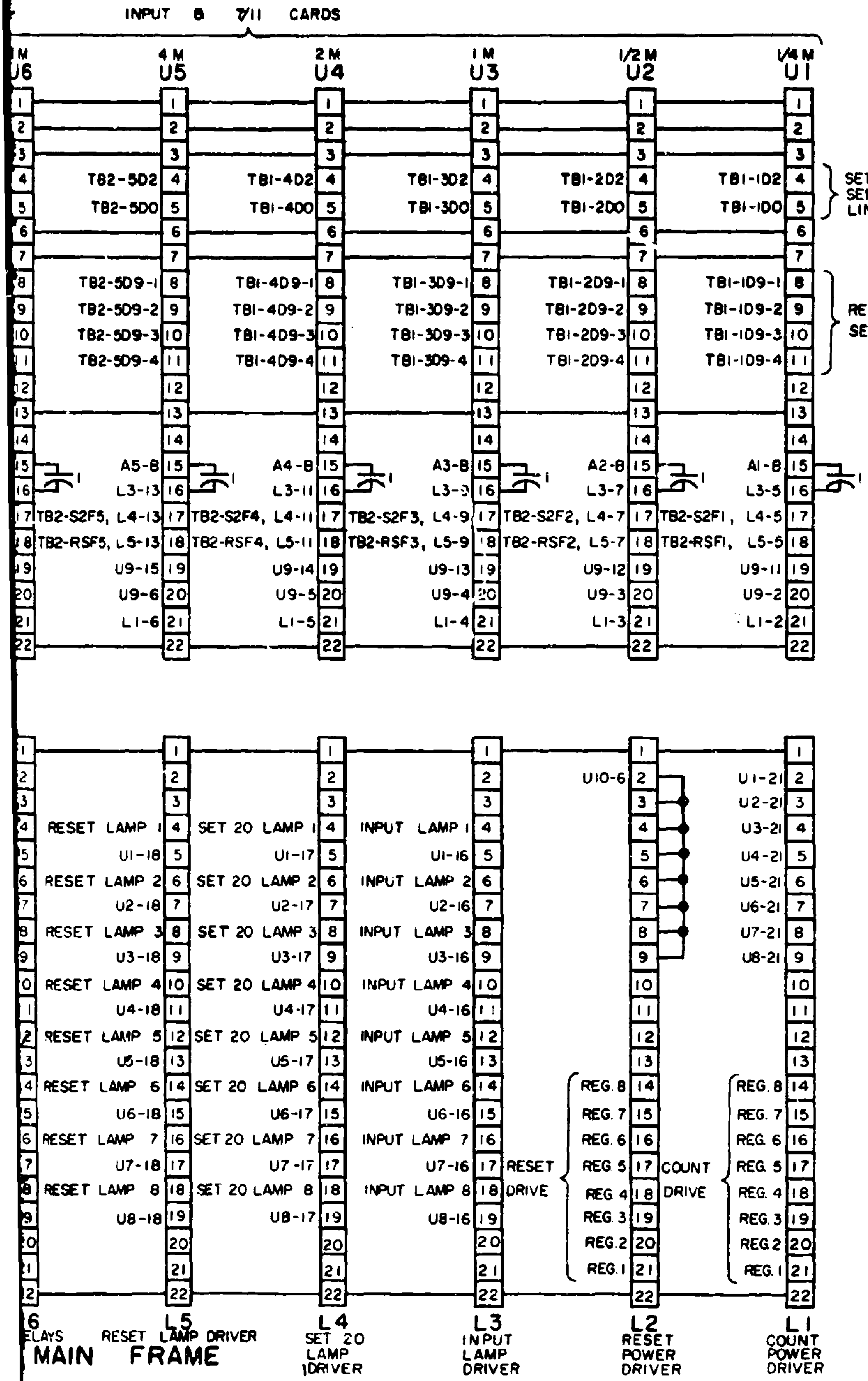

C3 CODE

1 – DIGIT 1
2 – DIGIT 2
3 – DIGIT 3
4 – DIGIT 4
5 – DIGIT 5
6 – DIGIT 6
7 – DIGIT 7
8 – DIGIT 8
9 – DIGIT 9
10 – DIGIT 0
11 – N.C.
12 – HI PUNCH
13 – N.C.
14 – HYPHEN
15 – TAB

B

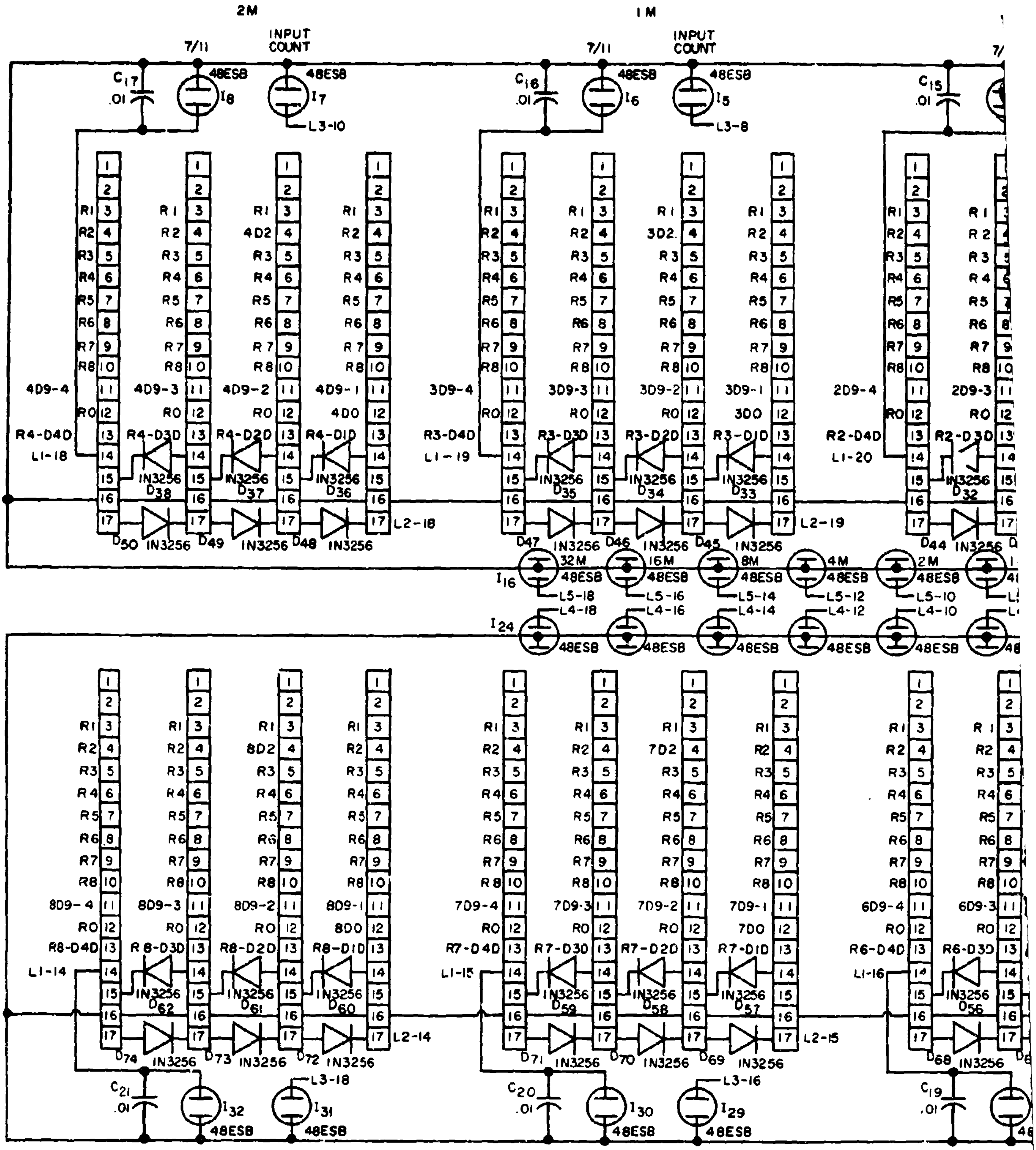

A

FIG. IV-12 FRONT PANEL REA

32 M

16 M

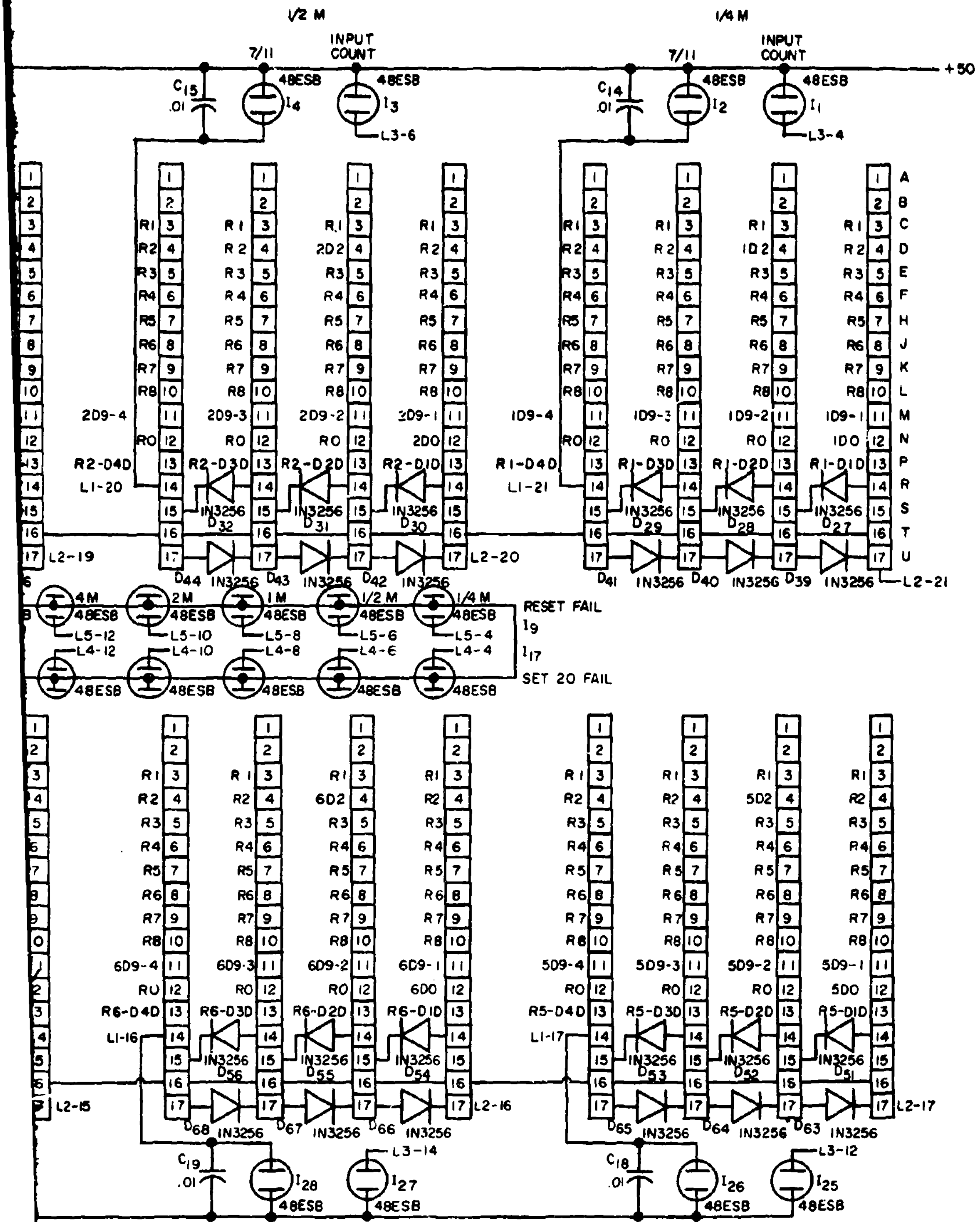

FRONT PANEL REAR WIRING

8 M

4 M

B

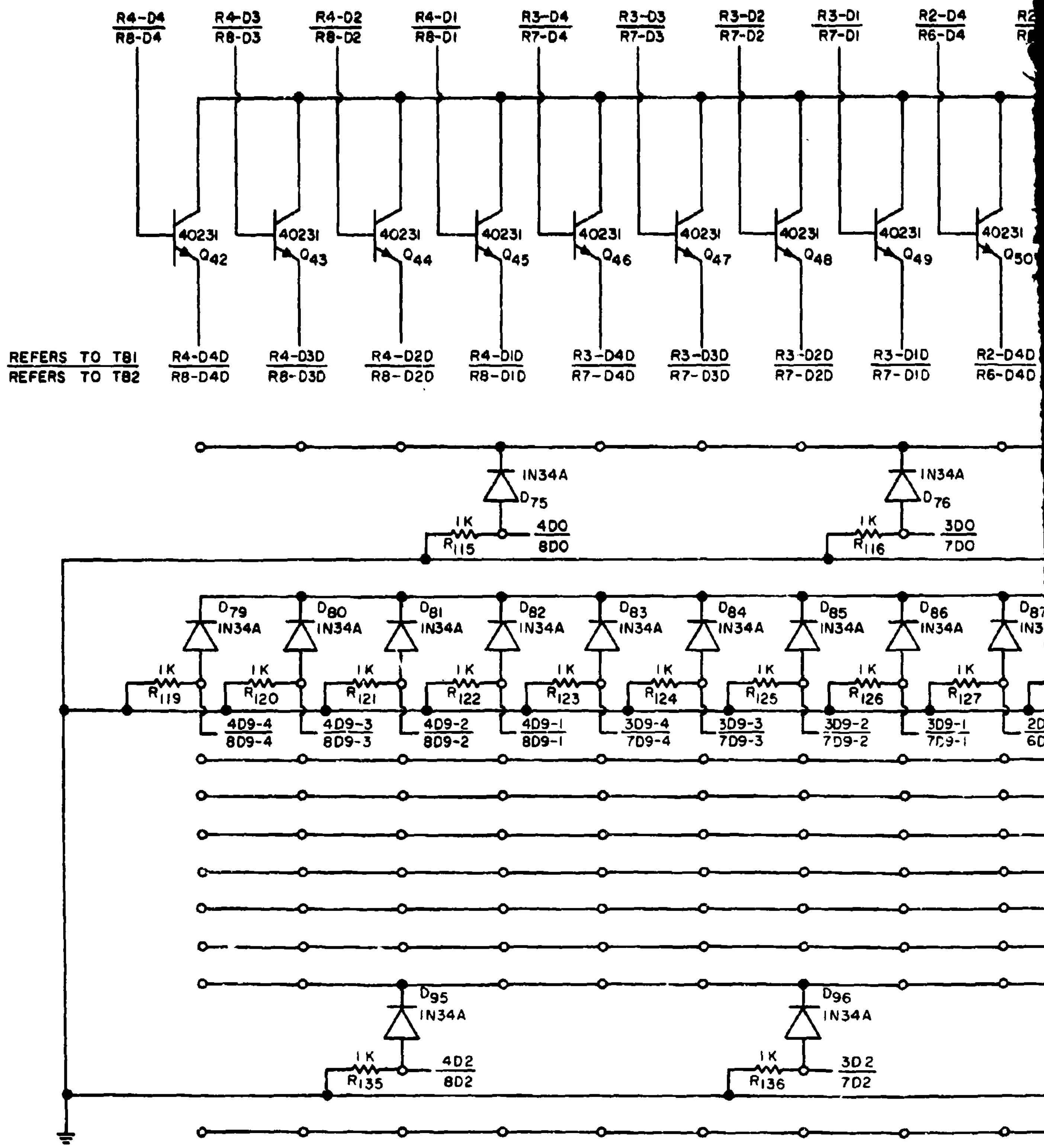

FIG. IV-13 DATA LINE

A

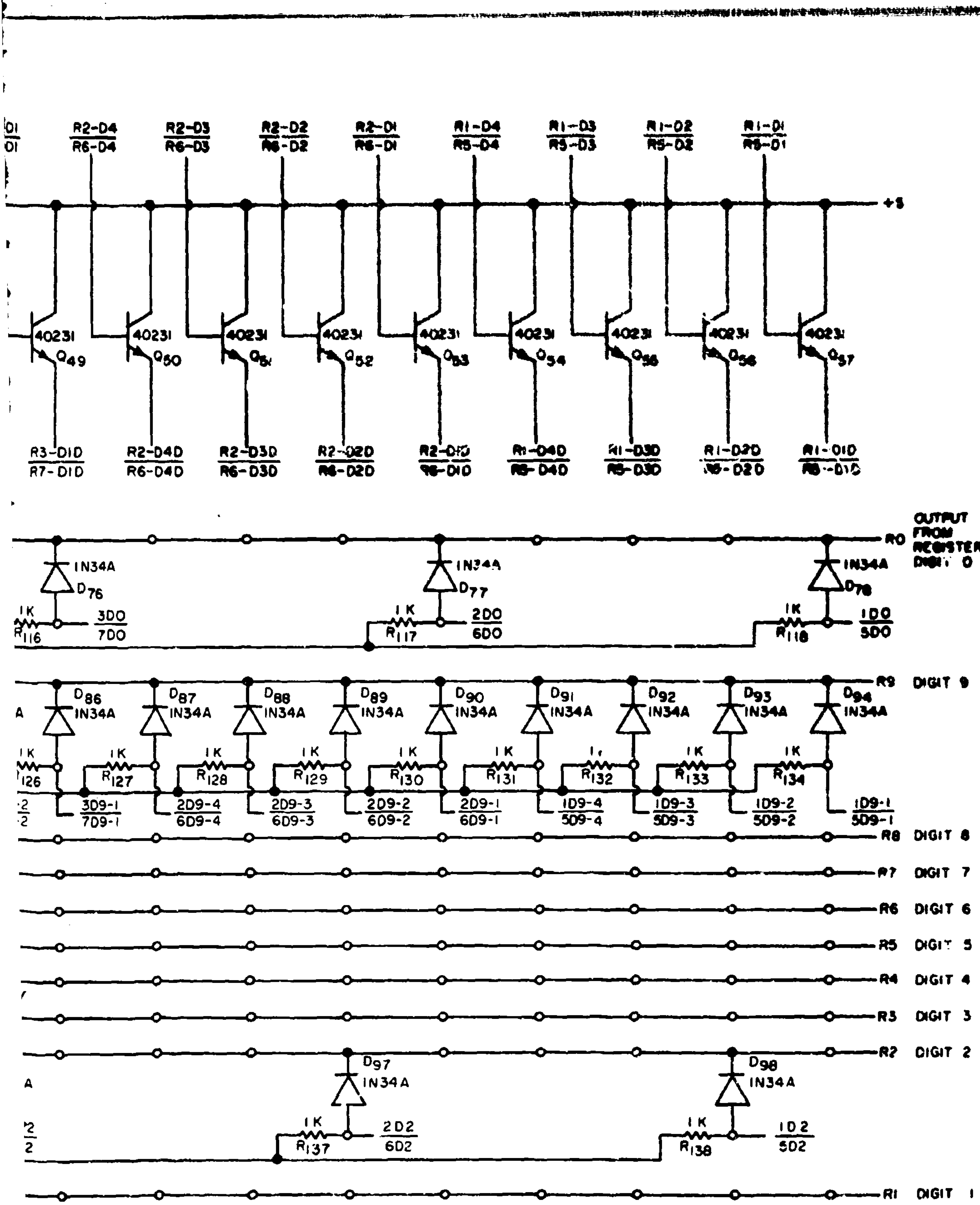

ATA LINE CONNECTIONS

B

Figures IV-10 through IV-14 show the signal flow pattern in the modified wind system and circuit wiring. It should be noted that integrated circuit (IC) modules in these and previous schematic diagrams are manufactured by Motorola. The IC signal levels are 5 volts.

The interconnection of the modified wind system to the control systems employed in the station trailers is given in Table IV-3.

B. Station Installation Characteristics

The station locations (see Fig. III-1) and configurations are schematically represented in Figures IV-15 and IV-16. The areal extent in the latter figures is a circle of 500 ft radius centered at the instrument tower.

The following tables show the soil characteristics at these stations.

Table IV-4. Soil Characteristics at Station A (Burleson County - 30° 29 min N - 96° 53 min W)

Depth	pH	O. M. %	P lb/acre	lb/acre	Ca lb/acre	Soluble salts lb/acre	Magnesium lb/acre	Na lb/acre
3 cm	5.1	1.3	1.2	116	1060	120	140	112
6 cm	6.3	0.8	2.4	46	620	120	110	112
12 cm	6.1	0.6	1.2	80	600	120	105	100
25 cm	6.5	0.5	3.6	30	420	120	110	100
40 cm	6.6	0.6	0	134	1200	120	475	100
65 cm	6.5	0.5	0	304	2540	120	>500	240
100 cm	6.1	0.2	0	324	1220	120	>500	476

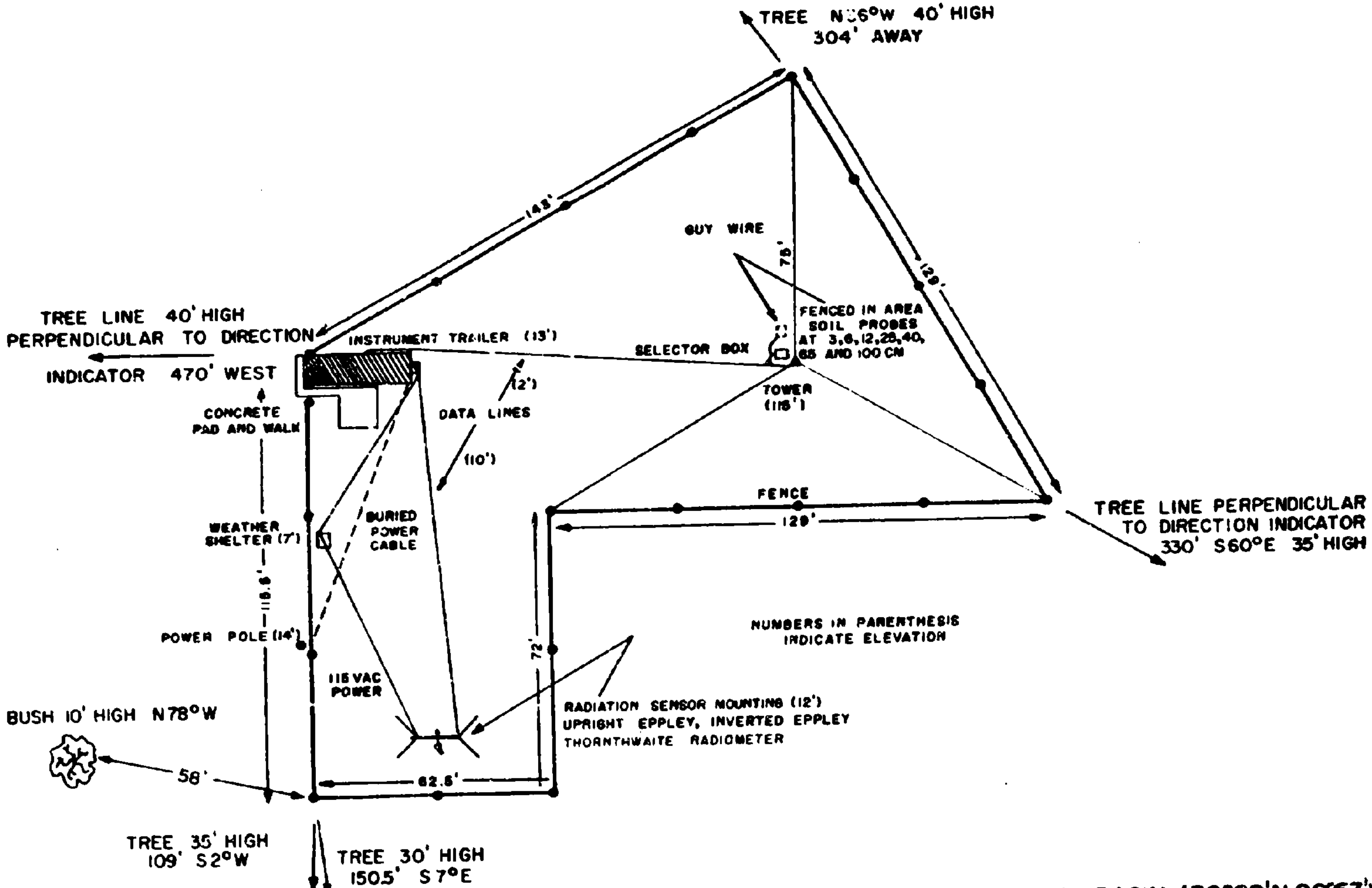

FIG. IV-15 SCHEMATIC REPRESENTATION OF STATION 'A' IN EAST YEGUA BASIN (30°29'N, 96°53'W)

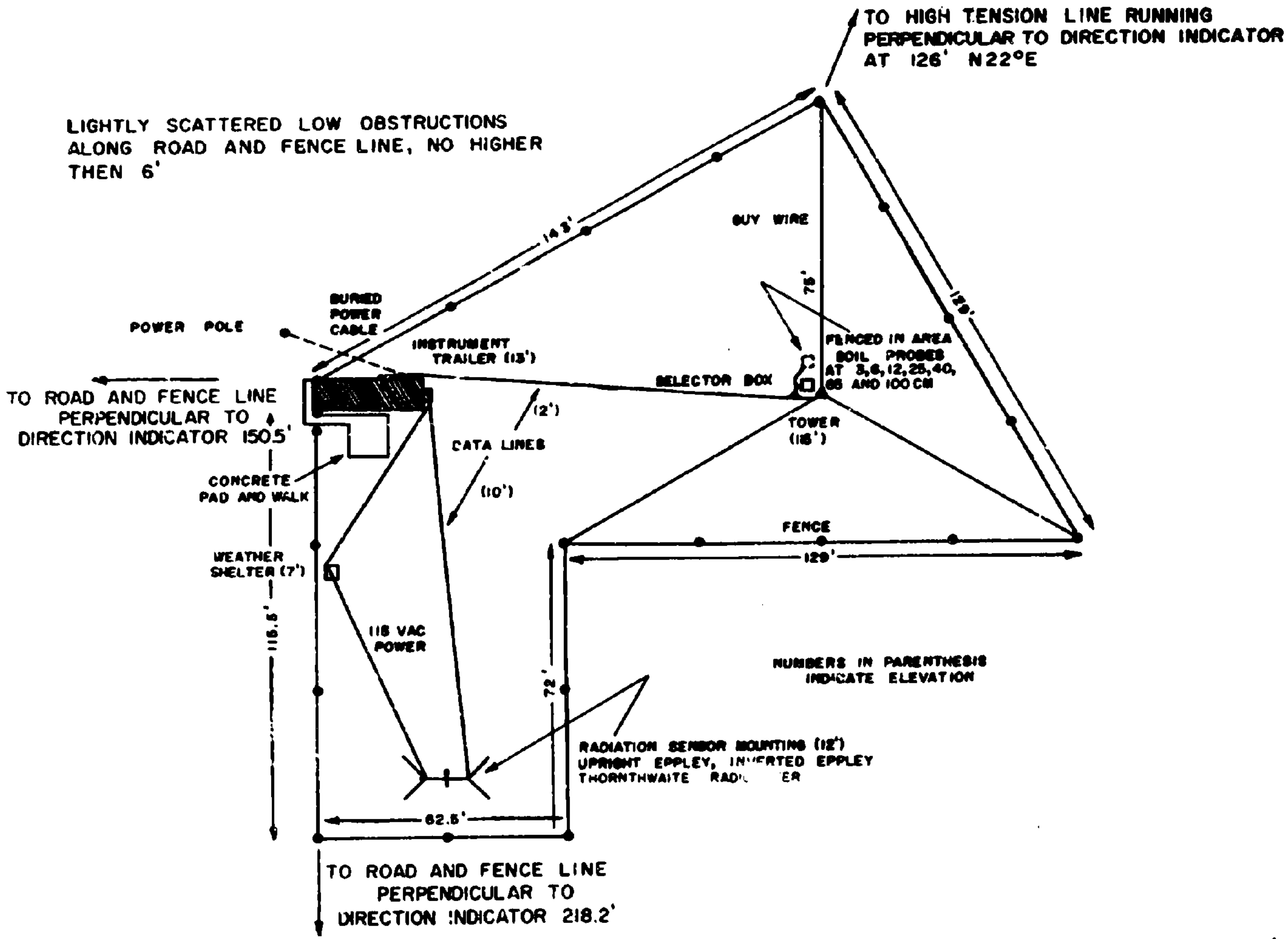

FIG. IV-16 SCHEMATIC REPRESENTATION OF STATION 'B' IN EAST YEGUA BASIN (30°32'N,91°58'W)

Table IV-5. Soil Characteristics at Station B (Lee County 30° 32 min N - 96° 58 min W)

Depth	pH	O. M. %	P lb/acre	K lb/acre	Ca lb/acre	Soluble salts lb/acre	Magnesium lb/acre	Na lb/acre
3 cm	6.7	0.5	6.2	382	2300	384	>500	620
6 cm	6.9	0.6	10.1	98	940	384	170	312
12 cm	7.7	0.4	20	464	2460	1104	265	430
25 cm	5.2	0.5	1.2	286	2840	288	>500	620
40 cm	5.4	0.5	1.2	232	2760	432	>500	1134
65 cm	6.1	0.4	1.2	196	3800	624	>500	1310
100 cm	7.1	0.3	1.2	186	3740	624	>500	1630

The soil type at Station A is similar to that classified as Bonham Loam while that at Station B is similar to the classification Tarrant Stoney Clay. Conductivity and specific heat determinations have not been made at this writing.

Both stations are located in pasture land in sparsely settled regions. The terrain can best be described y rolling with areas of medium to dense forestation ranging from 20 to 60 ft in height. These forested areas are scattered and tend to decrease in extent and frequency with distance from the Yegua Creek.

Stations A and B are completely self contained with respect to sensors, measuring systems, maintenance, calibration, and supporting equipment. Power is supplied from commercial sources (R. E. A.) as 230-115 volts, 60 cycle, single phase. Operation can be from motor driven generators.

As previously noted, the sensors outputs are converted to DC voltages and so scaled as to be numerically equivalent to conventional meteorological parameters. Calibration procedures for the sensors and the digital conversion system can be routinely performed without modification of the system itself, and in-line check procedures are incorporated to permit distinction between signal indication and correct operation.

The trailers housing the stations are 10 ton military semi-trailer vans (U. S. Army Model SKD 3809) of approximate dimensions 26 x 8 x 6.2 ft with an overall height of approximately 13 ft. The vans have been modified by installation of five windows, a side door, an air conditioner port, an interior lining of 1/2 in plywood, a floor covering of asphalt tile, and carrying boxes welded to the underside of the trailer for transport of cables, sensors, and station supplies.

The measurement tower is of triangular steel construction, 18 in on a side, made up of eleven 10 ft sections and one 5 ft section for an overall height of 115 ft (Rohn Model 40G). Triangular guying at 30 ft, 65 ft, and 95 ft is used to support the tower with concrete 'dead men' located 75 ft from the tower base as the guy anchors. The guys themselves are 3/8 in aircraft cable. The tower is supported by a concrete block, approximately 2 x 2 x 4 ft, in which the necessary bolts for securing the tower base platform are embedded. Erection of the tower is accomplished

by a floating gin pole which clamps to successive tower sections as construction proceeds. The weight of the 10 ft tower section is approximately 65 lb. The instrument arms are made of aluminum channel and 3/4 in aluminum tubing with the channel bolted to the tower side as support for the tubing which can be moved in and out from the tower. The arm installation at any level is so arranged that the anemometer cups and thermocouples are at the designated sensing elevation with the anemometer attached to the free end of the tubing, 5 ft from the tower side, and the thermochelter attached to the channel, 18 in from the tower side.

This completes the discussion of the modification and installation of the automatic meteorological station in the Yegua Watershed, except to note that the operation of these stations is conducted under Sub-task b. Operational scheduling and analytical procedures will be outlined in a technical report of that sub-task at a later date.

REFERENCES

Clayton, W. H., and B. J. Eckelkamp, 1963: Improvement, evaluation, and extension of capabilities of meteorological simulation. Final Rpt. Contract DA36-039 SC84942. Texas A & M Research Fdn., 63-1T.

Halstead, M. H., R. L. Richman, W. G. Covey, and J. D. Merryman, 1957: A preliminary report on the design of a computer for micrometeorology. J. of Met., 14.

King, B. L. D., 1963: An evaluation of heat flow transducers as a means of determining soil heat flow. M. Sc. thesis, Texas A&M University.

V. ANALOG MODELING

William H. Clayton and E. L. Deacon

The Themis portion of the analog modeling research being conducted at Texas A&M is primarily concerned with investigation of the applicability of various meteorological relationships commonly employed in model configurations. During the current reporting period, the main emphasis has been devoted to the frictional boundary layer and particularly to the concept and employment of exchange coefficients to provide necessary coupling of atmospheric model layers.

Although exchange coefficients are widely accepted as physically sound parameters describing turbulent flow characteristics, very little quantitative information is available and functional definition exists only as hypotheses. The basic definition of the exchange coefficient rests in the following equation, postulated by Wilhelm Schmidt (Sutton, 1953), based on an analogy of turbulent and laminar flow conditions as applicable to the flux of momentum.

$$\tau = \rho K_m \frac{dS}{dz} \qquad 1)$$

The term K_m in this relationship is the eddy coefficient for momentum, or eddy viscosity, which is presumed to be analagous to the kinematic viscosity of a fluid in laminar motion. The product ρK_m is the exchange coefficient.

The concept of analogy between the two flow patterns may

or may not be realistic. However, if one does accept the analogy then the definition of the exchange coefficient for momentum is as defined in Equation 1). Similar analagous reasoning leads to corresponding definitions for the eddy coefficients for heat and vapor, and no difficulties are encountered until an attempt is made to employ these coefficients in meaningful fashion in meteorological models. Such application necessarily involves usage of other meteorological relationships, often of the widely accepted variety, and this can lead to results that are questionable at best.

An illustration of this is afforded through any of the various diabatic profiles of wind, temperature, and vapor pressure that are relatively well known and employed. As an example, consider the following relations for wind and temperature given by Monin and Obukhov (1954),

$$\frac{dS}{dz} = \frac{u_*}{kz} \psi_1(\frac{z}{L}) \qquad 2)$$

$$\frac{d\theta}{dz} = \frac{\theta_*}{kz} \psi_2(\frac{z}{L}) \qquad 3)$$

where

$$L = - \frac{u_*^3 \bar{\theta} \rho C_\rho}{kgH} \qquad 4)$$

and

$$\theta_* = - \frac{H}{\rho C_\rho k u_*} \qquad 5)$$

All of the symbols employed have the usual meteorological designations as listed in the glossary at the end of this

report section. The functions ψ_1 and ψ_2 are not uniquely specified, but if the eddy coefficients for momentum and heat are assumed equal, then ψ_1 equal ψ_2. Further, if $|z/L|<1$, and $z >> z_o$, then the function can be approximated by

$$\psi(\frac{z}{L}) = 1 + \alpha\frac{z}{L} \tag{6)}$$

ignoring terms of order two and higher in a series expansion.

Substitution of 6) in 2) and 3) leads to the well known Monin-Obukhov profile relationships.

$$S = \frac{u_*}{k}[\ell n\frac{z}{z_o} + \alpha\frac{z}{L}] \tag{7)}$$

$$\theta - \theta_o = \theta_*[\ell n\frac{z}{z_o} + \alpha\frac{z}{L}] \tag{8)}$$

Substitution within 1), 3), 4), 7), and 8) yields

$$K_m = \frac{{u_*}^2 kSz\bar{\theta}}{\bar{\theta}Su_* + \alpha kgz(\theta - \theta_0)} \tag{9)}$$

Solving for u_* in 7) and substituting in 9), gives the eddy viscosity at height h as

$$K_{m,h} = \frac{k^2h[\bar{\theta}{S_h}^2 - \alpha hg(\theta_h - \theta_0)]^2}{\bar{\theta}S_h(\ell n\frac{h}{z_o})[\bar{\theta}{S_h}^2 + (1 + \ell n\frac{h}{z_o})\alpha hg(\theta_h - \theta_0)]} \tag{10)}$$

The value of α suggested by Monin and Obukhov is .6. Panofsky, Blackadar, and McVehil (1960), suggest α to be 4.5. No matter

the value, other than the trivial zero, it is seen that 10) can lead to negative values of K_m. Also, it can lead to K_m values that increase with decreasing wind speed. Neither of these possibilities are physically reasonable. To illustrate the preceding, Tables V-1 and V-2 below show $K_{m,h}$ values obtained from 10) for various wind and temperature values when h = 8 m, k = .4, $\bar{\theta}$ = 300 °K, g = 980 cm/sec^2, and z_0 = 2 cm. In Table V-1, α is chosen as .6 whereas in Table V-2, α is chosen as 4.5.

Table V-1. $K_{m,8}$ Values (cm^2/sec)

α = .6

S_8 m/sec	$(\theta_8 - \theta_0)$ °C				
	8	4	0	-4	-8
10	19152	20210	21364	22625	24009
5	7134	8638	10682	13612	18147
2.5	1420	2540	5341	21672	-19096

Table V-2. $K_{m,8}$ Values (cm^2/sec)

α = 4.5

S_8 (m/sec)	$(\theta_8 - \theta_0)$ °C				
	8	4	0	-4	-8
10	10576	14600	21364	34898	74721
5	1144	3040	10682	-47795	-12406
2.5	118	52	5341	- 3849	- 3520

This same physical inconsistency is met whatever profile relationships are used. However, use of a power profile for the wi ıd, and omission of direct consideration of a diabatic temperature profile improves the picture somewhat. For example, use of the Deacon profile.

$$\frac{dS}{dz} = \frac{u_* z^{-\beta}}{k z_o^{(1 - \beta)}} \qquad 11)$$

leads to the following expression for the eddy viscosity at height z

$$K_m = \frac{S k^2 (1 - \beta) z_o^{(1 - \beta)} z^{\beta}}{[(\frac{z}{z_o})^{(1 - \beta)} - 1]} \qquad 12)$$

Use of 12) depends on a functional definition of β. Professor Deacon suggests the following empirical relationship

$$\beta = 1 - 1.43Ri - 6Ri^2 - 10Ri^3 \qquad 13)$$

where Ri is the layer Richardson number between the surface and elevation h(z_o = 2 cm).

Substituting 13) in 12) and using the same values of h, $\bar{\theta}$, g, and k employed previously, leads to the K_m values shown in Table V-3. As noted previously, all inconsistency is not removed as can be seen for S_8 = 5 m/sec and $\theta_8 - \theta_0$ = -8°C.

Table V-3. $K_{m,8}$ Values (cm^2/sec)

S_8(m/sec)	$(\theta_8 - \theta_0)$, °C				
	8	4	0	-4	-8
10	15825	18513	21364	24337	27392
5	2197	5528	10682	16787	22559
2.5	0	60	5341	15218	26950

In the discussion of the Monin and Obukhov relationship, the question of physical contradiction rests with two concepts; the log-linear profiles, and the eddy viscosity definition. The Deacon profile introduces another factor, the Richardson number.

In view of the extensive employment of the latter as a stability criterion, it would seem illogical to question its worth. However, a careful analysis of the concepts utilized in its derivation provides some understanding why its determinations from profile measurements leads to numerous inconsistencies. In fact, one is led to believe that extensive employment of the Richardson number could be more a matter of discussion than practice.

Use of the Richardson number in objective modeling experiments requires application to finite layers. Thus in the determination of Table V-3, the layer Richardson number was defined as

$$Ri_{0}^{8} = \frac{gz_8(\theta_8 - \theta_0)}{\bar{\theta} S_8^{\,2}} \qquad 14)$$

Obviously the application of 14) to light wind gradients is limited. Presumably, one can retreat from such situations through

speculation concerning data reliability under such conditions, but it seems feasible to question also the inherent validity of a relation that is applicable to continuous phenomena when the relation incorporates discontinuity (as a second order pole).

Several possibilities exist to rectify this difficulty and the addition of a threshold wind, or turbulent anomaly to the mean wind, is efficacious. With this approach 14) becomes

$$Ri_{0}^{8} = \frac{gz_8(\theta_8 - \theta_0)}{\bar{\theta}(S_8 + b)^2} \qquad 15)$$

Use of this relation (b = 3 m/sec) with 12) and 13) gives the K_m values shown in Table V-4.

Table V-4. $K_{m,8}$ Values (cm^2/sec)

S_8(m/sec)	$(\theta_8 - \theta_0)$°C				
	8	4	0	-4	-8
20	40540	41630	42727	43835	44951
10	18007	19660	21364	23111	24892
5	6517	8489	10682	13024	15436
2.5	1565	3153	5341	7858	10332
1.25	217	1004	2670	4777	6547
.63	21	304	[illegible]	2755	3733
.31	2	100	668	1498	1998

The range of modified Ri in Table V-4 is 0 to $\pm$.2.

None of the values given in Table V-4 are mathematically or meteorologically inconsistent and the values of K are comparable to those obtained with other profile relations. Further, model solutions of the parameters of the frictional boundary layer are mathematically possible for wind and temperature values that were previously excluded and, no model degradation of previously included values occurs. Of course, this cannot be considered as an indication of meteorological correctness and further investigation is underway. Rather, it permits model experiments for further improvement of objective forecasting in the frictional boundary layer.

No rigorous justification exists for the introduction of the mean wind speed anomaly in the layer Richardson number, as shown in 15), other than its usage removes mathematical discontinuity. This type of justification is not without precedence in meteorology as is evidenced by the term z_o in the adiabatic and diabatic profile equations. However, z_o has been used so often in the literature that it is now accepted as a parameter representing the nature of the surface over which the wind (or other fluids) is flowing. In fact, tables of z_o (surface roughness) have been prepared from application (usually erroneously) of the adiabatic profile law, for various types of surfaces.

Extension of eddy coefficients determination above the layer of constant (with elevation) flux values is also being pursued.

The basic relationship is a modification of the equation suggested by Clayton, Covey, and Merryman (1957)

$$K_{m,z} = c\, K_{m,\ell} \frac{z}{Z}\left(1 - \frac{z}{Z}\right)^2 \qquad 16)$$

where Z is the vertical extent of the frictional boundary layer, ℓ is the vertical extent of the constant flux layer, and $\ell < z < Z$.

Use of 16) has been limited until now by too close coupling of $K_{m,z}$ with $K_{m,\ell}$ and unrealistic values of $K_{m,\ell}$. The latter has been resolved by the modified layer Richardson number and improvement of the former is being sought through modification of 16) by a stability parameter as indicated below.

$$K_{m,z} = c\, K_{m,\ell} \frac{z}{Z}\left(1 - \frac{z}{Z}\right)^2 (1 - \gamma Ri)^{\pm n} \qquad 17)$$

In this equation, n is an integer or an integer reciprocal. Ri is a modified layer Richardson number of the form given in 15).

Investigation in this area has not progressed sufficiently to justify conclusions as to useful applicability.

An approach to K_m determinations in the frictional boundary layer for wider extremes of stability is suggested by Professor Deacon. This approach, in part empirical, is directly addressed to the Low Level Meteorological Model.

Direct measurements of shearing stress as shown in Fig. V-1 as well as data from other researchers (e.g. Deacon 1953) support the following relationship

$$\frac{u_*}{z\partial S/\partial z} = kf(Ri) \qquad 18)$$

Results at more unstable conditions than Ri = -0.4 are as yet lacking as the usual unsteadiness of strongly unstable conditions makes it difficult to secure reliable observations. On the stable side, beyond Ri = 0.1, turbulence decreases further and recent work (Okamoto and Webb, in press) shows that turbulence in the usual sense has decreased to zero at a height of 2 m when Ri = 0.2. Radiative heat exchange is important when turbulence is small so 18) is not expected to hold beyond about Ri ~ 0.15.

Some simple linear approximations to f(Ri), as noted previously, have been used for near-neutral conditions but if applied over a wider stability range are found to be unsatisfactory. It is therefore feasible to investigate a non-linear form despite the added complexity in computation. Further, no formulation has been proposed which is valid for both stable and unstable conditions and it is necessary to treat them separately.

A formula proposed by Webb for unstable conditions fits the data of Fig. V-1 quite well but the 'Keyps' formula is but little different as may be seen from Lumley and Panofsky (1964, p 113, Fig. 3.3) and the latter has been used herein. This is

$$\frac{u_*}{z\partial S/\partial z} = k(1 - \gamma' Ri)^{1/4} \qquad 19)$$

in which γ' = 18 is suggested by Panofsky on the basis of

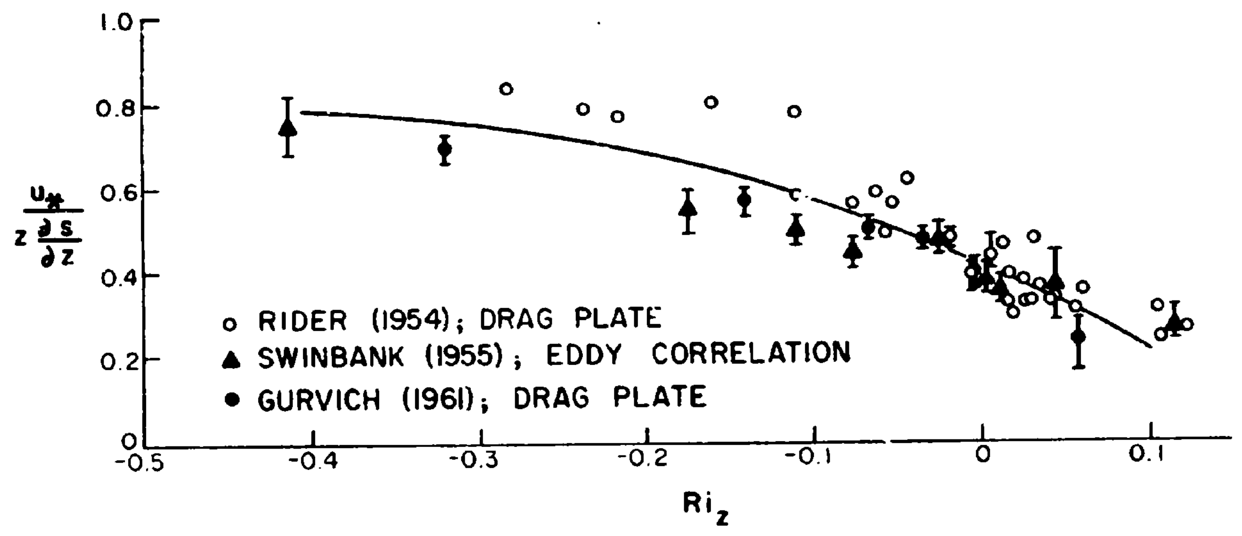

FIG. V-I THE VARIATION OF THE FRICTION VELOCITY / WIND GRADIENT RELATIONSHIP WITH STABILITY AS MEASURED BY THE RICHARDSON NUMBER (Ri).
(Where observations have been grouped, the vertical lines indicate the standard error of the mean).

observational material at O'Neill and elsewhere. Equation 19) can also be written as

$$P^4 + \gamma'(\frac{z}{L'})P^3 = ? \qquad 20)$$

in which $P = \frac{kz\partial S/\partial z}{u_*}$

and $L' = \frac{u_*(\partial S/\partial z)\theta}{kg(\partial\theta/\partial z)}$

On the assumption that the ratio of the eddy coefficients of heat and momentum is constant (γ), then L' is related to the Obukhov L by

$$L' = \gamma L \qquad 21)$$

In the following, use is made of the integrated form

$$S = \frac{u_*}{k}\{\ln\frac{z}{z_o} - \psi(\frac{z}{L'})\}$$

The function $\psi(z/L')$ has been computed by Panofsky and is reproduced in Fig. V-2.

An approximate solution for 20) for $(z/L') < 1$ is given by 7) which is assumed valid for stable conditions with $\alpha = 5$.

With other than linear approximations to 18) there is the difficulty that explicit relationships for u_* and K_m are unobtainable. This arises from the fact that u_*, for a given S_8, depends on the stability conditions from the surface up to 8 m and the stability conditions depend not only on temperature gradient but also on the

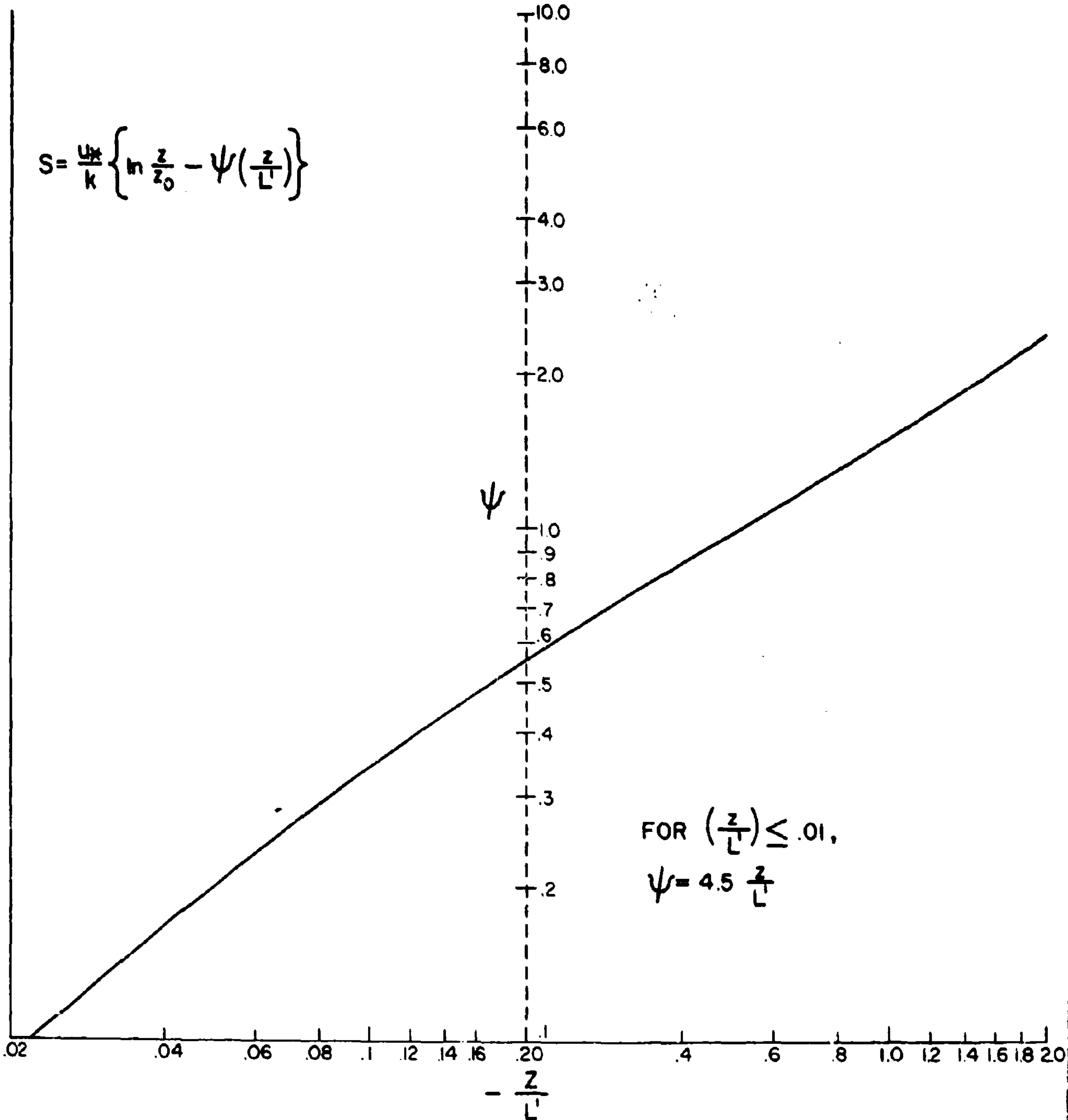

FIG. V-2 FUNCTION ψ FOR KEYPS WIND PROFILE (TAKEN FROM LUMLEY AND PANOFSKY: p. 113)

value of u_*. This makes it necessary to proceed by successive approximations as will be seen later.

Utilizing the preceding, the problem is to find u_*, $K_{m,8}$ and D_8 given:

S_8 = wind speed at 8 m height

θ_8, θ_0 = potential temperatures at 8 m and at the surface, and

z_o = the roughness parameter of the surface.

The stability criterion to be employed is a layer Richardson number for the surface to 8 m layer as shown in 14). With similarity between wind and temperature profiles it is easily shown that

$$(z/L')_8 = \frac{k Ri_o^8}{u_*/S_8} \qquad 23)$$

The procedure in establishing the relationship between u_*/S_8 and Ri_o^8 is as follows:

1) A rough estimate of u_*/S_8 is made for a given value of Ri_o^8 to obtain $(z/L')_8$ from Equation 23)
2) The $(z/L')_8$ estimate gives ψ_8 from Fig. V-2
3) With the given z_o for the surface and ψ_8 the value of u_*/S_8 is obtained from Equation [illegible]
4) The improved estimate of u_*/S_8 is employed in Steps 1 to 3 until no significant change occurs

For z_o = 2 cm the resulting relationship is the full line of Fig. V-3.

To obtain K_m knowing u_* one makes use of the flux equation

$$u_*^2 = K_m \, \partial S/\partial z$$

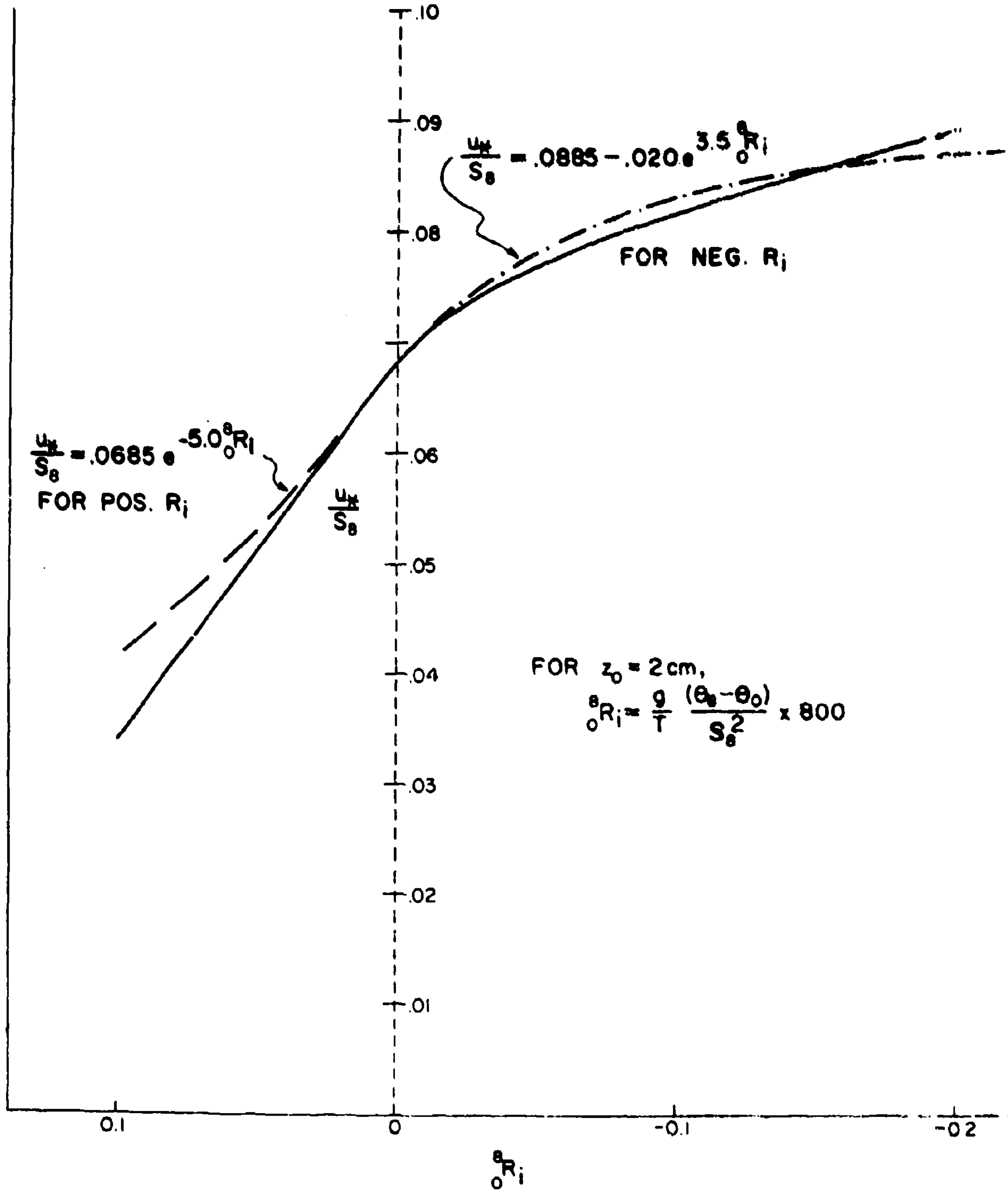

FIG. V-3 $\frac{u_*}{S_8}$ VERSUS ${}_0^8Ri$

which gives

$$\frac{K_{m,8}}{S_8} = (\frac{u_*}{S_8})(\frac{u_*}{z\partial S/\partial z})z_8 \qquad 24)$$

A graph of P versus z/L' constructed from Equation 20) gives the value k/P which is the quantity in the second bracket of Equation 24). As u_*/S_8 has already been obtained, $K_{m,8}/S_8$ is found. For $z_o = 2$ cm the resulting relationship is the full line of Fig. V-4.

The exchange coefficient D_8 defined by

$$u_*^2 = D_8 S_8 \qquad 25)$$

is obtained from u_*/S_8 as

$$\frac{D_8}{S_8} = (\frac{u_*}{S_8})^2 \qquad 26)$$

This graphed in Fig. V-5.

To apply these results in the LLMM analog computations it is necessary to fit simple mathematical expressions to the curves of Fig. V-3 and V-4. Expontential expressions appear the most suitable if different expressions are used for positive and negative Ri_0^8. They can be chosen to make u_*/S_8 and $K_{m,8}/S_8$ approach reasonable asymptotic values at large negative Ri_0^8. An exponential decrease of these values with increasing positive Ri_0^8 also has the merit of avoiding the negative values which can occur using linearized relationships.

The relationships shown in Fig. V-3, V-4, and V-5 as broken

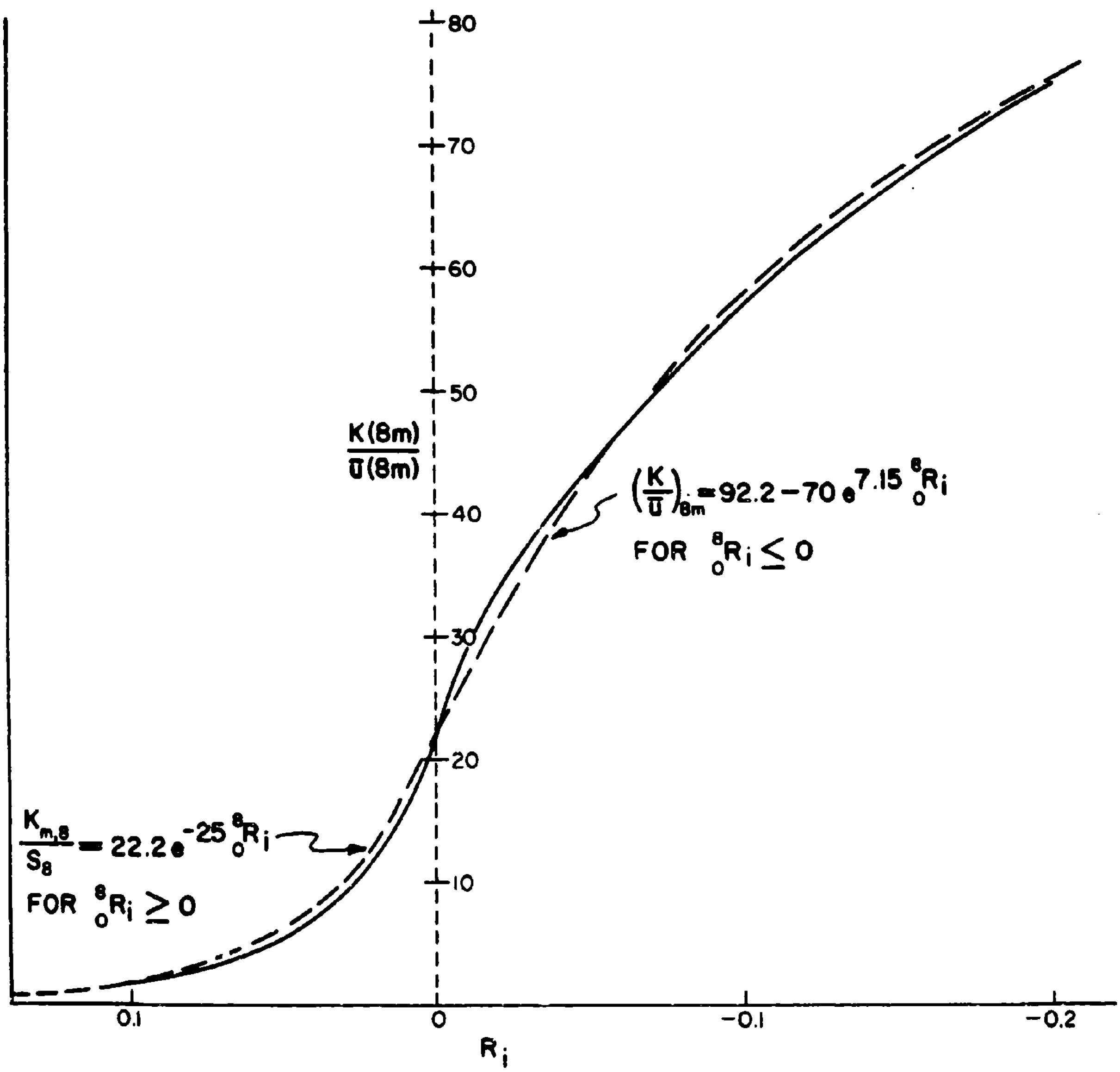

FIG. V-4 8m EXCHANGE COEFFICIENT VERSUS ${}^{8}_{0}R_i$ (FOR $z_0 = 2cm$).

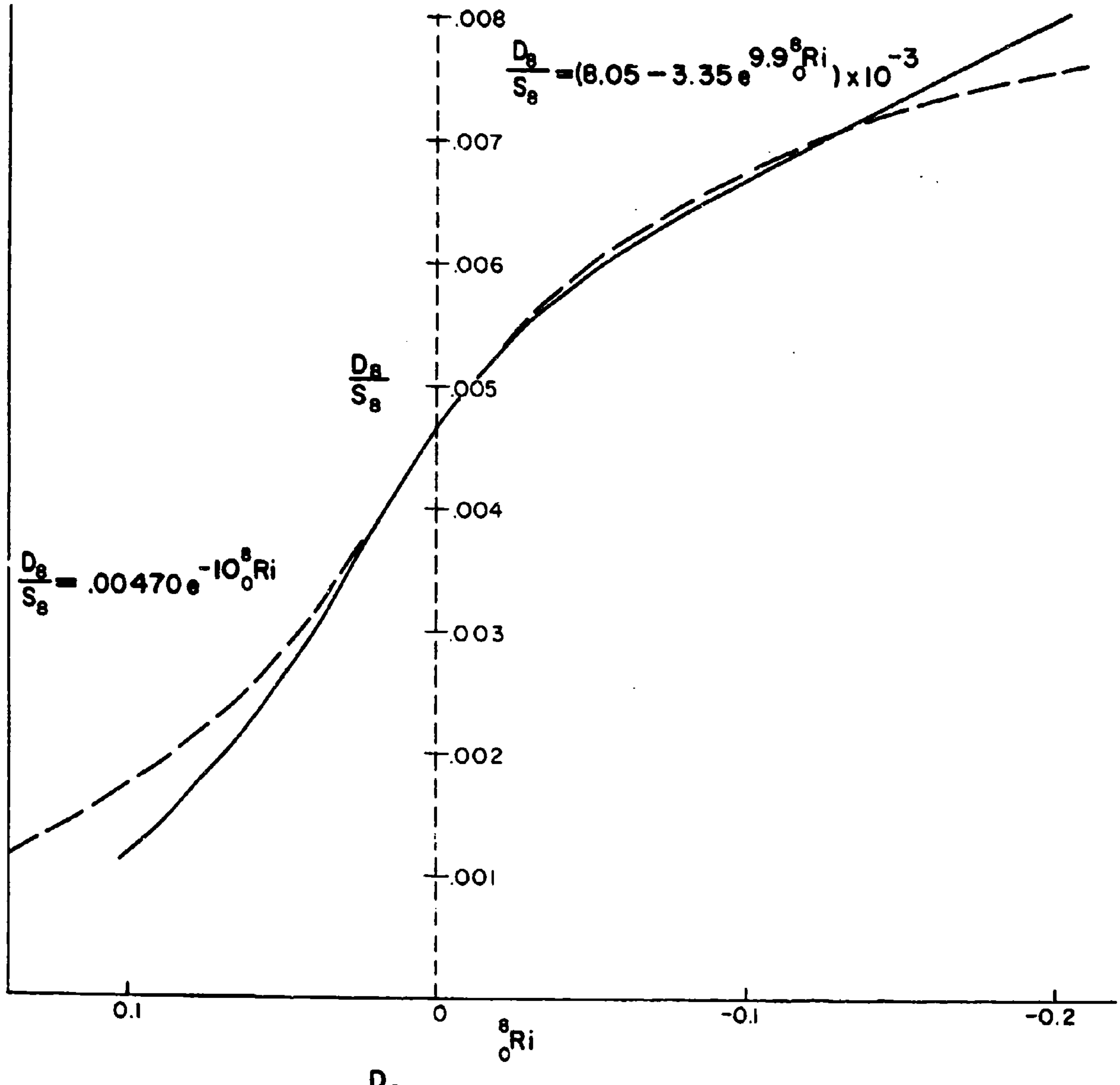

FIG. V-5 $\frac{D_8}{S_8}$ VERSUS ${}_0^8Ri$

lines are listed below.

Unstable conditions and $z_o = 2$ cm

$$u_*/S_8 = 0.0885 - 0.020 \exp(13.5 \overset{8}{\underset{o}{Ri}}) \quad 27)$$

$$D_8/S_8 = \{8.05 - 3.35 \exp(9.9 \overset{8}{\underset{o}{Ri}})\} \times 10^{-3} \quad 28)$$

$$K_{m,8}/S_8 = 92.2 - 70 \exp(7.15 \overset{8}{\underset{o}{Ri}}) \quad 29)$$

Stable conditions and $z_o = 2$ m

$$u_*/S_8 = 0.0685 \exp(-5.0 \overset{8}{\underset{o}{Ri}}) \quad 30)$$

$$D_8/S_8 = 0.00470 \exp(-10.0 \overset{8}{\underset{o}{Ri}}) \quad 31)$$

$$K_{m,8}/S_8 = 22.2 \exp(-25.0 \overset{8}{\underset{o}{Ri}}) \quad 32)$$

Similar calculations can be made for a number of other roughness values and the coefficients in Equations 27) to 32) graphed against z_o.

Table V-5 shows the various ratios to the 8 m wind for $z_o = 2$ cm.

Table V-5. Ratios of u_*, $K_{m,8}$ and D_8 to the 8 m Wind Speed Computed for $z_o = 2$ cm

$\overset{8}{\underset{o}{Ri}}$	$(z/L')_8$	$\frac{u_*}{S_8}$	$\frac{K_{m,8}}{S_8}$	$\frac{D_8}{S_8} \times 10^3$
+.10	1.202	.0341	1.6	1.16
+.06	0.515	.0478	4.4	2.28
+.04	0.300	.0547	7.2	2.99
+.02	0.133	.0618	12.0	3.82
0	0	.0685	22.5	4.69
-.01	-0.058	.0710	28.5	5.04
-.02	-0.112	.0730	33.5	5.33
-.03	-0.165	.0745	37.5	5.55

Table V-5—Continued

Ri_o^8	$(z/L')_8$	$\frac{u_*}{S_8}$	$\frac{K_{m,8}}{S_8}$	$\frac{D_8}{S_8} \times 10^3$
-.05	- .266	.0771	44.0	5.94
-.07	- .362	.0794	50.0	6.30
-.10	- .500	.0820	57.0	6.72
-.15	- .715	.0858	67.0	7.36
-.20	- .910	.0895	75.0	8.01

Direct comparison of Tables V-4 and V-5 cannot be made since the range of layer Richardson numbers in the former is limited. Approximately, however, $K_{m,8}$ values from Table V-5 are nearly a factor of 2 greater for negative Ri than those of Table V-4, an order of magnitude less for positive Ri, and, of course, good agreement exists for Ri = 0.

The question of an acceptable diabatic ind profile, for all stabilities, is far from settled and investigations continue. An empirical approach based on data collected at Stations A and B during their Dallas employment is the subject of a master's thesis by Mr. Richard Williams. It is expected that this thesis investigation will be completed in January 1969.

Several other areas are under study in the analog modeling activities. Assessment of these efforts will be deferred pending real-time forecast evaluations of the LLMM which are scheduled to begin in early 1969. These efforts, only partially under Themis

sponsorship, will be done cooperatively with the Meteorological section of Dugway Proving Ground.

GLOSSARY

b	turbulent anomaly to mean wind	(cm/sec)
c	parameter in the equation for K_m as a function of elevation	non-dimensional
C_ρ	specific heat of air at constant pressure	(cal/gm deg)
D_8	integral exchange coefficient for momentum between surface and 8 m	(cm/sec)
g	gravitational acceleration	(cm/sec^2)
h	elevation of constant flux level	cm
H	convective heat flux	(cal/cm^{2}sec)
k	Von Karman constant (.4)	non-dimensional
K_m	eddy viscosity	(cm^2/sec)
L	turbulent scale length	cm
P	normalized logarithmic wind shear	non-dimensional
Ri	layer Richardson number	non-dimensional
S	mean wind speed	(cm/sec)
u_*	frictional wind speed	(cm/sec)
z	elevation	cm
z_o	surface roughness length	cm
Z	elevation of upper limit of frictional boundary layer	cm
α	parameter in log plus linear diabatic wind profile	non-dimensional
β	parameter in Deacon wind profile	non-dimensional
γ	parameter in the equation for K_m as function of elevation and stability	non-dimensional

θ	mean potential temperature	deg C
θ_*	friction temperature	deg C
$\bar{\theta}$	mean potential temperature of layer	deg K
ρ	air density	(gm/cm^3)
τ	horizontal shear stress	$(dynes/cm^2)$
ψ	stability function	non-dimensional

REFERENCES

Clayton, W. H., W. G. Covey, and J. D. Merryman, 1957: Design of experimental meteorological simulators. Third Quarterly Progress Rpt. Contract DA-36-039 SC-74975. Texas A&M Research Fdn., 58-16T.

Deacon, E. L., 1953: Vertical profiles of mean wind in the surface layer of the atmosphere. Met. Office, London; Geophys. Mem. No. 91.

Gurvich, A. S., 1961: Measurement of drag in the surface layer of the atmosphere. Izv. Akad. Nk. SSSR. (Geophys. Ser.), 3, 458-466.

Lumley, J. L. and H. A. Panofsky, 1964: The structure of atmospheric turbulence. Interscience Publishers.

Monin, A. S., and A. M. Obukhov, 1954: Basic regularity in turbulent mixing in the surface layer of the atmosphere. USSR Academy of Science, Geophysical Institute, 24, 151.

Panofsky, H. A., A. K. Blackadar, and G. E. McVehil, 1960: The diabatic wind profile. Quart. J. Roy. Meteor. Soc., 86, 369.

Rider, N. E., 1954: Eddy diffusion of momentum, water vapour, and heat near the ground. Phil. Trans. Roy. Soc., 246, 481-501.

Sutton, O. G., 1953: Micrometeorology. McGraw-Hill.

Swinbank, W. C., 1955: Eddy transports in the lower atmosphere. CSIRO Australia, Div. Meteorol. Phys., Tech. Paper No. 2.

VI. TURBULENT FLOW DEFINITION THROUGH REYNOLDS STRESSES MEASUREMENTS

William H. Clayton

The design of the mobile Reynolds Stress facility has been completed and construction of the station has begun. Initially, the planning called for pulse sonics, using three four-head crossed-path systems at each of two measuring levels. The crossed-path systems were subsequently abandoned in favor of a single transmitter with six receivers arranged in a three dimensional orthogonal pattern at each level. Inasmuch as choice of the pulse type was largely based on construction of a prototype, it was felt that a more thorough study of continuous wave types should be pursued, since, the latter could lead to somewhat simpler analyzing and processing circuitry. It was later found, more or less as expected, that the continuous wave sonic continued to introduce excessive design complications to eliminate reflection interference, and consideration for this type sonic was abandoned and final choice was made of a pulse sonic with the single transmitter and six receivers, per level, configuration.

Analyses of various possible control systems, that is, small digital computers, was quickly completed, and twelve different manufacturers of such equipment were initially considered. However, design criteria, costing, power consumption, and size reduced the computer choice to four. These were:

1) Sigma 2-Scientific Data Systems
2) DEP 516-Honeywell
3) SEL 810A-Systems Engineering Laboratories
4) 2116B-Hewlett Packard

All of these computers are so-called third generation types, employing integrated circuitry and any of them would be adequate for the required purposes. Bid requests were submitted, but then deferred when it was realized that the interfacing problem was too heavily dependent on the computer to be employed to permit feasible project construction, and it was decided to incorporate external counting registers and computer interfacing as a part of the computer requirements. Modified specifications were submitted to the companies noted above and, after some reluctance on the part of one or two of the manufacturers, formal bid responses were received. The general specifications for the control computer were as follows.

1. Word length - 16 bit
2. Maximum memory cycle time - 3μ sec.
3. Memory capacity - 8K (16K as option if available in basic machine housing)
4. Hardware multiply and divide
5. ASR-33 teletype input - output with necessary interface (also ASR-35 as option)
6. Power requirements - 115/230 VAC, 60 cycle, single phase
7. Fortran IV - usage requirements as additional cost, hardware or software
8. Special features (in-board or out-board)
   a. One megacycle clock
   b. Sixteen registers (16 bit) which can be separately interrogated and cleared by the computer and which will separately accumulate clock pulses until a stop pulse is received from an external transducer. Each register must be supplied with an overflow indicator which can be recognized by the computer to identify incorrect data.

The successful bidder was the Honeywell Company, and the process controller, complete with external registers and interfacing, with ASR 35 teletype input/output was ordered in November of this year.

The use of sixteen registers is to accomodate the twelve sonic signals (six at two levels of measurement), two temperature signals at each level, and two spares.

Temperature measurements will be made with fast response thermistors whose outputs are converted to frequencies. The measurement of temperature, independent of the sonic system, is considered important inasmuch as the sonic temperatures, obtained from the sonic system, are dependent on vapor content of the air. In addition, independent temperature measurements will permit heat flux computations, using the two spare channels for vertical velocity determinations by other sensors, from two unrelated sources.

Planned housing for the mobile facility is shown in Fig. VI-1. This housing is a renovated and modified form of a former AN/GRC-26 radio station. Initial planning had called for the use of a housing of the pickup camper type, but the no-cost availability of the radio housing plus additional space made this a feasible substitution.

Station mobility is obtained through mounting of the housing on a 1 1/2-ton truck (obtained through the General Services Administration).

Planning is not complete as to tower and instrument support

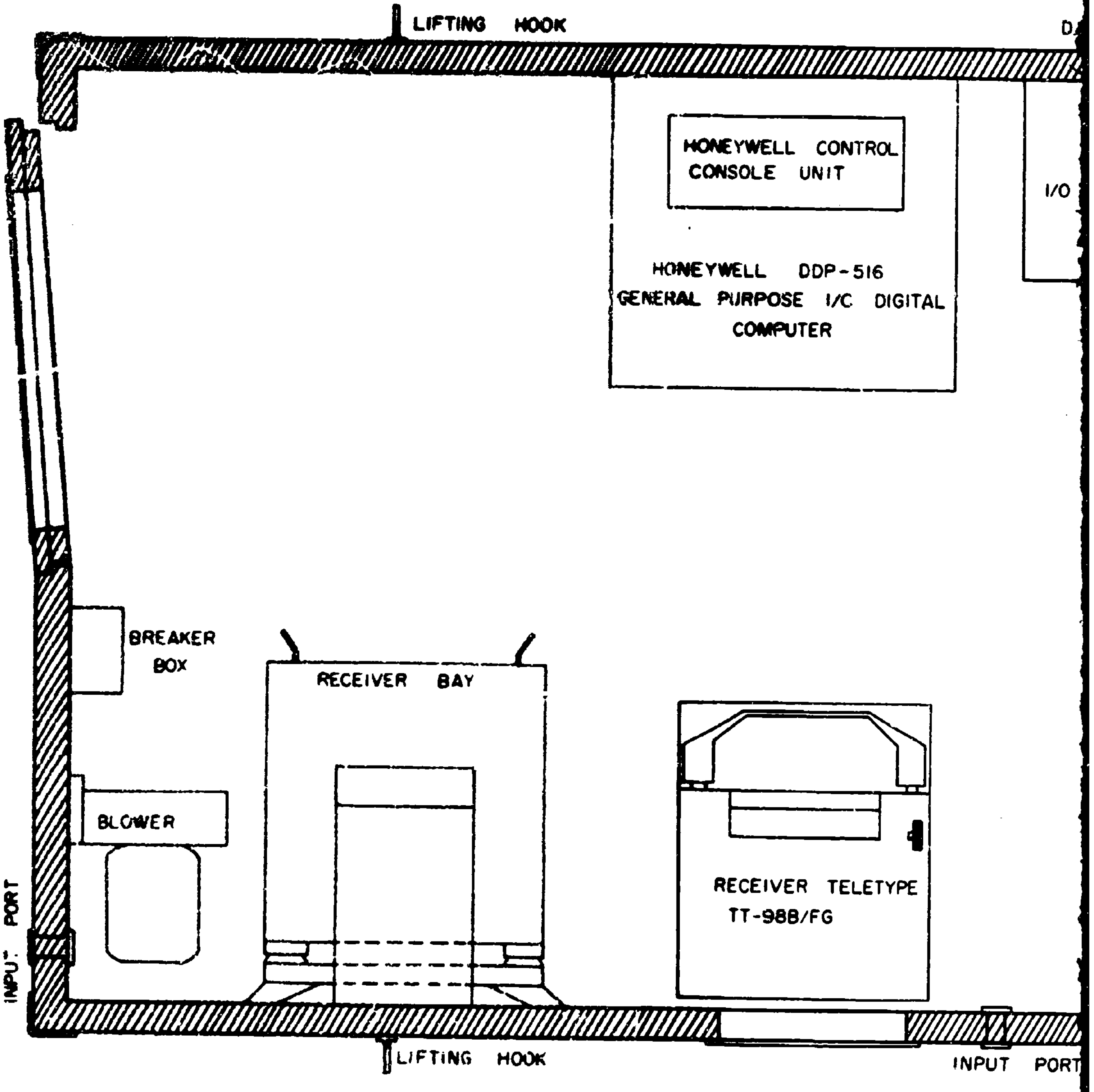

FIG. VI-1 REYNOLDS STRESS MOBILE

A

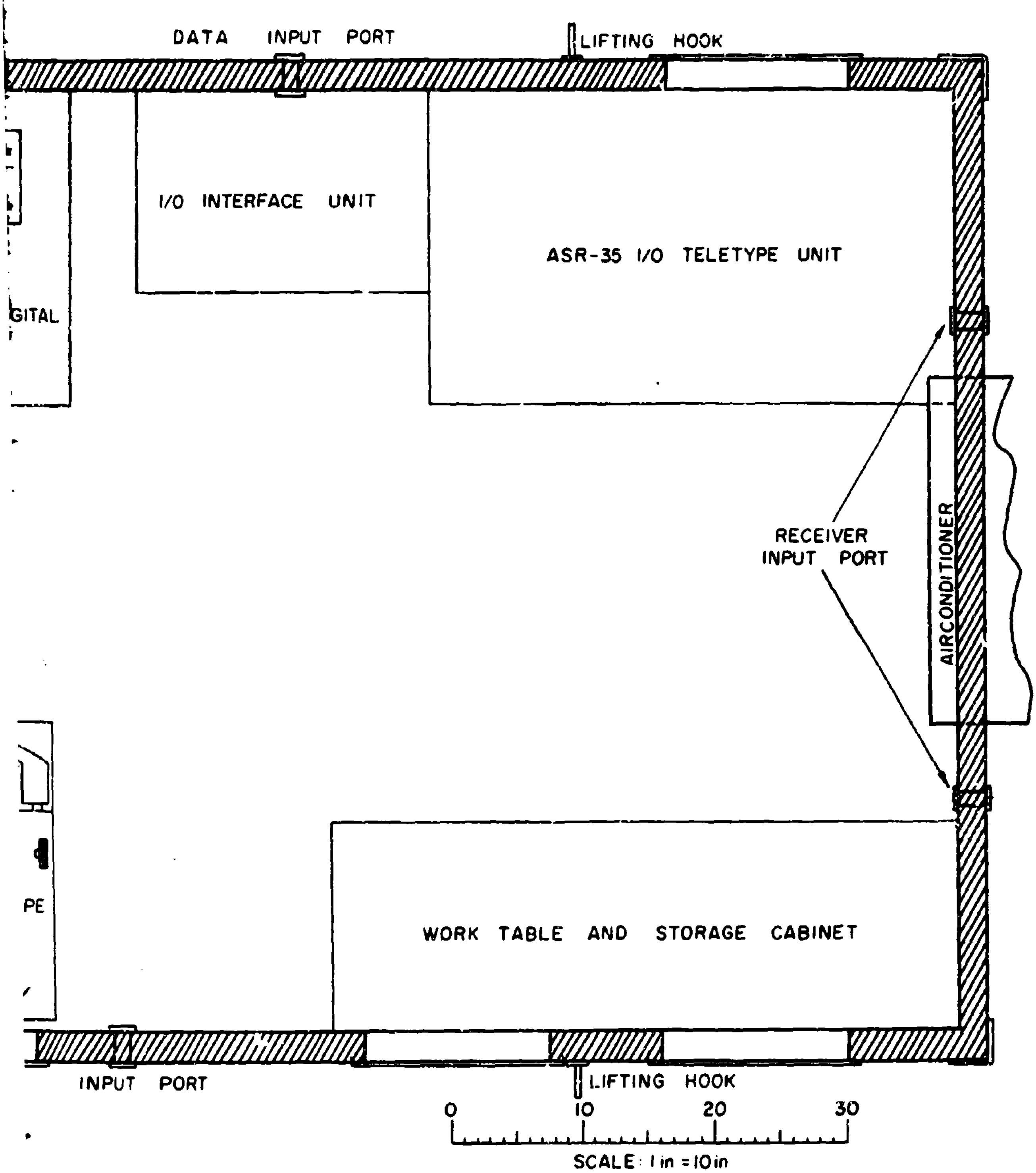

;S MOBILE LABORATORY

B

construction but tentative planning calls for a trailer configuration similar to the Rohn HD1-3-54G. This, or a similar type of tower, will permit reasonable mobility with regards to station transfer as well as rapid change of measurement levels.

The sonic heads and temperature sensors to be employed in this facility are still under study and final selection will not be made without consultation with other investigators in the sonic field. In this regard, visits are planned in early 1969, to the University of Washington (Dr. J. A. Businger), Iowa State University (Dr. Robert Stewart and Dr. Robert Post) and to the Air Force Cambridge Research Laboratories, Hanscom Field, Massachusetts (Dr. Chandran Kaimal).

The preceding discussion plus the 'ahead-of-schedule' status of this Sub-task is not intended to imply that completion of this facility is largely mechanistic and straightforward. Several problems remain to be solved of an anticipated nature and undoubtedly several unanticipated ones will be met. There can be no question that a large part of the difficulties will be engineering in nature, however, the theoretical implications of sonic anemometry are at present only unproved postulates and evaluation of these postulates is not expected to be routine. This is perhaps best indicated by noting that all of the researchers noted above have constructed successful prototype sonic anemometers, yet none of these devices have been consistently and gainfully employed in the field.

VII. MISCELLANEOUS

In the preceding review of Themis activities during the first year, attention has been focused on results and avoidance of detailed descriptions of unsuccessful and/or essentially logistical endeavors. This is particularly true for the data collection activities under Sub-task b, the calibration and installation procedures of the automatic meteorological stations under Sub-task c, and routine model evaluation and efforts also under Sub-task c. Some review of these activities have been given in the Quarterly Progress Reports and omission herein is strictly based on editorial concept. An idea of the magnitude of these omitted efforts may be afforded by noting that all of the originally proposed efforts are closely following the proposed schedule with the deviation, for the most part, being one of acceleration rather than retardation.

Two new efforts will be initiated during the second year. One under Sub-task b, the other under a new Sub-task e.

The first of these efforts "Anomalous Wintertime Precipitation in the Western United States and Related Meteorological Variables", will be directed by Dr. R. A. Clark. The research itself will largely be conducted by Mr. L. G. Cobb as a Ph.D. dissertation. A brief resume of the procedures that will be followed in conducting this research, given below, has been extracted from a proposal submitted by Mr. Cobb to the Technical Director.

The proposed research will investigate the deviations from the climatic mean monthly precipitation of the wet season for the Pacific coast of the United States. Relationships between the rainfall anomalies in the total problem will be investigated.

The monthly Climatological Data National Summary contains maps of the total precipitation, percentage of normal precipitation, average sea-level pressure, and departure of average pressure from normal, along with the average height and temperature and resultant winds for standard isobaric surfaces. These will be used to determine the months of significant anomalies (less than 75 percent or greater than 150 percent of the mean) of rainfall in the states of California, Oregon, and Washington for the period 1952-1967. The wet season (October-April) will be considered because only during those months does enough precipitation occur so that deviations from the average have real meaning.

From monthly mean radiosonde data for 12 stations located in the western United States, the flux of water vapor across the Pacific coast will be calculated for 40 months selected from the period 1952-1967. Ten months which are representative of each of the following four situations will be chosen for analysis: above-normal precipitation over the whole west coast region, below-normal precipitation over the whole west coast region, much-below-normal precipitation in the southern

half of the region and normal or greater precipitation in the northern half, and much-below-normal precipitation in the northern half and above-normal in the southern half of the area being considered. Calculations of the flux of water vapor will be made for the surface and each 50-mb level above to 400 mb by the technique used by Cummings and Franceschini. It is expected that a careful analysis of this data will reveal characteristic features of the flux of moisture for each station and situation, and will shed light on the question of whether increased precipitation is caused by a more efficient precipitation mechanism or a more abundant moisture supply (or both).

Mean monthly sea-surface temperatures are available for the eastern North Pacific Ocean for the period being investigated. These will be studied in conjunction with the analyses of water-vapor flux to see if the water temperatures significantly affect the water content of the air and the atmospheric pressure patterns.

The rainfall anomalies will be statistically correlated with the anomalies of the average sea-level pressure of that region to determine conditions associated with the pressure field which are conducive to abnormal precipitation. Most previous investigators have attempted to relate precipitation and upper-air patterns (mostly 700-mb); however, the present

study will utilize sea-level pressure because the pressure patterns at the surface reflect the behavior of the total atmosphere. A preliminary investigation has revealed very good correspondence between the anomalous component of the wind flow and areas of abnormal precipitation. Once the patterns of pressure anomaly that are associated with abnormal rainfall have been identified, theoretical relationships will be utilized to show what is occurring in the overlying atmosphere in terms of changes in moisture advection, convergence, and relative vorticity. The results of this study will be compared to previous studies of a more general nature.

The second new effort, directed by A. H. Thompson, is titled "The Change of Intensity in Cloud Systems Associated with Easterly Perturbations as They Move Over Areas of Differing Water Temperature". The research will be largely conducted by Mr. J. E. Arnold as a Ph.D. dissertation subject. A brief resume of the procedures to be employed in conducting this research, as given below, have been extracted from a proposal submitted by Mr. Arnold to the Technical Director.

The temperature field of the Caribbean Sea and equatorial western Atlantic will be examined through the use of commercial ship data available from the National Weather Records Center, Asheville, N. C., and from conventionally prepared northern hemisphere weather charts. It has been found that commerical

ship data, when averaged over a 7-day period, provide a reasonably good representation of ocean surface temperature. From composite sea-surface temperature charts of this nature the temperature of the ocean surface can be acquired for periods when active systems are propagating through the area of interest. It should be pointed out that although the temperature of the ocean acquired by this method is not always correct, i.e., it may be too warm or too cold, the temperature patterns are comparable to those obtained by research vessels.

The vertical thermal structure of the upper layer of the ocean also will be considered by the use of bathythermographs available from time to time in the area of interest and from historical data on the vertical thermal structure of the ocean. This information will be used to evaluate the capability of the ocean to supply or absorb heat during the periods studied and the effects that wind mixing would have on the surface layers on the oceans.

Surveillance of cloud systems moving through the area of interest will be accomplished using ESSA and Nimbus cloud photographs. Individual disturbances will be followed and the cloud activity recorded in terms of area and type of activity. The distribution of cloud activity about the disturbance will be examined on an interdiurnal basis from ESSA and Nimbus photographs and the cloud range during short periods,

i.e., during the day, will be studied from the ATS III photographs. This should provide informative data as to cloud distribution about a system over a water area of uniform temperature and the response of the cloud distribution as the disturbance passes over a region of strong surface temperature gradient. In addition to cloud examination, the ATS III photographs will be used to determine cloud motion in the vicinity of the disturbances studied.

A composite picture of the atmosphere will be obtained from existing radiosonde and surface stations situated around the region to be investigated. The patterns of divergence obtained from the rawindsonde and pibal measurements surrounding the Caribbean will be integrated with the patterns of divergence obtained from cloud motion (assumed to be representative of the wind field at cloud level) to arrive at an estimated field of vertical motion in the vicinity of the disturbance. The derived field of motion in the atmosphere and the sea-surface temperature field will be used as input data from which the life of the disturbance and associated cloud intensity will be evaluated.

With the above data it is proposed to take a period when traveling perturbations in the easterlies are known to exist in the Caribbean and western Atlantic region and maintain close surveillance of the region to find weak or moderate disturbances

entering the area of interest. It is anticipated that a sufficient number of disturbances will be found in one season, June–October, 1968, to enable an evaluation of the proposed technique to determine the relationship between cloud activity, intensity of the system, and sea-surface temperature field over which the perturbation passes.

The western equatorial Atlantic and the Caribbean Sea have been chosen as the geographic region for investigation because of the availability of data. The Caribbean Sea is surrounded by rawinsonde and surface reporting stations, enabling a basic framework of upper-air and surface stations to be used in connection with the satellite data. In addition, there is sufficient shipping within the area to enable reasonably accurate evaluation of the sea-surface temperature field. The region also is near the subpoint of the ATS III satellite, a feature definitely advantageous in determining cloud motion from the (Image Dissector Camera System) pictures. It is generally accepted also that the area of the Caribbean Sea is within the normal tracks of perturbations as the systems pass from the Atlantic toward the Yucatan Channel. Preliminary investigation of the Caribbean sea-surface temperatures as determined from commercial ship data and inspection of the oceanographic atlases reveal that sufficient gradients of

sea-surface temperature exist through the proposed time-period of study to evaluate realistically the proposed hypothesis.

It is intended to obtain ATS III photographs from the National Aeronautics and Space Administration for the construction of film strip loops to determine cloud motion. Tentative arrangements have been made with Mr. L. F. Hubert, ESSA, to have the National Environmental Satellite Center construct the film strip loops and send copies to Texas A&M. A loop projector system similar to that developed by Fujita at the University of Chicago will be constructed at Texas A&M. The technique of analysis described by Fujita will be used to determine cloud motion.

Finally, it should be noted that the activities of the second year will follow proposed schedules but with somewhat less rigidity than that employed during the first year. The efforts of the first year have, in a sense, been exploratory and, as anticipated, new lines of research have been opened, and these will be followed as time, staff, and facilities will allow. Primarily, these are changes in the originally proposed procedures which, necessarily, were tentative, and no basic changes in direction of the Themis efforts at Texas A&M are currently planned.

Security Classification

DOCUMENT CONTROL DATA - R & D

(Security classification of title, body of abstract and indexing annotation must be entered when the overall report is classified)

1. ORIGINATING ACTIVITY (Corporate author) Texas A & M Research Foundation College Station, Texas 77843	2a. REPORT SECURITY CLASSIFICATION
	2b. GROUP

3. REPORT TITLE

PREDICTION OF ENVIRONMENTAL PARAMETERS

4. DESCRIPTIVE NOTES (Type of report and inclusive dates)

First Annual Report for 20 September 1967 to 20 September 1968

5. AUTHOR(S) (First name, middle initial, last name)

K. C. Brundidge E. L. Deacon
W. H. Clayton V. E. Moyer

6. REPORT DATE	7a. TOTAL NO. OF PAGES	7b. NO. OF REFS
November 1968	150	35

8a. CONTRACT OR GRANT NO. DAAB07-68-C-0073	9a. ORIGINATOR'S REPORT NUMBER(S) Reference 68-23-A
b. PROJECT NO. 1T0-14501.B81A.00.09	
c.	9b. OTHER REPORT NO(S) (Any other numbers that may be assigned this report)
d.	TR ECOM-0073-1

10. DISTRIBUTION STATEMENT

This document has been approved for public release and sale; its distribution is unlimited.

11. SUPPLEMENTARY NOTES	12. SPONSORING MILITARY ACTIVITY
	U. S. Army Electronics Command Fort Monmouth, New Jersey AMSEL-B -TE

13. ABSTRACT

The research efforts for the first year on Project Themis at Texas A&M University have been directed along five primary research paths: analysis and prediction of atmospheric structure through use of dual-frequency radars and associated ground facilities; cumulus cloud dynamics; modeling studies of the frictional boundary layer; installation of two automatic meteorological collection stations in an instrumented watershed which is in the pattern of the radars; and design of a facility for direct measurement of the fluxes of momentum, heat, and vapor. The activities under these various headings are reviewed separately herein.

Security Classification

14. KEY WORDS	LINK A		LINK B		LINK C	
	ROLE	WT	ROLE	WT	ROLE	WT
1. Meteorology						
2. Modeling						
3. Radar Meteorology						
4. Cumulus Dynamics						
5. Instrumentation						
6. Simulation						